AN ABSTRACT OF THE THESIS OF

Joseph Arthur Martone for the Doctor of Philosophy in
Name of Student Degree

Mechanical Engineering presented on July 6, 1990
Major Date

Title: Sampling Submicrometer Particles Suspended in Near Sonic and Supersonic Free Jets of Air

Abstract approved: Redacted for Privacy
Richard W. Boubel

This experiment is concerned with sampling submicrometer particles in near sonic and supersonic flows. The study employed a high volume condensation aerosol generator to produce stearic acid particles having a geometric mean diameter of 0.8 μm and a geometric standard deviation of 1.28. The aerosol was diluted with dry air and accelerated to Mach 0.6, 0.8, 1.26, or 1.47 through a flow nozzle. Aerosol mass concentrations were determined using a small bore probe in the jet and by a large bore probe sampling isokinetically upstream of the jet nozzle. The results of both samples were compared to compute the sampling error associated with the high speed jet sample. The mass of stearic acid collected on polycarbonate membrane filters was determined by gravimetric and chromatographic methods. Studies at Mach 0.8 with four

sampling probes having inlet wall to bore area ratios ranging from 3.8 to 0.28 demonstrated that probe wall thickness effects are not significant when the sample is extracted isokinetically. Subisokinetic experiments using a knife edged probe showed relative errors of 124 ± 12% when sampling at 20% of the isokinetic condition. The subisokinetic results are compared favorably with the extended empirical results of other authors. For the supersonic cases it is shown that the subsonic velocity downstream of the sampling probe bow shock can be used in estimating the sampling error.

Sampling Submicrometer Particles Suspended in Near Sonic and Supersonic Free Jets of Air

by

Joseph Arthur Martone

A THESIS

submitted to

Oregon State University

in partial fulfillment of
the requirements for the
degree of

Doctor of Philosophy

Completed July 6, 1990

Commencement June 1991

APPROVED:

Redacted for Privacy

Professor of Mechanical Engineering
in charge of major

Redacted for Privacy

Head of Department of Mechanical Engineering

Redacted for Privacy

Dean of Graduate School

Date thesis presented July 6, 1990

Typed by Mary C. Harlow for Joseph Arthur Martone

ACKNOWLEDGEMENTS

I wish to express my thanks to the members of my doctoral committee for their efforts in regard to my graduate program. Their guidance and help has been greatly appreciated.

Much gratitude is extended to the many people at the National Aeronautics and Space Administration (NASA) Ames Research Center who helped design and fabricate the experimental equipment which was located at their facility. The invaluable assistance and generous cooperation of Mr. Homer Lem in using the NASA scanning electron microscope is greatly appreciated. The assistance of Aerotherm Acurex Corporation in the design and fabrication of the supersonic inlet sampling probe and Stoner Laboratories for their gas chromatographic sample analysis is gratefully acknowledged. Special thanks must also go to the Air Force Civil Engineering Center (AFCEC) whose interest and support made the project a reality.

The guidance of Professor R. W. Boubel, my major professor, has helped immeasurably throughout this investigation. Also, much gratitude is extended to Dr. Alan B. Chambers, for his help in facilitating the experimental program at NASA Ames Research Center. I want to thank Dr. Peter S. Daley, the AFCEC technical

monitor for this project, for his technical guidance and advice throughout the program. Finally, the support and understanding of my loving wife, Cathy and my children, Andrea and Rob was the key to bringing this study to fruition.

Doctoral Committee: R. W. Boubel, J. R. Welty, S. Kimura, P. Nelson, and D. Thomas.

TABLE OF CONTENTS

LIST OF FIGURES

LIST OF TABLES

LIST OF APPENDIX FIGURES

LIST OF APPENDIX TABLES

NOMENCLATURE

List of Symbols

A	=	Cross sectional area, also aspiration coefficient
A_b	=	Free jet sampling probe inlet bore area
A_p	=	Inlet area of settling chamber sampling probe
A_w	=	Front area of free jet sampling probe wall
A^*	=	Minimum cross sectional area of free jet supersonic nozzle
B	=	Coefficient related to ß(K)
C	=	Sample aerosol concentration
C_o	=	True or free stream aerosol concentration
C_s	=	Cunningham slip-flow correction
C'	=	Orifice constant
D	=	Outside diameter of sampling probe inlet
D_e	=	Exit diameter of free jet nozzle
D_p	=	Inside diameter of sampling probe inlet
d_p	=	Particle diameter
E	=	Probe collection efficiency
E_{max}	=	Maximum energy
Ep	=	Reduced probe collection efficiency

F	=	Various orifice factors
f	=	Function
f_p	=	Probe mass fraction ingested
G	=	Mass flowrate
g	=	Acceleration of gravity
H	=	Length of radioactive source for aerosol charge neutralizer
H_O	=	Null hypothesis
h_v	=	Velocity pressure
h_w	=	Orifice differential pressure
ID	=	Inside diameter
K	=	Stokes number
k	=	Specific ionization constant
Kn	=	Knudsen number
L	=	Length
M	=	Mach number
M_g	=	Geometric mean diameter by count
M'_g	=	Geometric mean diameter by weight
MW	=	Molecular weight
N	=	Coefficient depending on Stokes number
NS	=	Normal shock
n_∞	=	Equilibrium bipolar ion concentration
OD	=	Outside diameter
P	=	Pressure

P_{amb} = Ambient or atmospheric pressure

P_c = Collapsing pressure

P'_t = Operating gage pressure for settling chamber

P_f = Flowing pressure

Q = Volumetric flow rate

Q_a = Volumetric flow rate at actual conditions

Q_b = Volumetric flow rate at standard conditions

Q_m = Volumetric flow rate at desired conditions

R or r_o = Radius

R_g = Universal gas constant

R_p = Particle radius

Re = Reynolds number

R_s = Sample reflectance

R_w = Clean filter reflectance

r = Correlation coefficient

S = Line source strength for aerosol charge neutralizer, also standard deviation of the mean

S_o = Required source activity for aerosol charge neutralizer

SN = Smoke number

T = Temperature

T_b = Base temperature

T_f = Flowing temperature

t = Tube wall thickness, also t-statistic

t_{res} = Residence time

t^*	=	Ratio of residence time to neutralization time
U	=	Mean flow velocity at sampling probe inlet
U_o	=	Free stream velocity along the flow line passing through the axis of the probe
U'_o	=	Free stream velocity upstream of normal shock
V	=	Velocity
X	=	Length, also ordinate
X_c	=	Length of potential core
Y	=	Abscissa
α	=	Recombination coefficient
β	=	Beta energy
$\beta(K)$	=	Stokes number function
γ	=	Ratio of specific heats, also gamma energy
δ	=	Shock detachment distance
η	=	Inertial parameter
λ	=	Particle range
λ^*	=	Mean free path
μ	=	Linear absorption coefficient
μ_g	=	Gas viscosity
ρ	=	Fluid density
ρ_p	=	Particle density
ρ_{std}	=	Fluid density at standard conditions
σ_g	=	Geometric standard deviation

τ	=	Neutralization time
Φ_r	=	Non-Stokesian correction factor
Φ_s	=	Ratio of probe radius-to-shock detachment distance
Ψ_f	=	Particle impaction parameter

General Subscripts

1	=	Condition upstream of normal shock
2	=	Condition downstream of normal shock
e or exit	=	Condition at free jet nozzle exit
t	=	Total or stagnation condition

Dimensional Units

atm	=	Atmospheres
C	=	Celsius degree
cm	=	Centimeter
cm^3	=	Cubic centimeter
cmHg	=	Centimeters of mercury
cfm	=	Cubic feet per minute
F	=	Fahrenheit degree
fpm	=	Feet per minute
ft	=	Foot
gm	=	Gram
hp	=	Horsepower
in or "	=	Inch

in H_2O	=	Inches of water
in Hg	=	Inches of mercury
Lb_f	=	Pound force
Lb_m	=	Pound mass
l	=	Liter
m	=	Meter
min	=	Minute
Mev	=	Million electron volts
mm	=	Millimeter
mv	=	Millevolt
mCi	=	Millicurie
mg	=	Milligram
m^3	=	Cubic meter
psig	=	Pounds per square inch gage
psia	=	Pounds per square inch absolute
R	=	Rankine degree
sec	=	Seconds
scfm	=	Standard cubic feet per minute
%	=	Percent
Super script^{o}	=	Angular degree
μg	=	Microgram
μm	=	Micrometer

TERMINOLOGY

The following is a list of terms used in this study which may not be in common use, or which may have more than one common meaning.

Aerosol: A system consisting of fine particles, solid or liquid, in gaseous suspension. Because aerosols contain fine particles, they are characterized as a stable or quasi-stable system.

Aerosol charge neutralizer: A device that achieves electrical neutralization of aerosols (i.e. Boltzmann charge equilibrium) by mixing a charged aerosol with a mixture of positive and negative small ions generated in the gas phase of the aerosol by ionizing radiation.

Anisokinetic sampling: Aerosol sampling with an aspirating probe such that the sampling velocity is greater than or less than the free stream velocity.

Aspiration coefficient: Ratio of aerosol concentration of sample to free stream aerosol concentration.

Base conditions: The desired conditions associated with volumetric flow rate in orifice calculations and free jet airflow system. In this study, base pressure is 14.7 psia (76 cm Hg) and base temperature is 70 F (21.1C).

Boltzmann charge equilibrium: An equilibrium bipolar electrical charge on an aerosol as a result of the random thermal motion of bipolar ions and the frequent collisions of ions with particles. The charge distribution at equilibrium is described by Boltzmann's law.

Brazetyte: A registered trade name of the Truly Tubular Fitting Corporation that applies to stainless steel tube fittings especially designed to mate with actual tube OD sizes.

Cunningham correction factor: A correction to the law of fluid-flow resistance for particles with size of the order of the mean free path of the fluid molecules.

Filtration efficiency: The fraction of airborne particulate reaching a filter surface which is collected by that filter, on either a count or a mass basis, as found by subtracting the penetration

from unity. It may be shown as a ratio or as a percentage. Unless specified otherwise, efficiency on a mass basis is to be assumed in this study.

Filter velocity: The "average" gas velocity approaching a filter surface as found by dividing the total volumetric flow rate through the filter by the total filter cross-sectional area. It may be based on actual or standard conditions, and the terms should have consistent units. Also called superficial velocity.

Free jet: An unbounded axisymetric, near sonic or supersonic jet of air discharging into quiescent air at atmospheric pressure and room temperature.

Geometric mean diameter: The particle size at the 50th percentile for a log-normal particle size distribution.

Geometric standard deviation: The measure of dispersion for a log-normal distribution, the ratio of the 84.13 percentile to the 50th percentile.

Isokinetic sampling: A sampling method for aerosols whereby an aspirating sampling probe withdraws

aerosol such that the aerosol velocity at the sampling probe inlet is carefully matched to the free stream aerosol velocity, thereby eliminating sampling bias due to inertial separation of particles and gas at the sampling probe inlet.

Log-normal distribution: A statistical frequency distribution which is normal when plotted against the natural log of the variable.

Mach number: Ratio of the flow speed to the local speed of sound.

Magnehelic: A registered trade name of Dwyer Instruments, Inc., that applies to their line of diaphragm actuated precision gages that are used to indicate differential pressures of air or non-corrosive gases. In this study, Magnehelic gages measured differential pressures across the orifice flow meters in the particle sampling systems and pitot tube differential pressures.

Median: The 50th percentile demarkation for a distribution.

Monodisperse particle size distribution: A particle size distribution with values over a narrow range such that the sizes may be assumed to have a single, common value (homogeneous).

Near sonic: Mach number equal to or greater than 0.6 but less than 1.0.

Normal shock: The discontinuity, roughly normal to the flow direction that occurs with the sudden retardation of a supersonic flow near the front of an obstacle (in this study a sampling probe) in the flow stream.

Nuclepore: A registered tradename of the Nuclepore Corporation that applies to the unique membrane produced by using a patented irradiation and etching process on a polymer film. In the case of Nuclepore membranes, the film is polycarbonate plastic, chosen for its superior chemical resistance, thermal stability, transparency and availability.

Particle size: The "size" of a dust particle represented by the diameter of a circle whose area is the same as that of the actual particle as observed under a microscope.

Particle size distribution: The frequency of occurrence of particles of various sizes in a sample.

Particulate: Any group of particles or dust carried by a gas stream.

Particle stopping distance: The distance a particle would travel before coming to rest if projected with an initial velocity into a still fluid. Sometimes called particle range.

Pesticide grade acetone: Acetone that has been specially purified by a multi-step process that includes distillation in all-glass equipment making it suitable for pesticide residue analyses and the determination of trace hydrocarbons.

Polydisperse particle size distribution: A particle size distribution with values over a wide range such that a single value of size may not be assumed (heterogeneous).

Potential core: Zone downstream of the exit of a supersonic free jet where the free stream velocity equals the nozzle exit velocity. In this study, the

free jet particle sampling probe inlets were placed within the free jet potential core.

Probe wall effect: Errors (either over or underestimate) in measuring the true mass concentration of particles in a flowing aerosol with an aspirating probe even though the probe is properly aligned with the flow and isokinetic sampling is maintained. These errors can occur with "thick walled" sampling probes when solid particles may rebound from the leading edge or outer walls of the probe and be subsequently drawn in with the sample.

Probe blockage effect: A perturbation of the free stream velocity in the vicinity of the sampling probe inlet similar to the phenomenon which in this study is referred to as the probe wall effect.

Probe collection efficiency: Ratio of the measured aerosol concentration using an aspirating probe to the true aerosol concentration; also known as the aspiration coefficient.

Rayleigh limit: Maximum electrical charge on aerosol particles before the particles become mechanically unstable.

Shadowgraph: The photograph obtained using a supersonic flow visualization technique that relies on change in refractive index or light propagation speed which results from a change in gas density across shock waves.

Smoke: Particulate matter in an aircraft turbine engine exhaust that obscures the transmission of visible light.

Smoke number (SN): A dimensionless term used for quantifying aircraft turbine engine smoke emissions; its magnitude is related to the optical reflectivity of collected particles relative to the optical reflectivity of a clean filter.

Stagnation conditions: The maximum pressure or temperature a fluid (in this study air) could attain if brought to rest without the action of any viscous forces. Sometimes called the total pressure or temperature.

Standard conditions: The condition where the pressure is 14.7 psia (76 cm Hg) and the temperature is 60 F (15.6 C).

Stokes number: A dimensionless particle inertial parameter that is the ratio between the particle stopping distance and the diameter of the sampling probe.

Subisokinetic sampling: Aerosol sampling with an aspirating probe such that the sampling velocity is less than the free stream velocity.

Submicrometer particles: Particles with diameters less than 1 micrometer. A related term, fine particles, includes submicrometer particles and particles with diameters up to 10 micrometers.

Supersonic: Mach number greater than 1.0.

Superisokinetic sampling: Aerosol sampling with an aspirating probe such that the sampling velocity is greater than the free stream velocity.

SAMPLING SUBMICROMETER PARTICLES SUSPENDED IN NEAR SONIC AND SUPERSONIC FREE JETS OF AIR

INTRODUCTION

The Problem

Fine particles, those with diameters of 10 micrometers or less, are receiving increasing attention as a major air pollutant. It is well known, for instance, that many of the undesirable effects associated with particulate air pollutants, such as the effect on human health and atmospheric visibility, are due mainly to fine particles. The control of fine particles, therefore, is an important part of the problem of particulate air pollution control.

Aircraft turbine engine operation is a source of fine particles that is of special concern to the military and civilian aviation community. The awareness of air pollutant emissions from aircraft developed in the late 1950's with the introduction into service of turbine engine aircraft. Visible exhaust plumes from turbojet engines and increased levels of exhaust odors at airports gave rise to complaints against these perceptible manifestations of aircraft emissions. These complaints stimulated investigation into the nature and extent of aircraft emissions. Considering these studies, the

United States Environmental Protection Agency (EPA) determined that the magnitude of aircraft emissions was sufficient to warrant promulgation of emission standards for aircraft and aircraft engines (1).

In 1968, the Society of Automotive Engineers formed a committee on aircraft exhaust emissions measurement whose charge was the development of acceptable standards of measurement for the characterization of aircraft engine exhaust. The first order of priority was the measurement of smoke which by definition is the particulate matter in the engine exhaust that obscures the transmission of light (i.e. mainly fine particles). The result was the issuance of Aerospace Recommended Practice ARP 1179, "Aircraft Gas Turbine Engine Exhaust Smoke Measurement" (2). This recommended practice has in large part been adopted by the EPA. The method provides a relative index of smoke emissions called smoke number (SN) according to the following equation:

$$SN = 100\ [1-(R_S/R_W)] \qquad (1)$$

R_S = sample reflectance

R_W = clean filter reflectance

The procedure used for determining smoke number involves passing a known mass of engine exhaust gas through a filter and measuring the optical reflectivity of the collected particles. Dividing this result by the

clean filter reflectance yields a dimensionless term used for quantifying aircraft engine smoke emissions.

Thus, smoke number is an indicator of the relative visibility of the exhaust gas. The difficulty in attempting to use this procedure as a measure of particulate mass emitted is that the reflectivity is largely a function of the relative size of the particles collected, and may not necessarily be related in any discrete manner to the total mass of the sample. Champagne (3), for example, reports that the smoke number index can be identical for two particulate emission samples that differ in total mass by a factor of as much as two.

The EPA ambient air quality standards for particulate matter (4) are specified in units of mass per unit volume of air. Therefore, atmospheric dispersion models used to assess the impact of aircraft engine operations on ambient air quality require operating time weighted mass emission rates which consider each of the pertinent engine operating modes.

Currently, the usual procedure is to estimate mass emission rates from smoke number data using a smoke number-mass emission correlation such as suggested by Champagne (3) or Finch (5). A direct mass measurement of engine particulate emissions would provide a more accurate assessment of the gas turbine engine contribution to ambient air concentrations. The development of measure-

ment techniques for particulate emissions from aircraft turbine engines was considered by Johansen and Kumm (6). They employed the classical aspirating probe method to obtain an aliquot of the engine exhaust for analysis. Their recommendations included the following:

> It is recommended that the sampling apparatus developed in this program be used for additional research to attempt to correlate particulate emissions with smoke number and to relate this data to ambient air quality standards. This would enable further testing to study the effects of non-isokinetic sampling (and its effect on probe sampling efficiency), dilution, ambient dust ingested at the engine inlet, stratification of particulate concentrations in the engine exhaust plane, non-constant particulate emission rates, and particle size distribution.

Concern with current gas turbine engine particle sampling technology was also expressed by the Coordinating Research Council, Inc., which conducted a cooperative experimental program (7) to compare the results of several methods used to determine the amount and composition of particulate materials at the exhaust of a turbine engine. Nine participants from industry, government and military were included. Their conclusion was:

> Results of this program do not lead to many well-defined conclusions. Repeatability of the methods employed certainly is not as good as desired, but there is no way to tell what repeatability is reasonably attainable in

> practice. Likewise, agreement among the different methods is not as good as desired, but, again, there is no reliable way to determine why the methods do not agree or how well they can reasonably be expected to agree.
> There is one firm conclusion possible, however. Particulate measurement is still an art. In all the methods, a considerable amount of the measurement technique has not been quantified and the results in each case depend on the skill, patience and undocumented knowledge of the operator.

It is almost a certainty that aspirating probes will be an integral part of gas turbine exhaust sampling systems for many years, regardless of the analytical instrumentation and methods used for determining the pollutant character in the extracted sample. In view of the dissatisfaction with currently employed aircraft engine exhaust particle sampling methods, it was apparent that related fundamental research was required.

Statement of Purpose

Motivated by the demonstrated need to improve the accuracy of aircraft engine fine particle mass emission measurements, this experimental investigation was intended to examine certain parameters which would likely influence representative extractive sampling of submicrometer particles suspended in high speed flows. No attempt was made to simulate the chemical composition or temperature of a gas turbine engine exhaust, however the use of submicrometer particles was important since no

property of particles in a gas dominates their dynamic behavior more than size. Specifically, the primary purpose of this study was to determine whether or not mismatches in the sampling velocity and the free stream velocity has a significant effect on the sampled aerosol mass concentration when small bore aspirating probes are used to extract submicrometer particles from near sonic and supersonic free jets. Of secondary importance was the effect of the sampling probe inlet wall thickness and the effect of shock front passage on sample representativeness.

In conjunction with the specific purposes of this study, methods and/or procedures were developed to accomplish the following:

1. Isokinetic sampling of submicrometer particles in near sonic and supersonic free jets.
2. Generation of large quantities of uniformly sized, spherical, electrically neutral submicrometer particles.
3. Acceleration of submicrometer particles to near sonic and supersonic velocities.
4. Determination of the size distribution of submicrometer particles collected on polycarbonate membrane filters.
5. Determination of the mass of the collected aerosol particles.

6. Shadowgraphs of sampling probes in supersonic free jets.

Preliminary Comments

The most common and usually most important reason for sampling particles in gas streams is to determine the mass concentration and/or size distribution of the particles as they exist in the free stream. In this case, the sampling method is said to be representative when the mass concentration and particle size distribution derived from the sample is the same as the particle mass concentration and particle size distribution in the undisturbed flow.

The classical method for sampling particles suspended in a gas stream uses an in-stream, front facing, aspirating probe to extract an aliquot of the aerosol flow. The particles are retained for subsequent laboratory analysis by passing the sampled volume through a particle collection device. Although non-interferring, remote monitoring systems usually based on the optical properties of the particles, may eventually be widely employed, it is very likely that extractive sampling methods will continue to be the reference technique for characterizing particle emissions.

Particles may have sufficient inertia such that particle motion may deviate from the gas flow streamline

pattern in the vicinity of the sampling probe inlet. Thus, the representative sampling of particle laden streams may be influenced by such things as sampling velocity, sampling nozzle shape, and probe alignment. Fine particles, however, have generally not been considered in particle sampling studies on the presumption that their behavior is essentially the same as the gas in which they are suspended. Thus, previous investigators have dealt with relatively large particles and low stream velocities.

The conclusions of early investigators led to general guidelines for representative sampling of particles having diameters greater than three to five micrometers. Among these are the requirement for maintaining a sampling velocity at the probe inlet which is equal to the free stream velocity, a condition known as isokinesis or isokinetic sampling. The use of a front facing knife edged probe aligned with the flow and having an inlet diameter not less than 6.35 mm is also a practice recommended to preclude sample biasing at the sampling nozzle inlet.

These guidelines are sufficient to permit representative results in the majority of particle sampling situations. However, in recent years there has been an increasing requirement for obtaining representative results in sampling environments that are significantly

different from those for which the sampling guidelines were developed. The sampling of stratospheric particles with probes mounted on high speed aircraft and sampling smoke emissions at the exhaust plane of an aircraft gas turbine engine or a solid rocket motor nozzle, are examples where submicrometer particles in sonic and supersonic flows are encountered. In these situations it is often impractical to sample isokinetically with a large bore probe (i.e. D_p > 6.35mm.) because of the large volume of sample gas which must be handled. Consequently, the presumption of faithful flow following particles is made, and sampling is performed sub-isokinetically with probe bores as small as 1.0mm diameter. The present study attempts to provide additional guidance for the case of such particles in high speed flows.

Limitations

In this experimental study, spherical, essentially monodispersed, submicrometer particles were generated, accelerated through a jet nozzle and then sampled in the free jet. The most direct application of these results is in sampling methodology for aircraft turbine engine particle emissions. There are, however, certain incomplete parallels. The most obvious is that the experimental apparatus was not a combustion source of particles, thus any high temperature effects other than mere gas

density corrections cannot be derived from the data. In addition, smoke particles are not spherical but lacy carbonaceous agglomerates (8, 9), however, they do have aerodynamic equivalent diameters which define their dynamic behavior as spheres. Stockham (8) found particles at the exhaust plane of a J57 engine operating at 75% normal power to have mass median diameter (MMD) of 0.11 μm with a geometric standard deviation of 1.63. Johansen and Kumm (6) found particles with a MMD of 0.3 to 0.5 μm in the exhaust of a TPE 331 turboprop engine. The present study used 0.8 μm diameter particles.

Since the most dramatic inertial effects occur at high velocity, only the upper range of gas turbine engine exhaust velocities were considered. Free jet velocities ranged from Mach 0.6 to Mach 1.47. This compares with maximum gas turbine engine sea level exhaust velocity values of from Mach 1.27 (10) to Mach 1.39 (11). Higher exhaust velocities are possible when engines are operated at altitude conditions. Although of minor importance compared with particle size and velocity, it was desirable to experimentally generate an aerosol concentration that was within the range typically found in gas turbine engine exhausts.

Most aircraft particulate emission measurements have been concerned with particulate matter on a dry basis (12); that is, with the liquid droplets removed from the

sample stream or with the sampling and collecting system maintained at a sufficiently elevated temperature to avoid any vapor condensation. Current ranges of turbine engine exhaust particulate concentrations (dry basis) are listed in Table 1. In the present study, aerosol concentrations ranged from 1.5 to 10.4 mg/m^3.

Table 1. Current Ranges of Aircraft Engine Exhaust Particulate Emission Concentrations (12).

	Engine Operation			
	Idle	Approach	Cruise	Take-off
Dry Particulates (mg/m^3)	0-200	5-150	6-60	2-150

To evaluate and characterize particulate emissions from aircraft gas turbine engines, proven methods must be used to obtain representative samples. It was expected that the confidence in such sampling methods would be significantly improved by the results of this investigation. The study employed small bore, front facing, aspirating probes to obtain samples of submicrometer particles suspended in near sonic and supersonic free air jets. The work was not an attempt to develop a sampler or sampling method to use in the discharge environment of a gas turbine engine. However, the experimental results

provide fundamental data to evaluate the effect of aniso-kinetic sampling in high speed flows as well as pio-neering information concerning the representativeness of particulate sampling in supersonic free jets.

Comments on Dimensional Units

There is a complicated mixture of units in the various disciplines associated with the processes and applications of aerosol sampling, and it is not uncommon to see units of feet per minute and micrometers in the same report. Also, in the present report, available instrumentation resulted in data being recorded with such units as inches of water, grams, inches and micrometers. To try to reduce the seriousness of the problem, a list of appropriate conversion factors is given below:

1 ft	=	30.5	cm
1 ft/min	=	0.058	cm/sec
1 ft^3/min	=	472.	cm^3/sec
1 gm/ft^3	=	$3.53 \ (10)^{-5}$	gm/cm^3
1 in	=	2.54	cm
1 in^2	=	6.45	cm^2
1 in^3	=	16.4	cm^3
1 in H_2O	=	0.187	cm Hg
1 Lbf/in^2	=	5.17	cm Hg
1 Lbm	=	454.	gm
1 Lbm/ft^3	=	0.0160	gm/cm^3
F	=	32 + (9/5) C	
R	=	460 + F	

LITERATURE REVIEW

Representative Sampling of Aerosols

The primary requirement in aerosol sampling is the representativeness of the sample; the sample must be correct with respect to particle concentration, particle size distribution, chemical composition, etc. In practice, two substantially different cases of sampling are encountered--from flowing and from stationary aerosols. The present discussion is restricted to the former case--the sampling of aerosols flowing through pipes, gas ducts, nozzles, etc. as well as atmospheric aerosols in the presence of wind. In addition, we are concerned with "classical" sampling methods through a sampling probe which is front facing and aligned with the gas flow.

To assure the acquisition of representative aerosol samples, isokinetic sampling is usually required. Isokinetic sampling is defined as the situation where the gaseous sample is withdrawn at the same velocity as the gas stream at the point of sampling (Figure 1-a). The concept of isokinetic sampling is germane to this investigation and demands a thorough description.

If the velocity at the sampling nozzle inlet does not match that of the gas stream, an erroneous sample is

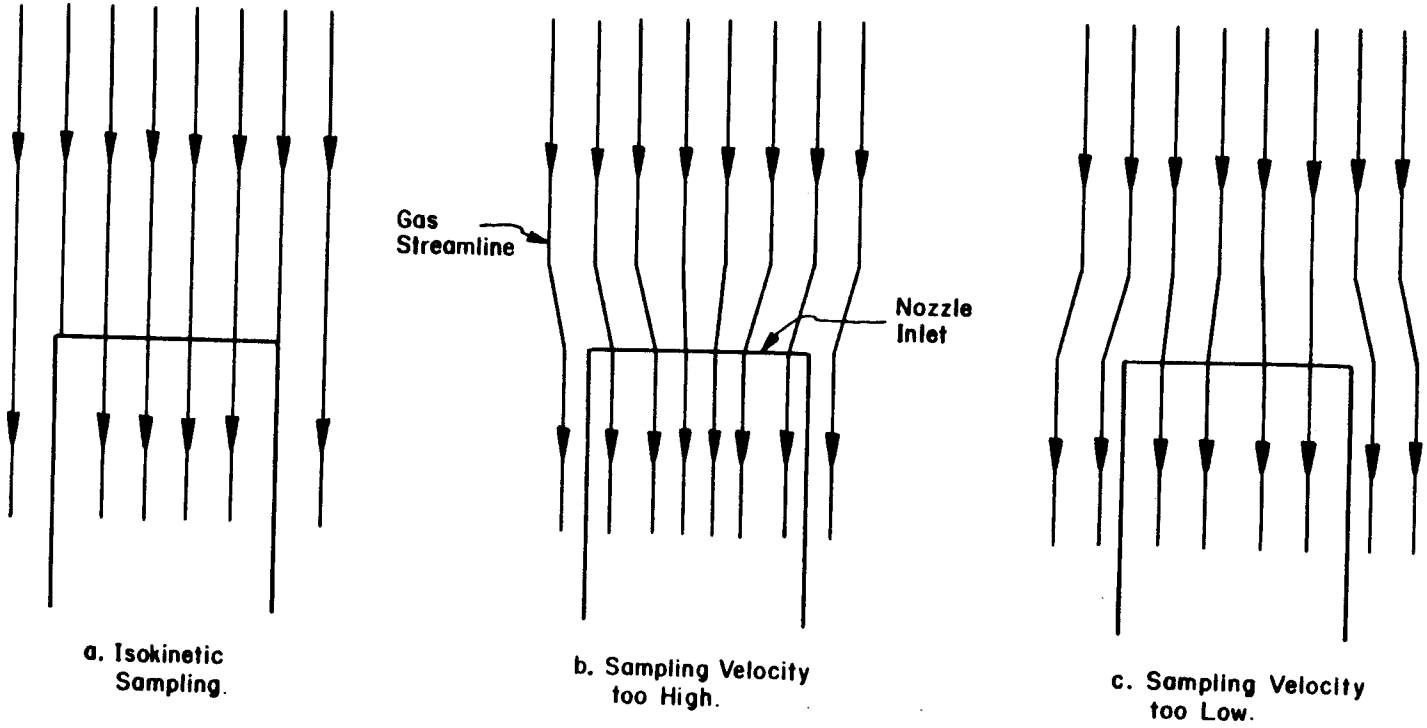

Figure 1. Gas flow patterns at the sampling nozzle inlet.

collected as a result of particle inertia. When the sampling velocity is less than the gas stream velocity (Figure 1-c), part of the approaching stream is deflected. The light particles tend to follow gas streamlines and do not enter the probe, but heavier particles, due to their inertia, continue along their previous path and enter the nozzle. As a result, a high proportion of the heavier particles are sampled and the total particle mass is therefore greater than expected. On the other hand, if the sampling velocity is greater than the main stream velocity, (Figure 1-b), the gas stream will converge towards the nozzle inlet carrying the lighter particles into the nozzle. The heavier particles will tend to continue along their original path because of their greater inertia and thus miss the nozzle. The collected sample will contain a relative excess of the lighter particles and the particle mass will be in error on the low side.

Recommendations for isokinetic sampling date back to 1911 when Brady and Touzalin (13) made measurements with coal dust. Numerous articles have appeared since, but the major emphasis has been on relatively large particles (>3 μm) and on the incompressible (< Mach 0.3) flow regime. Other authors have made the same observation (14) (15). Therefore, this review is limited to the most significant incompressible results and a discussion of

factors relating them to the experimental program.

Early investigators (1930's 40's, 50's) realized that a number of conditions must be fulfilled in order to insure representative aerosol samples. The requirements for isokinesis has already been mentioned. In addition, Hemeon and Haines (16) determined that the axis of the sampling probe should be parallel to the flow lines in a duct, otherwise the aerosol concentration (C) in the sample would be less than in the duct (C_o) and the aspiration coefficient (C/C_o) would be less than 1. Particle inertia is again the culprit; sampling probe misalignment causes selective withdrawal of smaller particles without as many of the larger particles as are actually present.

Studies (17) (18) using sampling probes with inlet nozzles having thick walls and obtuse edges demonstrated a narrow ring-like stagnant zone in front of the probe inlet wall which could only be penetrated by particles with sufficient inertia resulting in an increase of the aspiration coefficient. Thus, a third condition was added: the walls of the sampling probe inlet should be infinitely thin. The nearest practical approach to this is that of thin tubing ground to a knife-edge at a small cone angle. In addition to the above mentioned conditions, some authors (19) (20) suggest a lower limit of 6.3 mm for the sampling nozzle inlet diameter.

For practical purposes in incompressible flows, it is relatively easy to satisfactorily obtain the conditions for probe size, shape, and alignment; however, strict isokinesis is difficult to maintain. In addition, an isokinetic sampler is of necessity much more complex, expensive and difficult to operate than one that does not need to follow the gas flow velocity; thus anisokinetic sampling is desirable if the resulting errors are small or can adequately be estimated. Therefore, it is necessary to know what error results from a given mismatch in free stream (U_o) and sampling velocity (U). This question has been studied both theoretically and experimentally.

Effect of Anisokinetic Sampling

Historically, experimental investigations concerning anisokinetic sampling have dealt with relatively large particles (greater than 4 μm diameter) and low velocities. Some of these studies have resulted in generalized empirical expressions to fit the experimental data. Parker (15) uses the Stokes number (K) as an approximate but convenient guide to indicate when isokinetic sampling is necessary. Based on an examination of theoretical and experimental deposition studies, Parker (15) suggests that isokinetic sampling is required if:

$$0.05 < K = (\rho_p d_p^2 U_o C_s)/(18\ \mu_g D_p) < 50 \qquad (2)$$

where:

K = Stokes number

C_s = Cunningham slip-flow correction

U_o = ambient flow velocity along with the flow line passing through the axis of the probe.

ρ_p = particle density

d_p = particle diameter

μ_g = gas viscosity

D_p = diameter of sampling probe inlet (inside diameter)

Voloshchuck and Levin (21) made theoretical calculations and found that the approximate formula for the aspiration coefficient (A) could be written in the form:

$$A = C/C_o = 1 + [(U_o/U) - 1]\ ß(K) \qquad (3)$$

where:

C = aerosol concentration of sample

C_o = aerosol concentration free stream

U = mean flow velocity at probe inlet

U_o = ambient flow velocity along the flow line passing through the axis of the probe

$ß(K)$ = Stokes number function

Other authors have correlated their experimental data using the form of Equation 3 with different expressions for ß(K). Zenker, as reported by Fuchs (22), sampled vertical air streams containing spherical glass beads or limestone dust with particle diameters from 7 to 73 μm. For Stokes numbers between 0.06 and 14 and values of U/U_o between 0.4 and 2.5, ß(K) was found to be:

$$ß(K) = 1 - N \qquad (4)$$

where:

N = dimensionless coefficient depending only on the Stokes number.

Davies, as reported by Belyaev and Levin (23), suggests the following formula:

$$ß(K) = 1 - [1/(1+4K)] \qquad (5)$$

Belyaev and Levin (23) used the same form as Equation 5 to correlate their data. They employed flash illumination to study the aspiration process for willow pollen (aerodynamic diameter 24 μm) and Lycopodium spores (aerodynamic diameter 17 μm) near a sampling probe inlet. The sampling errors were determined from the limiting trajectories of particles entering the sampling nozzle.

For probes with very thin (0.1 millimeter) walls their results were accurately approximated by:

$$ß(K) = 1 - [1/(1 + BK)] \quad (6)$$

where:

$$B = 2 + 0.62\ (U/U_o) \quad (7)$$

Equations 6 and 7 are applicable for U/U_o between 0.18 and 6.0 and a Stokes number between 0.18 and 2.03.

Rader and Marple (24) conducted a numerical investigation of sampling bias through cylindrical probes for both isokinetic and anisokinetic conditions for thin-and thick-walled probes. Based on a dimensional analysis of the problem and on the assumptions of a physical model, five dimensionless groups, Re, U/U_o, D/D_p, K, and $\rho/(\rho_p C_s)$ are identified that specify the aspiration coefficient, A. Previously undefined terms are:

D = outside diameter of sampling probe

Re = tube Reynolds number = $(\rho D_p\ U)/\mu_g$

ρ = fluid density

$\rho/(\rho_p C_s)$ = slip-modified density ratio

The tube Reynolds number and the slip-modified density ratio were shown to have only a minor influence in determining A. Using the remaining groups--velocity ratio, diameter ratio, and the Stokes number--Rader and Marple (24) calculated results that were in good

agreement with the experimental data of others such as Belyaev and Levin (23) and Martone et al (25).

The results of these relatively recent authors suggest that anisokinetic sampling errors might be significant even for submicrometer particles if sampled in high speed air flows with small bore probes. The errors predicted by these expressions are greater than would be predicted by the empirical relationships presented in the often cited, but considerably older, work of Badzioch (26) and Watson (27).

In a supersonic flow, a shock front would be located either at the bow of, attached to, or swallowed in, the aspirating probe. There apparently have been no experimental studies to determine anisokinetic sampling errors when using aspirating probes for sampling supersonic dust laden gases. Parker (15) briefly acknowledges the problem; he states that:

> isokinetic sampling in a unity Mach number flow appears theoretically impossible unless the interior of the probe tapers to allow subsonic diffusion to occur; furthermore, shock wave systems which form around the probe at these conditions give added complexities to sampling.

Recently, Forney and McGregor (28) theoretically considered the collection efficiency of a thin-walled cylindrical probe sampling nondiffusing particles of low concentration suspended in a supersonic stream. It was

demonstrated that the probe capture efficiency is influenced by particle inertia, departures from Stokes drag, gas compressibility, and the probe ingestion rate. By defining an effective Stokes number in terms of the particle stopping distance downstream of the shock, which includes the effects of non-Stokesian drag and slip flow; and rescaling the Stokes number with the shock detachment distance, the reduced probe collection efficiency was shown to be correlated with a single universal curve (Figure 2). This similarity parameter should be useful in attempts to correlate the particle deposition for any geometry in a supersonic stream. Both of the most recent publications cited above, Rader and Marple (24) and Forney and McGregor (28), cite the published version of this work, Martone et al (25) as unique for its experimental consideration of subisokinetic sampling from near-sonic and supersonic flows.

Effect of Nozzle Shape

Sampling nozzle configuration has an effect on the accuracy of particulate sampling by affecting the pattern of gas flow streamlines. The ideal shape is a probe with infinitely thin walls. The nearest practical approach to this, according to Parker (15), is that of thin tubing ground to a knife-edge at a small cone angle. Whiteley and Reed (17) evaluated several different types of probes

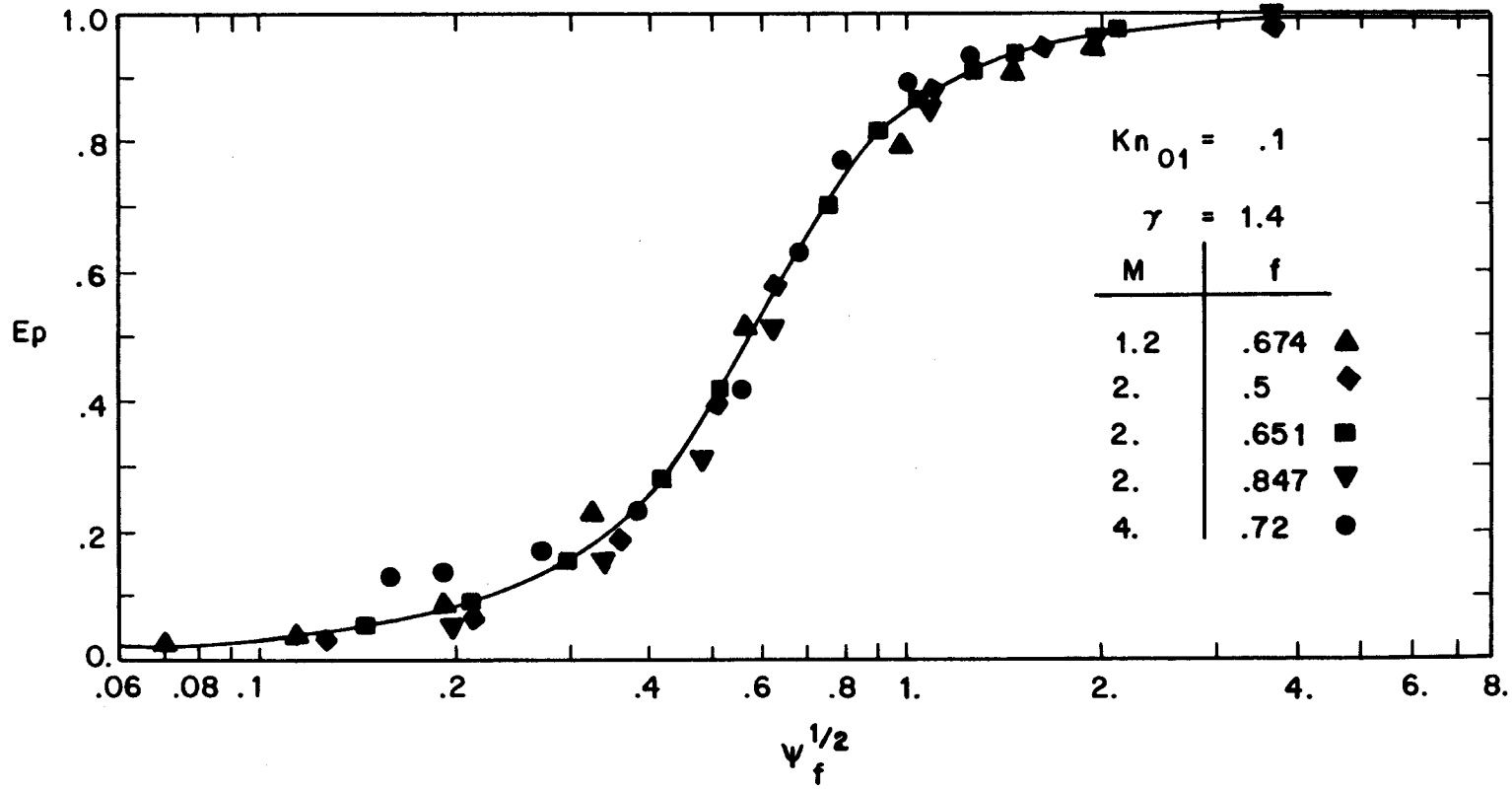

Figure 2. Reduced sampling probe collection efficiency versus the particle impaction parameter, Ψ_f.

by simultaneous sampling in a dust chamber using coal fly ash from a precipitator and found that blunt-edge probes produce significant errors and that sharp edged probes of various probe angles produce essentially equivalent results. Walter, however, as reported by Parker (15), observed that a thick walled tube, although ground to a knife-edge, produced distortion of the streamlines and gave low and erratic values for concentration when sampling in a dust-laden atmosphere. Dennis and Samples (18) investigated the flow characteristics of five different probe shapes and found results similar to Whiteley and Reed (17).

As part of their numerical investigation of sampling bias, Rader and Marple (24) considered thick-walled probes and found that: (1) even isokinetic sampling does not ensure a representative sample, (2) probe thickness plays a minor role for superisokinetic sampling (i.e. $U/U_o > 1$), and (3) for subisokinetic sampling, a thick-walled probe may actually provide a sampling efficiency that is closer to unity than a thin-walled probe.

Effect of Probe Alignment

It is necessary to align the probe in the direction of the incoming gas stream in order to obtain a representative sample of the particulate materials present. Misalignment of the probe causes selective withdrawal of

smaller particles without as many of the larger particles as are actually present; hence, an error in measurement. Work by the National Council for Air and Stream Improvement (29) as reported by Cooper and Rossano (30) recommends permitting a maximum error of plus or minus five degrees in probe alignment with the direction of the gas stream. The sampling probes in this study were properly aligned with the flow for all tests; in other words, the effect of probe alignment was not studied.

Effect of Nozzle Size

There is a suggested lower limit to the diameter of sampling nozzles used in particulate determinations for two reasons. First, systematic error is introduced by selectively excluding large particles because of inadequate cross-sectional area. Second, the volume of the source gas sampled per unit time decreases by the 1.5 power as the nozzle cross sectional area decreases, thus tending to magnify any random errors. The ASME (19) and Los Angeles County (20) recommend a minimum sampling nozzle of 6.3 mm diameter. Cooper and Rossano (30) note that Hemeon and Haines (16) found that for small size particles (5 to 25 micrometers) there was no significant difference between nozzle inlet diameters of 3.2, 6.3, and 9.5 mm. On the other hand, they (30) also report studies by Miller et al (31) in which consecutive samples

from a waste wood fired boiler were taken using 4.8, 6.3 and 9.5 mm diameter sampling nozzles; particulate concentrations measured when using the 4.8 mm diameter nozzle were substantially below that of the other two sizes.

Experimental Design Considerations

Free Jet Air Flow System

This project required a high speed air flow apparatus to accelerate the monodisperse test particles to the desired subsonic and supersonic Mach numbers without producing a significant slip velocity between the particles and the air. Ideally, the flow apparatus could not limit the system run time and, more importantly, could not produce any flow irregularities that would significantly alter the homogeneity and particle morphology of the generated aerosol. In addition, the flow system had to be supplied with relatively particle free, dry air to minimize interference by particles which might result from system contamination (i.e., oil etc.) or condensation of water vapor.

Early in the program it was decided that an open free jet was the easiest and most economical type of test section to construct that would hopefully meet the requirements outlined above. Also, an unbounded air jet would more closely simulate the flow condition at the discharge plane of an aircraft jet engine than would a two dimensional test section with solid walls. It was

also decided to build the free jet apparatus at the National Aeronautics and Space Administration Ames Research Center because they had a wind tunnel quality air supply that would not restrict expected experimental run times and, equally important, the expertise to oversee the design, assembly, calibration and safe operation of the required equipment.

The air supply system at Ames was known to be dry (i.e., <1 ppm water vapor); wind tunnels using the same air operate at up to Mach 3.5 without condensation problems. Also, the air supply was assumed quite free of particles greater than 0.1 micrometer diameter. This assumption is based on the experience of laser anemometry research where it is necessary to seed the air supply with 0.1 to 1.0 micrometer diameter particles to obtain a sufficient number of signals during velocity measurements. In any case, the background particle levels in the air supply were to be determined experimentally.

With regard to the effect of the test particles on the performance of the flow system, the following conditions were expected based on information contained in the literature (32) (33) (34) (35) (36) and personal communication (37) with Dr. S. L. Soo. First, the effect of the particles on the gas dynamics of nozzle flow would be negligible for the particle sizes, mass concentrations and temperatures involved in this project. In other

words, all the equations used to predict mass flows through the flow nozzles, exit Mach numbers, and free jet thermodynamic conditions would not need to be modified to account for the presence of particles. Furthermore, reference experimental data concerning the physical dimensions, velocity character, and turbulence levels of particle free unbounded jets were, for the most part, assumed as applicable for this study. In addition, the velocity lag (i.e., particle slip velocity) would be very small for nozzles of any substantial length. Also, it was not expected that particle deposition on the flow nozzle walls would be a serious problem. A uniform particle mass concentration distribution at the nozzle exit plane was not assumed and a sampling traverse was necessary to determine the particle mass concentration profile.

Another important general feature of the flow system is that it was, in all regards, axisymmetric. For example, the region upstream of the flow nozzles (i.e., settling chamber) was a cylinder and the test particles were introduced on a centerline in a manner which provided thorough mixing. The flow nozzles themselves were three dimensional designs which produced axisymmetric, parallel, uniform flow at the nozzle exit plane. Both of these matters are discussed in more detail in the next chapter.

When the experimental approach was formulated there was some concern about the interaction of expansion waves when a shock free supersonic stream of gas emerges from a nozzle into a free space and how this interaction might influence the experimental results. Upon further examination of the character of axisymmetric free jets it became evident that the best place to sample was in a region upstream of any expansion wave interaction; the so-called potential core of the jet. The potential core is a region near the nozzle exit in which the velocity is equal to the discharge velocity. It extends for a definite distance from the nozzle exit; on the order of one nozzle diameter downstream.

Figure 3 (38) shows, for the two dimensional case, the interaction of two expansion waves when a shock free supersonic stream of gas emerges from a duct into a free space. Table 2 (38) presents the various Mach numbers corresponding to the states of the gas in the jet shown in the figure.

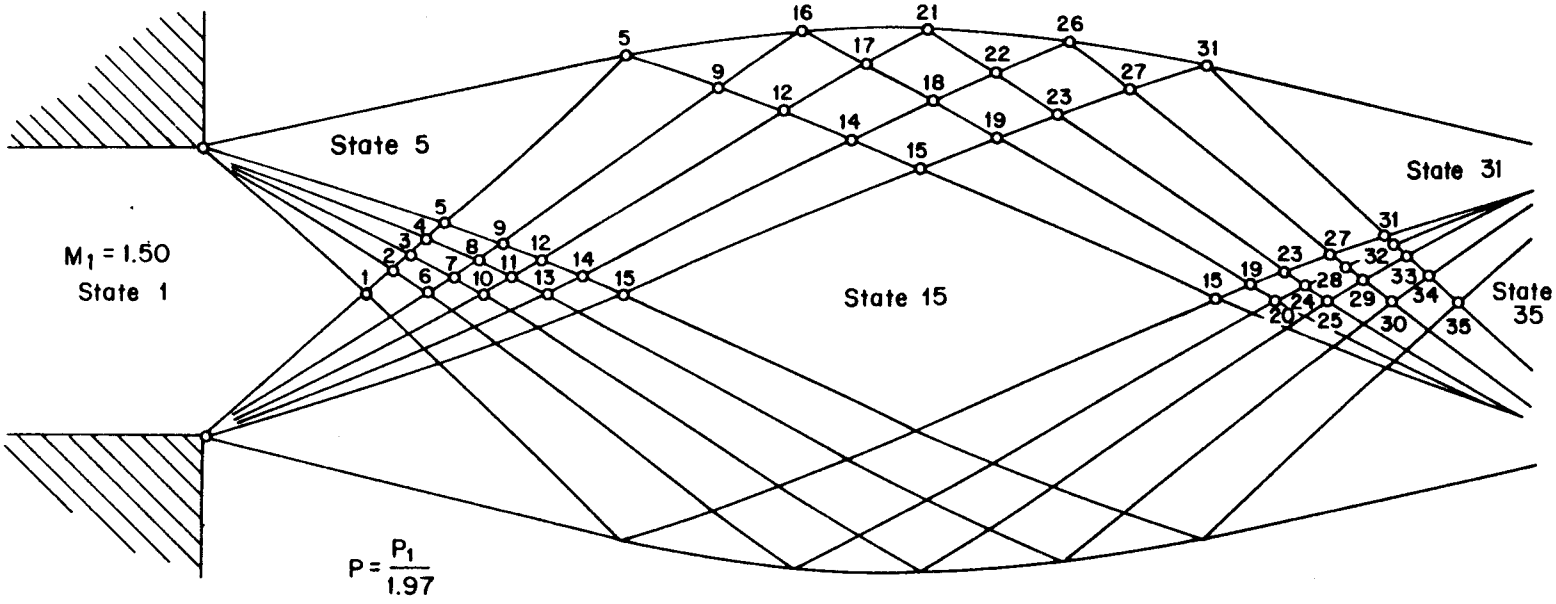

Figure 3. Expansion wave interaction in a two-dimensional supersonic gas jet.

Table 2. Mach numbers corresponding to the states of the gas in a supersonic free jet.

State	Mach No.	State	Mach No.	State	Mach No.	State	Mach No.
1	1.50	10	2.01	19	2.275	28	1.89
2	1.65	11	2.115	20	2.105	29	1.79
3	1.75	12	2.225	21	1.95	30	1.69
4	1.85	13	2.225	22	2.055	31	1.95
5	1.95	14	2.34	23	2.16	32	1.795
6	1.80	15	2.455	24	1.995	33	1.695
7	1.905	16	1.95	25	1.89	34	1.595
8	2.01	17	2.06	26	1.95	35	1.50
9	2.11	18	2.165	27	2.055		

Aerosol Sampling Systems

The aerosol sampling systems consisted of an aspirating probe to withdraw an aerosol sample, a filter membrane to collect aerosol particles, a prime mover (i.e., oiless rotary vane vacuum pump) to establish the desired sampling rate, and a calibrated orifice meter to measure the sampling rate.

During the supersonic sampling experiments the sampled aerosol would be decelerated to subsonic velocities. This would occur as a normal shock located either in front of the sampling probe (bow shock), at the probe inlet (attached shock), or within the sampling probe (swallowed shock). One of the objectives of this study was to determine the effect of shock front location on the representativeness of the sample. In order to study the conditions of an attached shock and a swallowed shock, the supersonic sampling probe had to be designed

with a supersonic inlet (i.e., supersonic diffuser). The program proposal suggested a tapered convergent probe inlet to allow subsonic diffusion to occur. However, further investigation revealed that internal supersonic deceleration in a converging passage is not easy to establish. In fact, design conditions cannot be achieved without momentarily overspeeding the inlet air or varying the probe geometry (39). This, clearly, is not a desirable feature for a particle sampling probe inlet. Fortunately, this starting problem can be avoided altogether by using a simple divergent inlet. In this case, with sufficiently low back pressure, it is possible to accelerate the internal flow within the divergent portion of the sampling probe before decelerating it in a shock (39). Figure 4 depicts the various possibilities for shock front location relative to a probe tip situated in supersonic flow (40).

During individual tests, generated aerosol was collected on Nuclepore filters; the filters were analyzed to determine the mass concentration and particle size distribution of the retained particles.

Nuclepore filters were chosen for use in this study because their performance as a fine particle collection media and in electron microscopic analysis has been well documented by Augustine (41). In comparing the polycarbonate plastic film Nuclepore filters with fiber

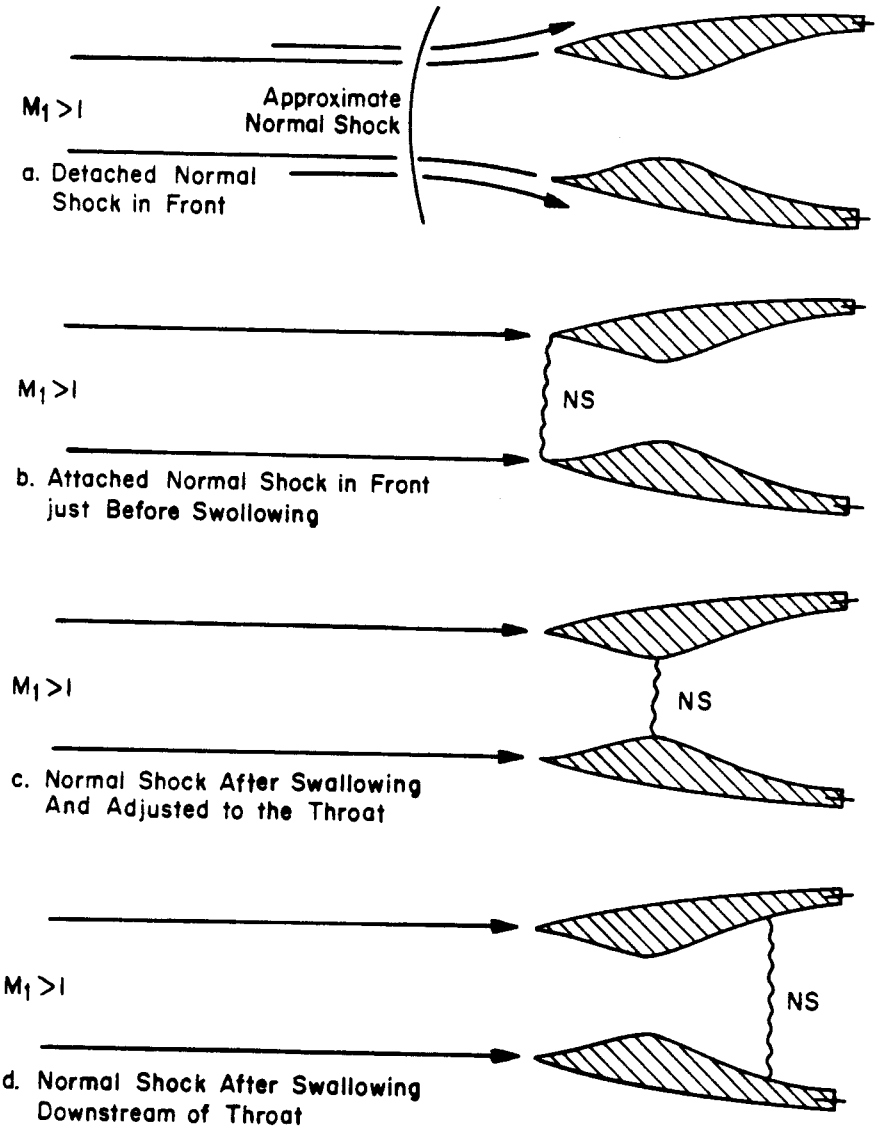

Figure 4. Four supersonic inlet flow configurations.

filters, Augustine (41) notes that the flow rate through Nuclepore filters is approximately four times that through a fiber filter of comparable pore size. Nuclepore filters also make an excellent substrate for electron microscopy and are fairly easy to prepare for microscopic examination. Nuclepore filters do have poorer particle retention characteristics than fiber filters but their efficiency is quantifiable, removing much of the disadvantage (41).

Based on Augustine's (41) analysis of Nuclepore filter collection efficiencies, filters with a nominal pore diameter of 0.4 μm would insure essentially a 100% sampling efficiency for the particle size examined in this work. The use of 142 mm diameter filters would allow filter face velocities to be maintained in the optimum collection efficiency range of between 20 and 40 cm/sec (42).

Aerosol Generation

This program required an aerosol generator that could produce large numbers of spherical, monodisperse, electrically neutral, particles. The particle size output of the generator had to be between 0.1 and 1.0 micrometer diameter and the generator had to be constructed to permit operation at pressures up to 50 psig and hydrostatic testing at 225 psig.

The aerosol generator selection was a major effort during the design phase of the program. The use of Dow polystyrene latex spheres was rejected mostly because the extreme hydrosol dilution required to achieve monodispersity would have resulted in a very low particle concentration. Several aerosol generation methods were rejected either because they were too new to be considered reliable (e.g. fluidized bed) or involved the construction of intricate and/or expensive equipment (e.g. transpiration cooled anode operated in a high intensity arc). Certain commercially available units were rejected because they were not constructed to discharge an aerosol at pressures much above atmospheric pressure.

After evaluating the literature, making a survey of commercially available equipment, and considering the recommendations of experts (43) (44) (45), it was decided to employ an aerosol generator whose operation was based

on successive evaporation and recondensation of the aerosol material. Credit for the development of this type of generator is generally given to Sinclair and LaMer (46) and/or Rapaport and Weinstock (47), subsequently several authors have described slightly modified and improved versions of the original design (48) (49) (50) (51) (52). In this program the aerosol generator is referred to as a LaMer type generator.

The LaMer generator produces monodisperse liquid droplets or solid particles by controlled condensation of vapor upon nuclei. In the earliest versions a liquid was evaporated and condensation nuclei were produced separately and added to the vapor. In recently used versions a liquid containing a nucleating agent is atomized and passed through an electric heating zone where the polydisperse droplets evaporate. Since the liquid is intentionally not perfectly pure, a small residue remains which later serves as condensation nuclei. As soon as the vapor becomes supersaturated in the condensation zone, an equal amount of liquid is formed around all nuclei thus yielding droplets of equal size. The volume of the droplet is approximately proportional to the ratio of the amount of liquid per cubic centimeter to the number of condensation nuclei per cubic centimeter. This ratio can be varied by changing the size distribution of the initial aerosol (52).

In this study, anthracene was used as the nucleating agent. The use of anthracene for this purpose was initially suggested by Preining (51) and, more recently, has been used by Tomaides et al. (49) to improve the performance of LaMer type generators. Anthracene was used because it has a considerably higher melting point (217C) than the corresponding aerosol material (e.g. stearic acid, m.p. = 69C). Therefore, it provided a source of stable nuclei on which the vaporized aerosol material could condense when cooled.

In theory, as described above, the ultimate particle size produced by the LaMer generator depends on the amount of vapor available for condensation relative to the number of condensation nuclei. In practice, Tomaides et al. (49) report no significant difference in the quality of dioctyl phthalate (DOP) or di-2-ethylhexyl phthalate (DEP) aerosols when the anthracene concentration was changed between 0.1 and 1 gm/l. Thus, experimentally, a convenient method to alter the vapor/nuclei ratio is to change the size distribution of the initial aerosol. A common method for doing this is to dilute the liquid in the atomizer with an easily evaporated solvent (e.g. alcohol). This was not desirable in this program because the solvent might have condensed in the supersonic test section.

Tomaides et al. (49) reports that aerosols produced by condensation generators can be electrically charged. This is undesirable because a significant electrical charge on the particles greatly influences aerosol behavior. Charge can affect the penetration of an aerosol through a filter, its deposition on surfaces, the efficiency of a sampler, and the concentration profile of an aerosol passing through a duct or nozzle. Since the behavior of electrically charged particles was not of interest in this study, it was decided to include an aerosol charge neutralizer as part of the aerosol generating system. The neutralizer brings the charged aerosol to a Boltzmann charge equilibrium by mixing the aerosol with bipolar ions. The bipolar ions (i.e. a mixture of positive and negative small ions) are conveniently generated in the gas phase of the aerosol by ionizing radiation from radioactive materials.

The interest in an analytical method specific for trace amounts of stearic acid materialized because of the requirement to determine the amount of stearic acid collected on the Nuclepore filters and deposited on the sampling probe and filter housing walls during a test. A simple gravimetric analysis alone was ruled out because of the small amount of expected sample (i.e., on the order of micrograms).

After a rather broad based literature search for quantitative analysis methods for trace amounts of non-volatile organic acids, it was discovered that a gas chromatographic technique was routinely used by personnel in the Agricultural Chemistry Department at Oregon State University. Basically, the method involves getting the stearic acid into solution by washing, for example, the Nuclepore filters or sampling probes with a suitable solvent, quantitatively converting the stearic acid to its methylester, and analyzing the resulting solution using a gas chromatograph equipped with an ethylene glycol succinate column and a flame ionization detector. The method would easily accommodate washings that contained as little as 0.1 microgram of stearic acid. This is discussed more thoroughly in the next chapter and in Appendix D.

Particle Deposition

So far the problem of particle deposition in the sampling train has not been addressed. This possibility did not significantly affect the determination of the mass concentration of the aerosol because the deposit could be recovered and added to the main part of the dispersed phase. Generally, particle deposition in the sampling train could cause serious errors in determining particle size when the sampled aerosol has a polydisperse

particle size distribution and the particle deposition mechanism(s) are size selective. In this work, however, this difficulty was avoided because the aerosol was nearly monodisperse.

It did not appear apriori that particle deposition would seriously affect sampling effectiveness in the present case. First, any deposition due to electrostatic charge would be minimized because the generated aerosol would initially be brought to a state of neutral charge distribution and the use of plastic construction materials was avoided. Diffusional deposition of particles on the walls of the sampling probe would be negligible because, as calculated by Fuchs (22), this effect is only significant for particles of nearly molecular size.

Because the flow in the sampling system would be strongly turbulent, inertial particle deposition on the probe tip and sampling line walls could be significant. Fuchs and Sutugin (53) for example, note that considerable deposition occurs in conical sampling probes even in the case of highly dispersed aerosols. Sehmel (54), however, reports less than 1% deposition of particles with diameters less than 3 micrometers in conical nozzles used to sample gas flows isokinetically at velocities up to 45 ft/sec. Sehmel (55) also has shown that for fully developed turbulent flow in straight tubing, 10 feet

long, with diameters ranging from 0.6 to 1.15 inches and flow rates up to 12 and 40 cfm respectively, that particle deposition for 1 μm particles is generally less than 0.1 percent.

Recently, Ivie et. al. (56) experimentally considered internal wall deposition characteristics of several different supersonic particle probes. Using test particles with diameters of 1.0, 1.5, 2.0, and 2.5 μm, the average losses were 14-22%. In general, deposition increased with increasing particle size.

EXPERIMENTAL PROGRAM

Objective and Technical Approach

The basic objective was to examine the use of small bore aspirating probes for representative sampling of submicrometer particles suspended in near sonic and supersonic air flows. The experiments were designed to independently evaluate the importance of three factors which may likely effect the representativeness of the sample with regard to particle size and mass concentration. First, the effect of varying the ratio of probe wall to bore area normal to the flow was studied in near sonic free jets (i.e., probe wall effects). Next, the effect of subisokinetic sampling in near sonic flows was investigated. Finally, the effect of subisokinetic sampling in supersonic flows was determined.

The experimental approach to this study was simple in concept; submicrometer particles (d_p = 0.8 μm, σ_g = 1.28) were injected into an air stream and accelerated to the desired velocity (Mach 0.6, 0.8, 1.26 or 1.47) through a sonic or supersonic nozzle. Experimental probes were used to sample aerosol particles at the free jet exit while a conventional isokinetic sampling probe upstream of the nozzle was used to withdraw a sample assumed to accurately represent the true aerosol concen-

tration. Differences between the two observations reflected errors due to conditions at the free jet sampling probe inlet. Figures 5-8 illustrate the experimental equipment.

Free Jet Air Flow System

Clean, dry, oil-free air at a nominal pressure of 10.5 atm was delivered to the experimental system. Constant air flow was maintained by manually controlling the static pressure in the settling chamber. Downstream of the aerosol generator inlet line the diluted aerosol was passed through a wide angle diffuser and three 40 mesh screens to spread the flow and reduce turbulence. The aerosol then traveled approximately 0.76 m before being sampled by the settling chamber sampler and accelerated through the appropriate 5.08 cm exit diameter flow nozzle. The aerosol was exhausted as a free jet into still room air. The experimental sampling probe inlets were placed 1.3 cm from the nozzle exit, well within the "potential core" where the jet velocity is equal to nozzle exit velocity. The location of the sampling probes in the "potential core" was confirmed by 14 point X-Y velocity traverses of the free jet at each Mach number. The jet velocities, also measured at 1.3 cm from the nozzle exit, were for all traverse points within two percent of the maximum jet velocity.

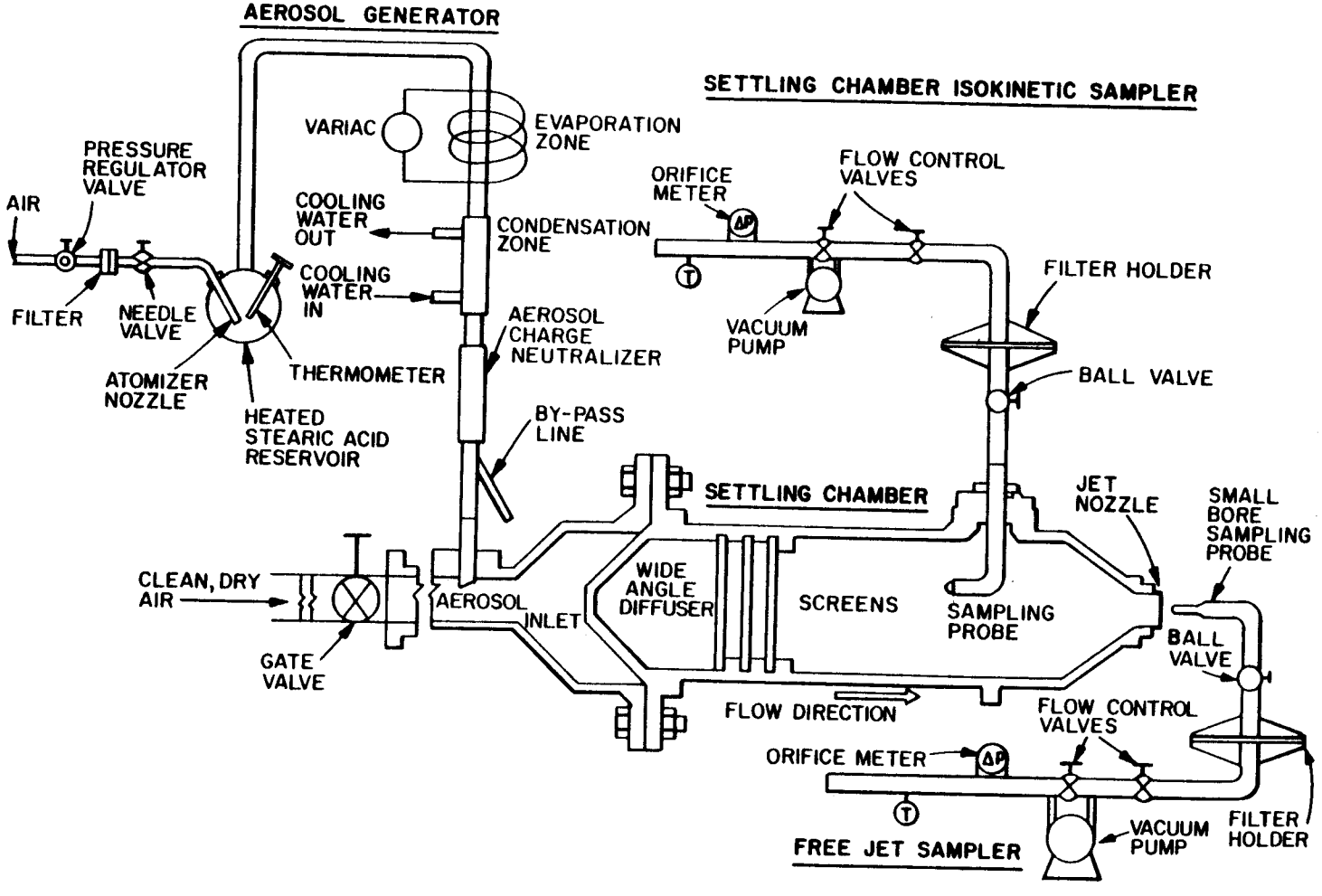

Figure 5. Experimental equipment schematic drawing.

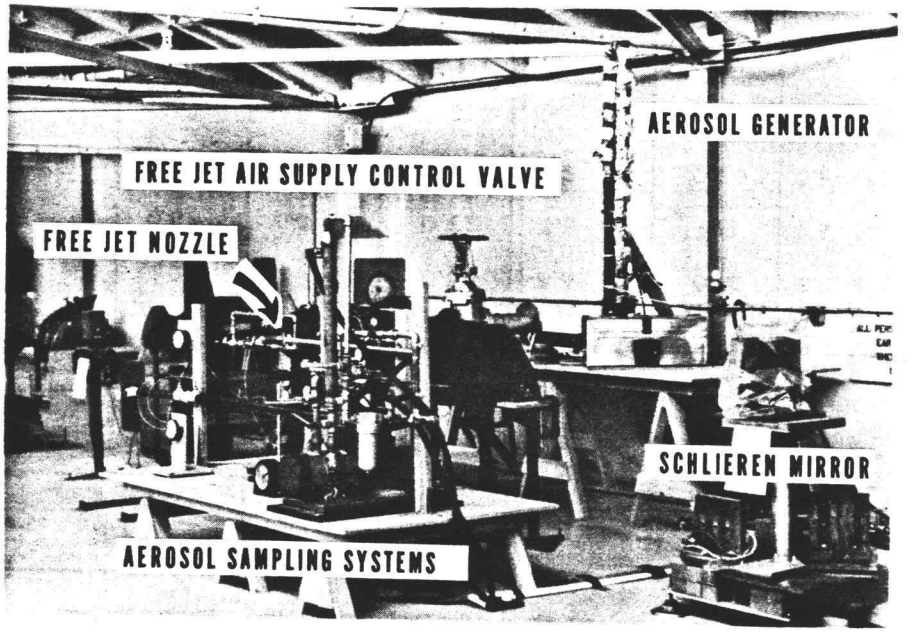

Figure 6. Overall view of experimental equipment.

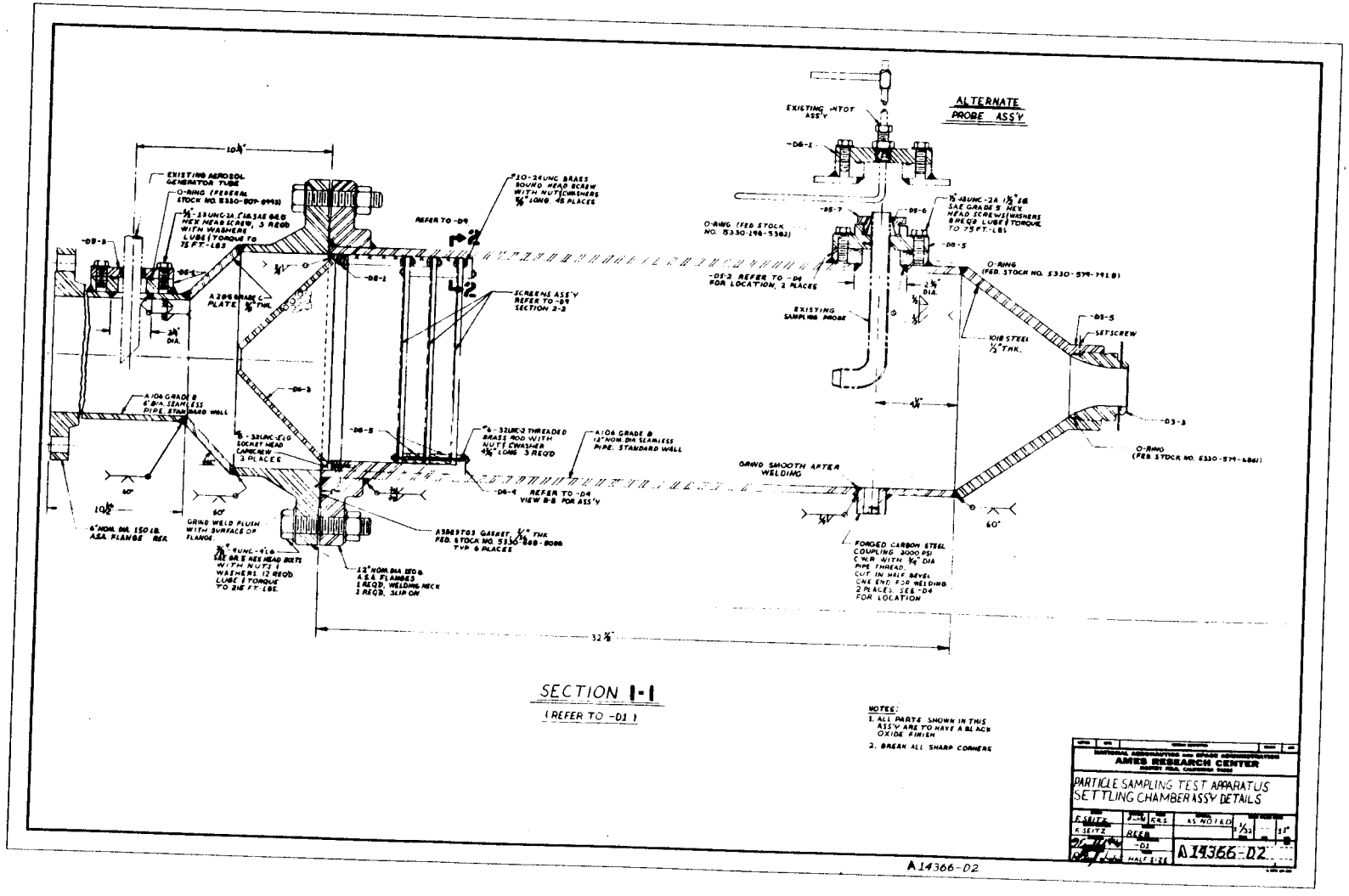

Figure 7. Free jet air flow system.

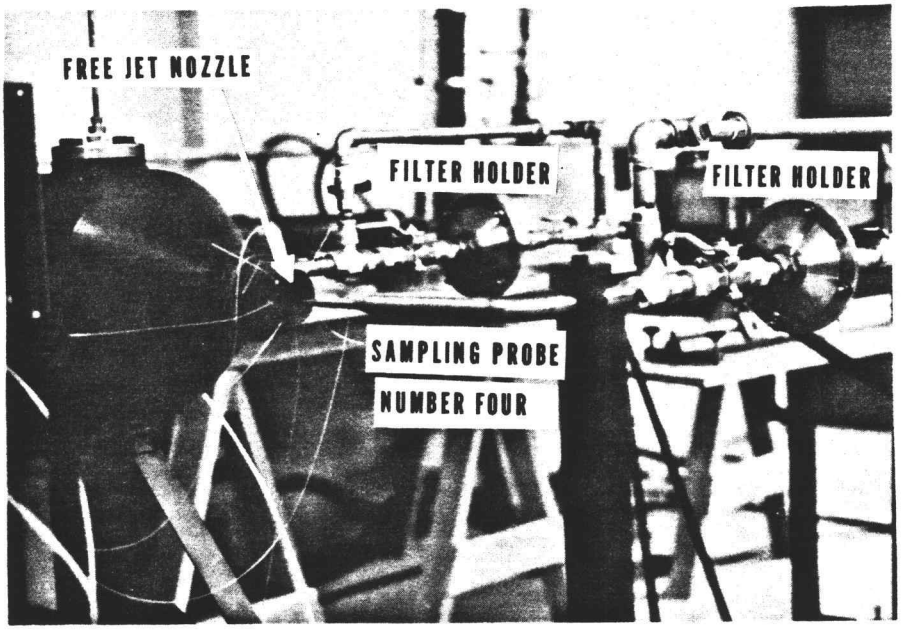

Figure 8. Sampling probe number four in the free jet.

One subsonic and two supersonic axisymmetric flow nozzles were designed and fabricated for this study. The subsonic nozzle design was a standard ASME long-radius, low-ratio type (57) while the supersonic nozzle contours were generated by the computerized version of a design method due to Sims (58). The subsonic nozzle was used to achieve exit Mach numbers of 0.6 and 0.8 while the properly expanded supersonic nozzles proved to produce exit Mach numbers of 1.26 and 1.47. The free jet air flow system and flow nozzle design and performance are discussed more fully in Appendix A.

Aerosol Generation

The aerosol generator shown in Figure 9, was a high-volume (30-45 l/min) condensation unit. Stearic acid was chosen as the aerosol material because it results in nearly spherical particles. One tenth weight percent anthracene was added to provide a stable source of condensation nuclei.

An aerosol charge neutralizer containing a 10 mCi ^{106}Ru - ^{106}Rh beta radiation source was used to bring the aerosol to an equilibrium Boltzmann charge distribution. The neutralizer design was based on guidelines presented by Cooper and Reist (59).

Particles were collected on 142 mm diameter, 0.4 μm pore size, polycarbonate membrane filters (i.e. Nuclepore

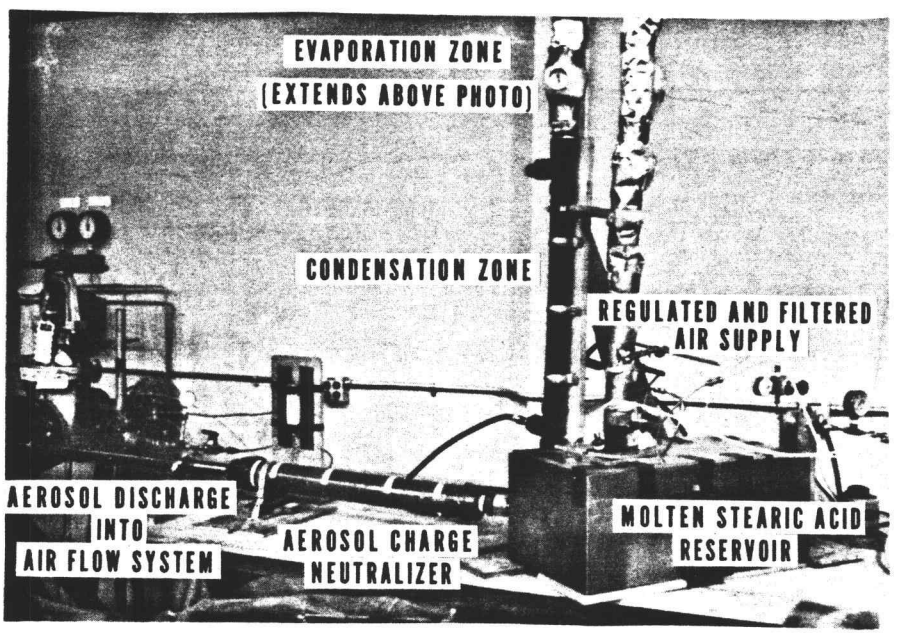

Figure 9. High volume condensation aerosol generator.

filters). To size particles, a small piece of the filter membrane was mounted on a cylindrical brass stud which could be staged directly into a JSM-U3 scanning electron microscope (SEM). The size of the particles was determined by direct counting of the particle images on the micrographs. A minimum of 100 particles was counted for each sample sizing. Figure 10 is a typical SEM micrograph.

The average of 22 particle size samples taken in the free jet and the settling chamber gave a geometric mean particle diameter of 0.8 μm (std. dev. 0.06) and a geometric standard deviation, σ_g of 1.28 (std. dev. 0.04). The output of the condensation aerosol generator was on the order of 10^6 particles/cm^3.

Aerosol generator design and performance are discussed more thoroughly in Appendix A. Particle size data are more fully treated in Appendix G.

Aerosol Sampling Systems

Both the free jet and settling chamber samplers employed front facing aspirating probes, polycarbonate membrane filters, oiless rotary vane vacuum pumps, and calibrated orifice meters. The membrane filters were held in specially constructed, double o-ring sealed, stainless steel filter holders. Orifice meter calibration over a range from 0.014 to 0.85 standard m^3/min was accomplished

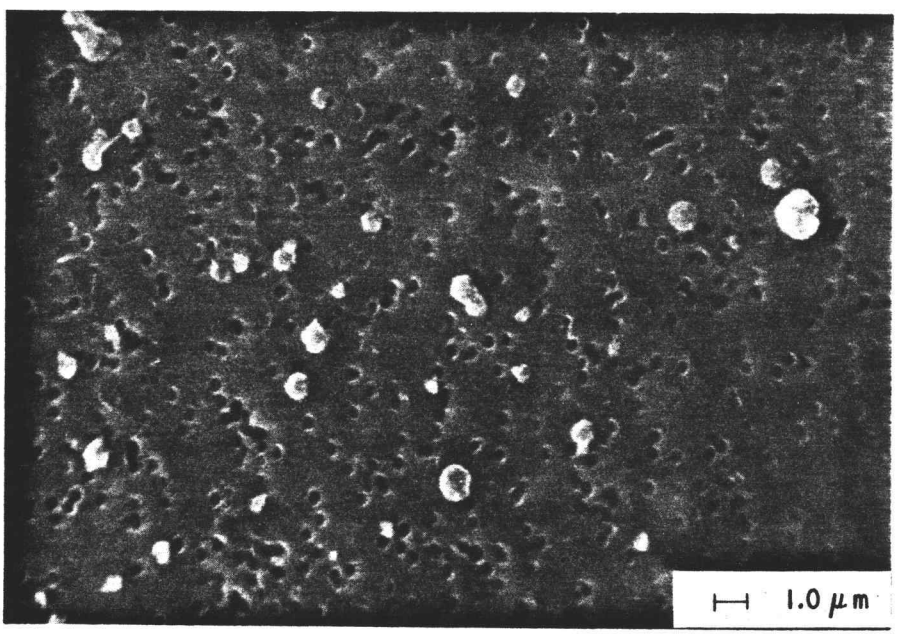

Figure 10. Scanning electron micrograph of stearic acid particles.

by a method (60) involving the use of a saran bag with a known volume. Figure 11 is a generalized schematic of the sampling systems.

The probe used to sample isokinetically in the settling chamber had a large bore (19.1 mm) and a low cone angle (4^{o}) to insure representative sampling. The required isokinetic sampling rates were determined from velocity data obtained during 22 point X-Y pitot tube traverses of the settling chamber. The settling chamber sampling probe was accurately located and held at the site of velocity measurements using a scale on the sampling probe and a lockable insert fitting on the settling chamber. Velocity profiles in the settling chamber were very flat at all test conditions. All velocities, except within 2.54 cm of the settling chamber wall, were within 16% of the maximum velocity. The average velocity in the settling chamber ranged from 5.4 m/sec at Mach 1.47 to 6.3 m/sec at Mach 0.8.

Four sampling probes, shown in Figure 12, each with a different inlet wall to bore area ratio (Table 3) were used in the free jet sampling system. All the probes were used to evaluate probe wall thickness effects when sampling isokinetically in a Mach 0.8 free jet; however, only the knife edged probe (number 4) was used in the anisokinetic studies at all Mach numbers.

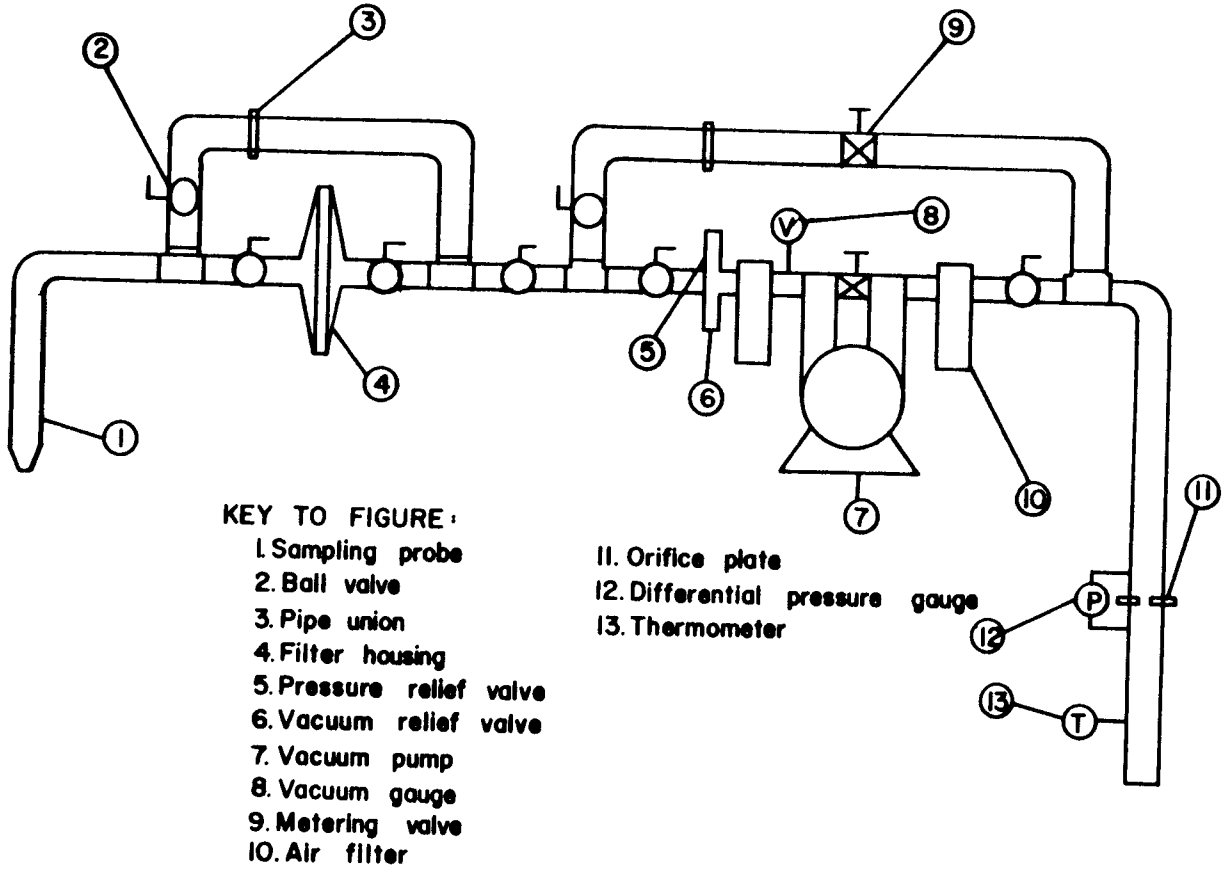

Figure 11. General arrangement of the free jet and settling chamber particle samplers.

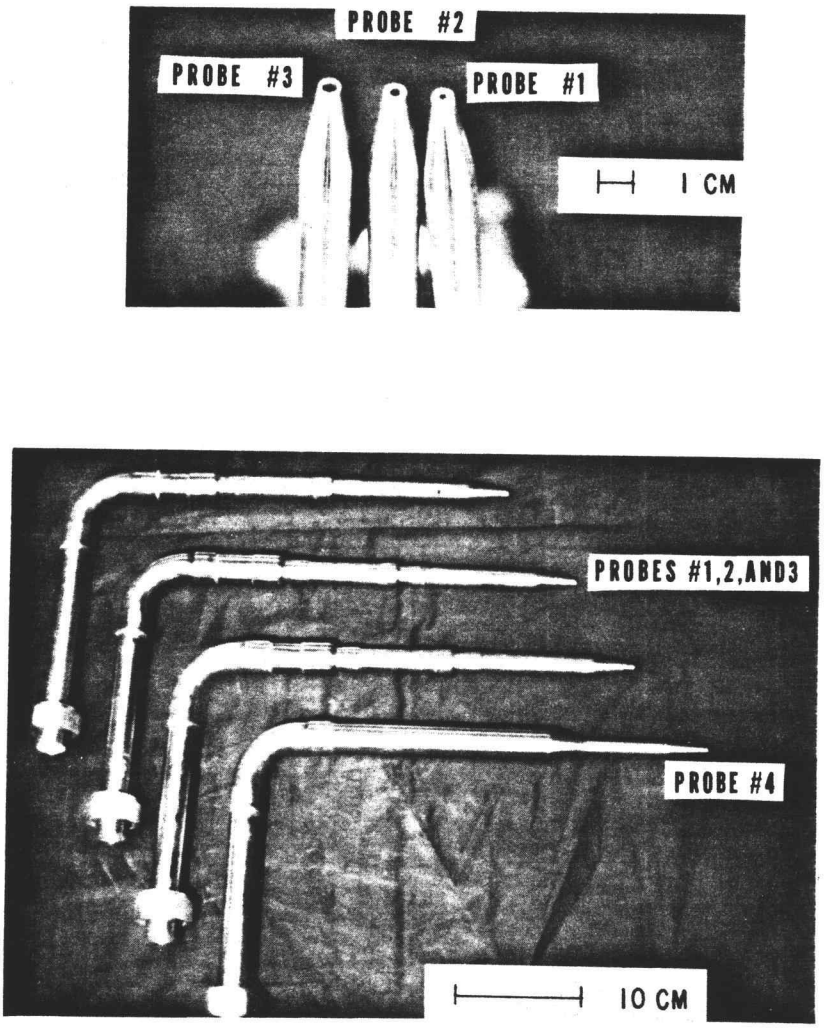

Figure 12. Small bore sampling probes for free jet.

Table 3. Aerosol concentration in a Mach 0.8 free jet determined by different sampling probes.

Probe number	Outside diameter of probe inlet, D (mm)	Inside diameter of probe inlet, D_p (mm)	Wall to bore area ratio A_w/A_b	Aerosol concentration, C (mg/m^3) Mean	Std. dev.
1	6.05	2.77	3.77	9.3(3)*	1.23
2	6.12	3.96	1.39	8.4(4)	0.67
3	6.17	5.16	0.436	9.3(4)	0.63
4	5.08	4.50	0.277	8.0(4)	0.44

*( ) number of observations

Probe number 4, shown in Figure 13, was designed by Aerotherm Acurex Corp., Mountain View, CA as a divergent supersonic inlet. For low supersonic Mach numbers, the divergent inlet portion, with sufficiently low back pressure, accelerates the flow to the vicinity of Mach 2. The flow is decelerated in a shock pattern within a constant area cross section immediately downstream of the divergent inlet. The constant area cross section is also intended to enhance the pressure recovery characteristics of the probe. The supersonic inlet portion of the sampling nozzle has an intentional surface roughness to reduce the tendency of the shock to move once it is swallowed by the probe. Figure 14 is a set of shadowgraphs showing probe number 4 submerged in a Mach 1.47 free jet with no probe flow, at $U/U'_o = 0.5$, and at $U/U_o = 1.0$ (shock swallowed). To obtain the shadowgraphs, a parallel beam of light produced by a point source and converging mirror was passed through the working section of the nozzle exit. Shock waves then appeared on a screen/camera as dark and light bands corresponding to the sudden increase and decrease in density gradient across the shock.

The aerosol sampling system design is treated more completely in Appendix A. The free jet air flow system baseline data is presented more completely in Appendix B.

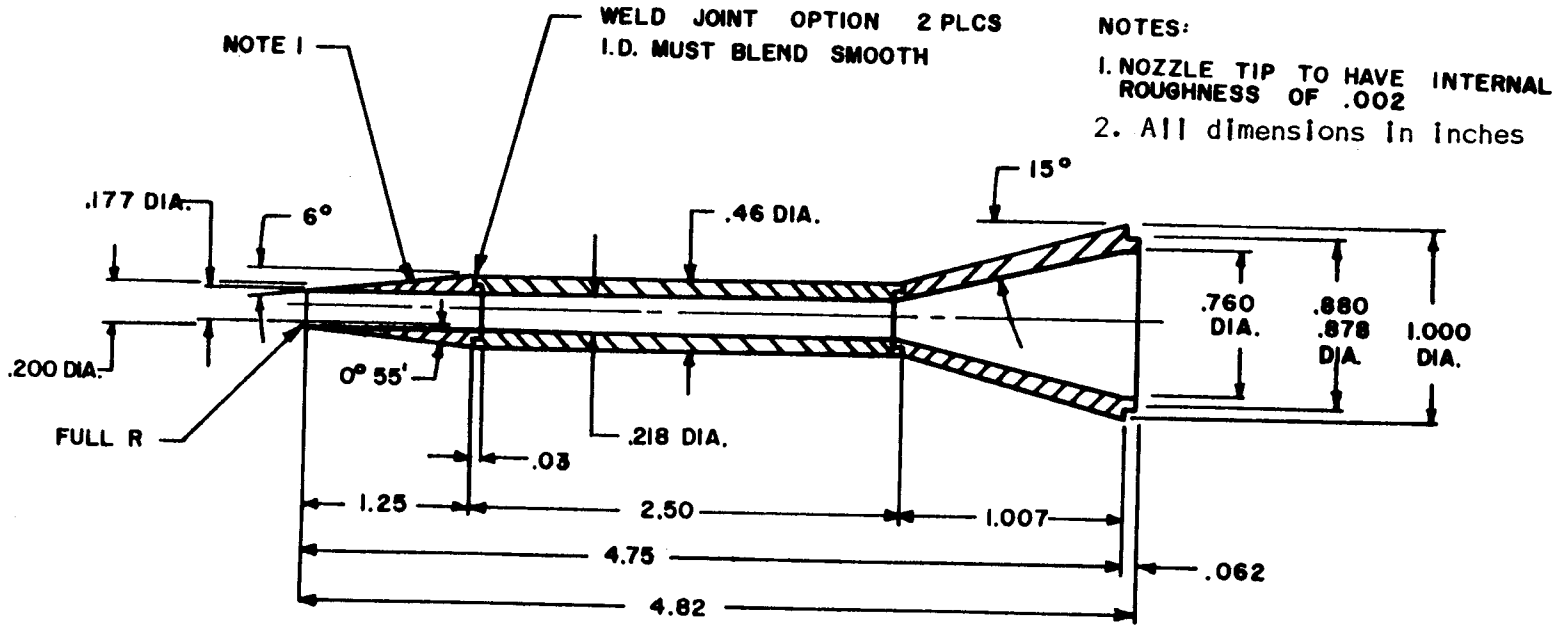

Figure 13. Supersonic inlet for sampling probe number four.

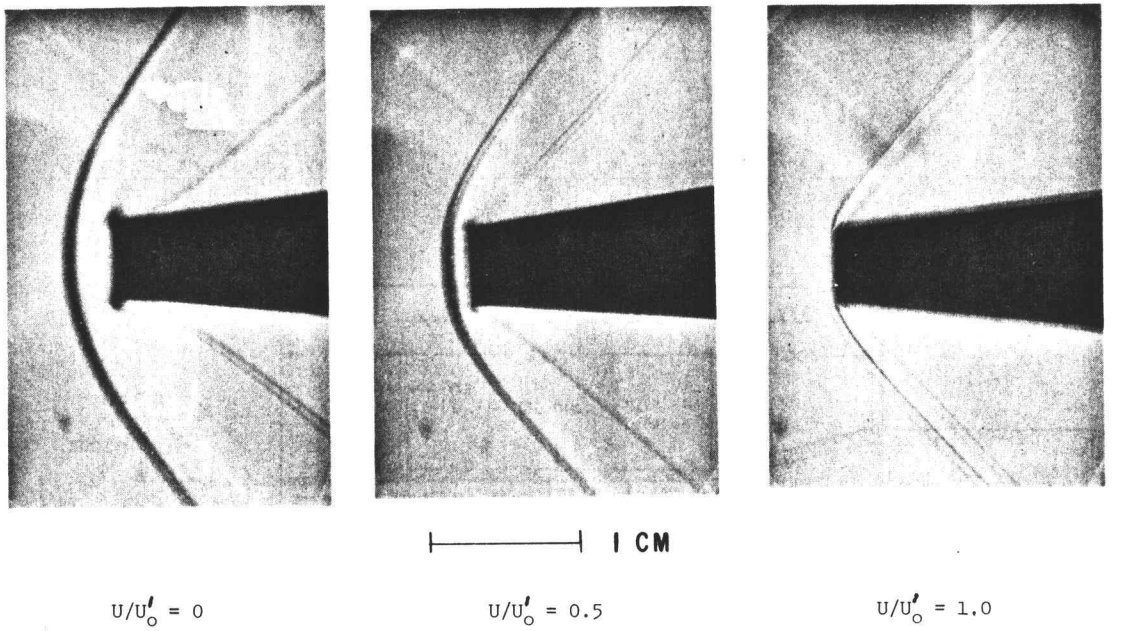

Figure 14. Shadowgraphs of probe number four in a Mach 1.47 free jet.

Determination of Stearic Acid Mass

In the free jet and settling chamber sampling systems, stearic acid particles were collected on polycarbonate membrane filters. The mass of stearic acid collected on a particular filter was determined by gravimetric and gas chromatographic techniques. The gravimetric determinations were used to make rapid, approximate computations and therefore no extraordinary precautions were used to insure their accuracy. It was found that sample handling and weight reproducibility were greatly enhanced by exposing the filter to a small alpha radiation source to eliminate static charges on the filter just before a weighing. The range of sample weight gains, excluding blanks, was from 0.75 to 16 mg.

The gas chromatographic method involved washing the filters with diethylether and converting the dissolved stearic acid to its methylester before separation in a gas chromatograph equipped with a flame ionization detector. Sampling probe deposits were determined similarly after washing the probes with pesticide grade acetone and careful evaporation of the acetone. In both filter and probe wash analyses an amount of non-interfering organic acid (heptadecanoic acid) was added as an internal standard.

All chromatographic analyses were performed by Stoner Laboratories, Inc., Santa Clara, California. A

method verification study showed that, within the experimental range, essentially 100 percent stearic acid recovery from the Nuclepore filters could be expected even after a storage time as long as a week (See Appendix D).

A paired t statistical comparison of 223 gas chromatographic and corresponding gravimetric results indicated no significant difference (see Appendix E). However, only the chromatographic results were used in the final computations.

Procedures

System Operation

Obtaining experimental data involved phased operation of the aerosol generator, the free jet system, and both particle sampling systems. First, the aerosol generator was permitted to thermally equilibrate using dry, filtered purge air. Then, with clean wind tunnel air in the free jet system, flow control valves in both particle samplers were adjusted to achieve the proper sampling rate; the vacuum pumps were used only if required. Following a momentary shut down, aerosol was permitted to enter the settling chamber and the chamber was brought to proper stagnation pressure. After operating for about one minute, the particle samplers with pre-set sampling rates were activated for a five minute sampling period. When a sample was taken for particle size analysis the sampling time was ten to fifteen seconds; however, the sampling was performed at the midpoint of a usual five minute run.

After collection, the samples to be used for particle sizing were prepared for SEM examination while the preweighed filters to be used for particle mass concentration calculations were placed in glass petri dishes until they could be reweighed and subjected to gas chromatographic analysis. Probe washings awaiting gas

chromatographic examination were stored in glass sample bottles fitted with teflon lined screw caps.

Aerosol Concentration Profiles

Table 4 summarizes the concentration profile results at Mach 0.6, 0.8 and 1.26 for both the free jet and settling chamber. The mean and standard deviation of the concentrations measured on the centerline were comparable with the mean and standard deviation of all the data points obtained during a traverse. For this reason it was assumed that average concentration in either the settling chamber or free jet could be adequately determined by samples taken on the center line. Table 4 also shows that the mean deviation between the settling chamber and free jet concentrations was 11%. This good agreement allowed settling chamber samples to be used as the reference aerosol concentration (C_o) during the probe wall effects and anisokinetic sampling studies. Complete aerosol concentration profile data is given in Appendix F.

Blanks

During the course of the experiments many blank filter samples were submitted for analysis. Ten Nuclepore filters carried through sample handling procedures, but not used in either sampling system, gave an average result of +0.07 mg. This amount was considered negligible since in 95% of the samples the correction would be less than 2.0% of the filter weight gain; in the

Table 4. Summary of aerosol concentration profiles.

	Settling chamber concentration (mg/m^3)				Free jet concentration (mg/m^3)			
	All traverse points		Centerline samples		All traverse points		Centerline samples	
Mach no.	Mean	Std. dev.	Mean	Std. dev.	Mean	Std. dev.	Mean	Std. dev.
0.6	8.23(13)*	1.00	7.9(5)	0.54	8.5(13)	0.70	8.7(5)	0.88
0.8	6.7(19)	0.82	6.8(9)	0.62	7.6(19)	1.11	7.6(9)	1.02
1.26	2.9(11)	0.34	2.7(3)	0.28	3.2(11)	0.20	3.1(3)	0.07
1.47	-	-	1.7(3)	0.11	-	-	2.0(3)	0.09

Footnote a: ( ) Number of samples used to determine mean value.

worst case, the possible error was less than 9%. Twenty-two filter samples were obtained in the settling chamber and in the free jet without the aerosol generator operating. These indicated whether particle re-entrainment from the settling chamber wall, screens, or wide angle diffuser was significant. The analysis showed that particle re-entrainment would account for at most a 0.5% error in the computed reference aerosol concentration, C_o. Complete blank sample data is given in Appendix H.

Probe Washes

Although the free jet and settling chamber sampling probes were washed with acetone between sampling periods, not every probe wash was retained for analysis. Average probe wash values were used with the filter weight gain to compute the total sample weight gain. Twenty-six settling chamber probe washes indicated that the average probe deposit was 2% of the amount deposited on the filter (std. dev. 1%); 46 free jet sampling probe washes gave an average probe deposit that was 12% of the filter weight gain (std. dev. 5%). Complete probe wash data is given in Appendix H.

Other Data

During the course of experimentation certain other data were also accumulated. For example, the initial supersonic sampling tests made extensive use of a sha-

dowgraph system to determine the location of the shock relative to the free jet sampling probe as a function of sampling rate. Velocity determinations within the settling chamber were made with a standard pitot tube connected to a 0.-0.25in H_20 Magnehelic differential pressure gage. The Mach number at the nozzle exit was determined from tabulated isentropic flow relations after measuring the static pressure drop across the nozzle, P_{exit}/P_t. The stagnation pressure, P_t, in the settling chamber was measured with a calibrated large dial Wallace and Tiernan gage capable of measurements to the nearest tenth of a psi. Each of the flow nozzles was fitted with four pressure taps to determine true static pressure at the nozzle exit, P_{exit}.

The orifice plates used to measure flow rates in both particle sampling systems were calibrated using a method involving a saran bag with a known volume (60). During calibration, Magnehelic differential pressure gages were used to determine the pressure drop across the orifice; the identical gages were used during actual tests.

Appendices A-D contain additional details on the equipment and methodology including: supersonic free jet nozzle design, orifice meter calibration, aerosol generation and charge neutralization, supersonic sampling probe design, and stearic acid chromatographic analysis.

Experimental Scenario

A general sequence of the data collected is presented below. Many items were preliminary experiments necessary for system evaluation and calibration. The experiments of primary interest, marked with an asterisk (*).

General Experimental Sequence

A. Using the subsonic flow nozzle, determine exit Mach number as a function of settling chamber stagnation pressure. For supersonic nozzles, determine exit Mach number at the critical pressure ratio of the nozzle.

B. Using a standard pitot tube, make velocity traverses in the settling chamber for each desired exit Mach number.

C. Using velocity data from item B, determine that the settling chamber sampler can sample isokinetically.

D. Using the subsonic flow nozzle, determine that the free jet sampler can isokinetically sample near sonic free jets. Also, determine the range

of sampling velocities attainable with each of the four sampling probes when used in the near sonic free jets.

E. Using a shadowgraph, determine shock front location relative to sampling probe number 4 as a function of sampling rate for each supersonic nozzle.

F. Sample background particles in settling chamber and in free jet to determine any interference with stearic acid analysis methods.

G. Operate aerosol generator and introduce stearic acid particles into settling chamber, then collect particles on center line of settling chamber for the determination of particle size and mass concentration. Make replicate runs to determine the reproducibility of the aerosol generator. Make traverses of the settling chamber to determine the particle concentration profile.

H. Periodically and at the end of procedure G, run blanks in the settling chamber and free jet

sampling systems to determine if background stearic acid levels become significant; inspect screens and walls in settling chamber for evidence of particle deposition.

I. Based on settling chamber stearic acid concentration profiles, select a single sampling location which best represents an average concentration.

J. Using probe number 4, sample isokinetically at the free jet exit plane to determine stearic acid concentration profiles in near sonic free jets. Choose one location to represent an average free jet stearic acid concentration.

*K. Using all four jet sampling probes to sample isokinetically at Mach 0.8, determine probe wall effects.

*L. Select the probe with minimum wall effect and use it to take extensive data on subisokinetic sampling at Mach 0.6 and 0.8.

*M. Determine stearic acid concentration profiles in supersonic jets with the probe number 4 operated so that the shock is swallowed by the probe. Establish a sampling location to represent the average concentration of stearic acid in the supersonic free jets.

*N. Using probe number 4, study subisokinetic effects in Mach 1.26 and 1.47 free jets.

RESULTS

Probe Wall Effects

Four sampling probes with wall to bore area ratios ranging from 0.28 to 3.8 were used to isokinetically sample stearic acid aerosol on the center line of a Mach 0.8 free jet. The intention was to demonstrate sampling errors due to the probe inlet wall thickness. Replicate samples were taken with each probe; the results are presented in Table 3. Using the 15 data points, no linear correlation (correlation coefficient, $r = 0.35$) could be obtained between the sampling probe wall to bore area ratio, A_w/A_b, and the relative percent error $[(C - C_o)/C_o)] \times 100$.

This finding is in good agreement with the numerical calculations of Rader and Marple (24). They found that for Stokes numbers approaching 0.1 and sampling velocity ratios of 1.0, the aspiration coefficient, A, is 1; even for probe diameter ratios, D/D_p, up to 2.5. In this work, D/D_p, ranged from 1.1 (probe number 4) to 2.2 (probe number 1) and the Stokes number ranged from 0.1 to 0.14 (Table 5). For larger Stokes numbers or velocity ratios much greater or less than 1, Rader and Marple (24) predict significant effects on A.

Table 5. Experimental conditions used by various authors to develop subisokinetic correlation equations.

Author	Particle sizes (μm)	Aerosol Material	Stokes Number Range	U/U_o Range	U_o Range (m/sec)
Present work	0.8	stearic acid	0.10-0.14	0.1-1.0	199-422
Davies[1]	3 to 25	zinc sulfide	0.01-2.5	0.008-0.8	1.2-13.4
Belyaev-Levin	17 and 24	pollen and spores	0.18-2.03	0.18-6.0	2.0-7.9
Zenker	7 to 73	glass beads limestone dust	0.06-14	0.4-2.5	3.0-35.0
Badzioch	19 to 27	silica and zinc	0.5-0.95	0.22-5.0	7.6-24.1
Watson	4 and 32	spores	0.02-3.2	0.44-2.3	4.5

1 Davies analysis based on experimental data obtained by Sehmel (54).

Anisokinetic Studies

Sampling probe number 4 was used to sample at less than isokinetic conditions ($U/U_o<1.0$) on the center line of free jets having Mach numbers of 0.6, 0.8, 1.26 and 1.47. The average result of isokinetic samples taken simultaneously in the settling chamber was used as the reference concentration, C_o. Figure 15 shows the experimentally determined relative percent sampling errors, $[(C - C_o)/C_o] \times 100$ as a function of the percent of the isokinetic sampling velocity $[(U/U_o) \times 100]$ for each Mach number. A nonlinear regression analysis of the data gave:

$$C/C_o = 0.69 + 0.31\ (U_o/U) \pm 12\% \qquad (8)$$

Equation 8, shown graphically in Figure 15, predicts relative sampling errors greater than 124% for $U/U_o < 0.2$.

For the supersonic cases the percent of isokinetic sampling and the Stokes number were initially computed using the supersonic free jet velocity, U'_o. However, when a bow shock exists, the stream velocity is subsonic between the shock front and the sampling probe inlet. If the bow shock is considered to be a normal shock, the subsonic velocity may be predicted from normal shock relationships. For example, compressible flow

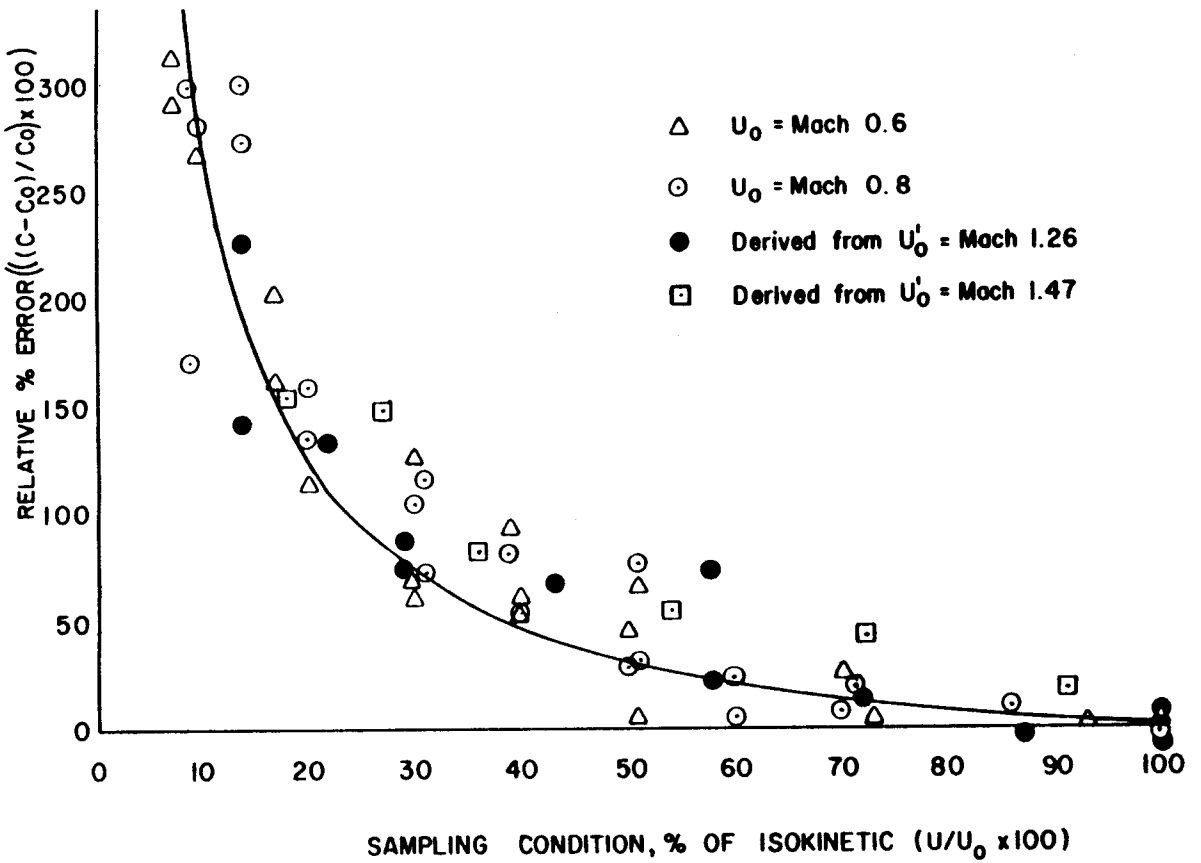

Figure 15. Relative aerosol concentration errors for subisokinetic velocity ratios.

tables (61) show that for a Mach number of 1.26 (M_1) the Mach number ratio across a normal shock (M_1/M_2) will be 1.56, or M_2=0.81. Thus, the actual Mach number immediately upstream of the sampling probe inlet is Mach 0.81. This concept is illustrated in Figure 16.

Using the post shock subsonic velocity as U_o, the percent of isokinetic sampling was recomputed for the Mach 1.26 and 1.47 free jets. These derived data points are included in Figure 15. The good agreement between the derived data and the data actually obtained at subsonic free jet velocities suggests that, within the experimental limits, supersonic subisokinetic sampling errors can be estimated using the subsonic velocity which exists downstream of a sampling probe bow shock to compute the sampling velocity ratio, U/U_o.

Interpretation of Results

Figure 17 compares the subisokinetic errors predicted by Equation 8 with the results of other authors for a Stokes number of 0.12. Even though previous investigators used relatively large bore probes and low speed flows, they studied a Stokes number range that approached or included the Stokes numbers encountered in the present study (i.e. $0.1 < K < 0.14$). The experimental results also compared well with predictions using the theoretical approach attributed to Forney and McGregor (28) (See

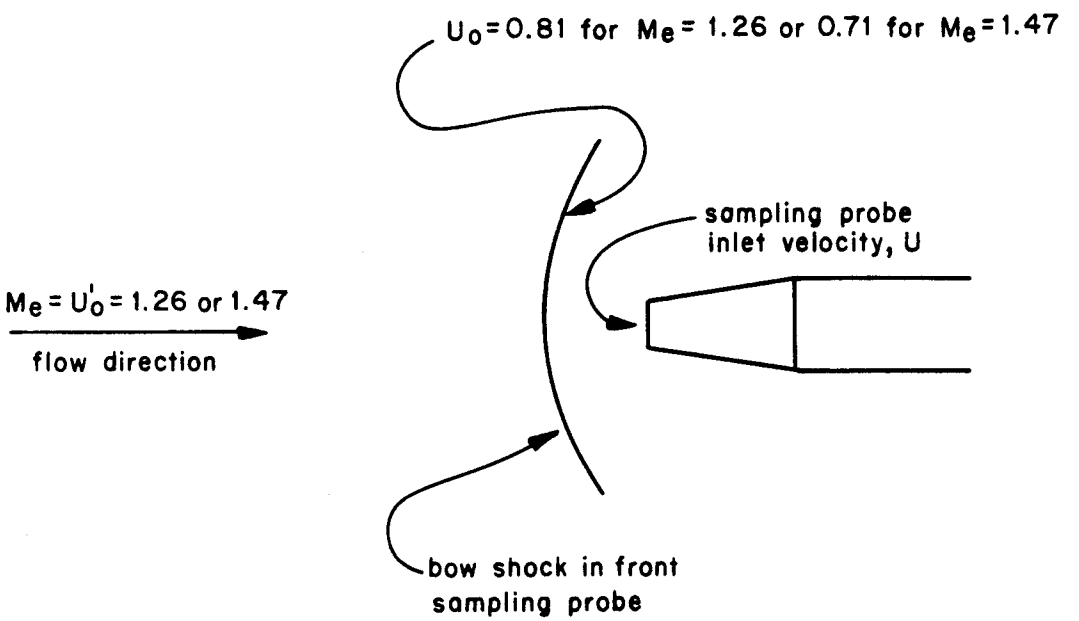

Figure 16. Relationship of U'_o, U_o, and U for supersonic free jets.

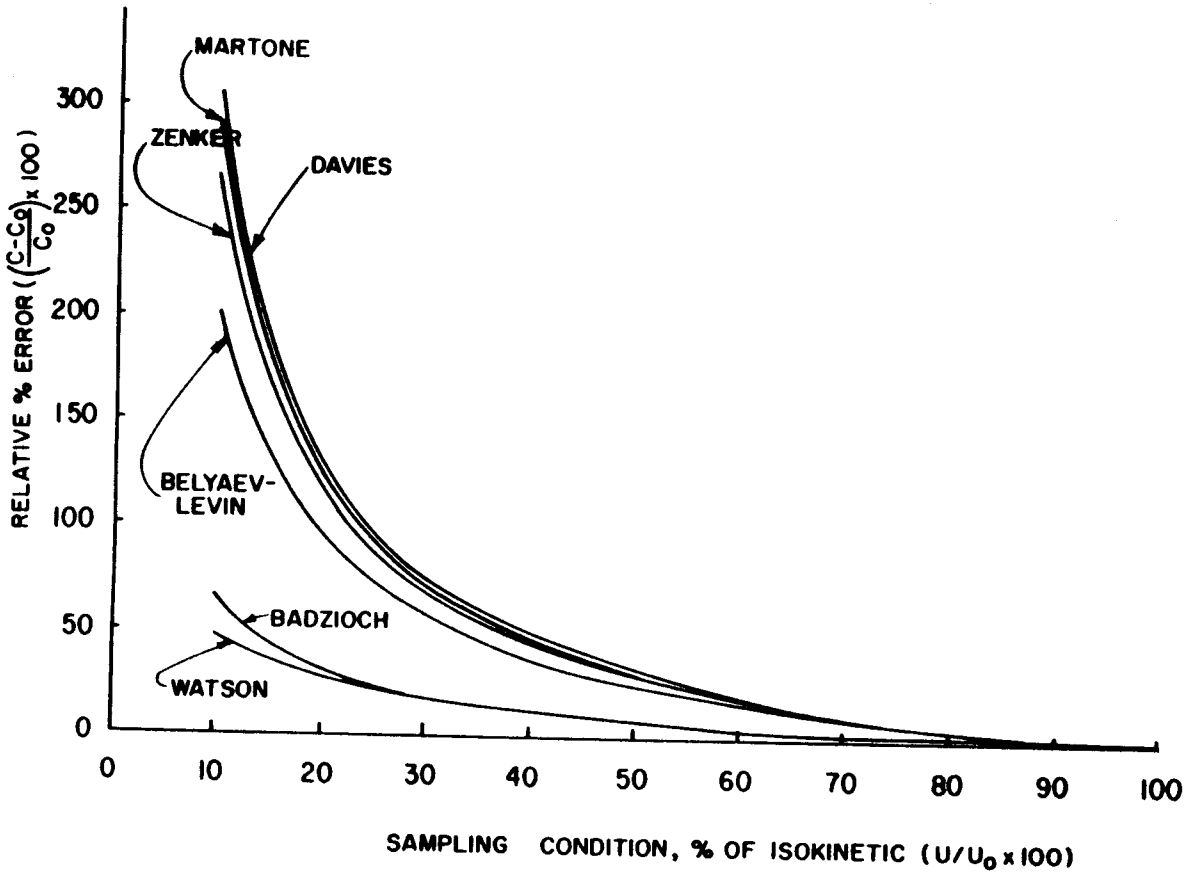

Figure 17. Comparison with the results of other authors for a Stokes number of 0.12.

Appendix K). The good agreement between the results of the present study and the relatively recent experimental work of Zenker, as reported by Fuchs (22), Belyaev and Levin (23), and Davies, as reported by Belyaev and Levin (23), and the theoretical work of Forney and McGregor (28) demonstrates the usefulness of these correlations for predicting sonic range, subisokinetic sampling errors when the Stokes number of the particle nozzle system is near 0.1. Table 5 compares the experimental conditions used by these authors in developing their predictive equations for anisokinetic sample errors.

Generally, the results suggest that the coefficient, $\beta(K)$, in the generalized aspiration equation (Equation 3) depends on the Stokes number and on the velocity ratio, U/U_o. Furthermore, the results support the theoretically developed notion of a universal similarity parameter to correlate probe collection efficiency in a supersonic stream.

This fundamental research was, in part, motivated by the real world concerns about the sampling efficiency of aircraft turbine engine smoke probes. As shown in Appendix L, the subisokinetic results given above allow prediction of sampling errors for aircraft turbine engine smoke probes.

CONCLUSIONS AND DISCUSSION OF ERRORS

Conclusions

In this study, aerosols containing spherical stearic acid particles with a geometric mean diameter of 0.8 μm and a geometric standard deviation of 1.28 were sampled with small bore, front facing aspirating probes in near sonic and supersonic unheated free jets. The conclusions are:

1. The sampling probe wall to bore area ratio, A_w/A_b in the range from 0.28 to 3.77 does not affect the sampled aerosol concentration C, when sampling isokinetically in Mach 0.8 free jets.

2. Relative concentration errors of approximately 124% are encountered when sampling in Mach 0.6, 0.8, 1.26 and 1.47 free jets, if the sampling velocity is 20% of the free stream velocity.

3. With supersonic free stream Mach numbers less than 1.47 the subsonic velocity downstream of the sampling probe bow shock can be used with subsonic subisokinetic data to estimate sampling errors. Therefore, representative samples can be obtained by matching the sampling velocity with the post shock subsonic velocity rather than the free stream supersonic velocity.

Discussion of Errors

There are three basic categories of errors to be considered: (1) instrument errors, (2) experimental errors and (3) statistical errors.

Instrument Errors

(1) Six temperature readings were involved with each test. The stagnation temperature in the settling chamber, the flowing temperature of air through the orifice meters in the settling chamber and free jet sampling systems, the temperature of molten stearic acid in the aerosol generator reservoir, and the aerosol temperature in the evaporation zone and condensation zone of the aerosol generator. Temperature readings could be made to within +/- 1F. The aerosol generator temperatures were used to monitor performance of the aerosol generator and to detect system upsets and were not used in any calculations. The settling chamber stagnation temperature and orifice meter flowing air temperatures, although measured and recorded, were assumed to be 530R for the purpose of calculation. This is discussed further in the next section as an experimental error.

(2) Two pressure measurements were involved with each test. The ambient pressure, measured with a labora-

tory quality mercury in glass barometer to the nearest tenth millimeter of mercury, and the settling chamber stagnation pressure, measured to the nearest tenth psi with a large dial calibrated pressure gage. The accuracy of the pressure gage was +/- 0.2 psi for the range of measured pressures. Calibration data is given in Appendix A. The ratio of ambient to stagnation pressure determined the nozzle exit Mach number and the isentropic flow conditions listed in standard compressibility tables. Based on the precision of the pressure measurements, the exit Mach number could be controlled to within +/- 0.005M or less than 0.5% error in exit Mach number.

(3) Differential pressure gages were used to measure pressure differences across the aerosol sampling system orifice plates and the difference between total and static pressure when pitot tubes were used for velocity measurements in the settling chamber or free jet. The accuracy of these devices is +/- 2% of full scale. This gage inaccuracy translates to a velocity or flow rate measurement error of less than 3%.

(4) For each test, the calculation of settling chamber and free jet aerosol concentrations involved a time measurement of the aerosol collection period.

Errors in measuring time were small, probably less than 0.5%.

(5) The mass of stearic acid collected on the Nuclepore filters and in sampling probe washes was determined by a gas chromatographic technique described in Appendix D. The recovery of known amounts of stearic acid added to untreated filters and acetone solutions averaged 101% and 102%, respectively, over the range of one to ten milligrams. The weight of stearic acid collected was determined to the nearest 0.01 mg. Since total filter weight gain was always greater than 0.75 mg, the error in stearic acid determination was less than 2%.

(6) Particle size was determined by direct counting of particle images on photomicrographs obtained with a scanning electron microscope. Particle images were measured to the nearest 0.1 mm which corresponds to 0.03 μm at 3000 x magnification. Since the particle geometric mean size was 0.8 μm, the error associated with the sizing of an individual particle was about 4%. Particle size did not directly enter into calculation of sampling errors, but particle size was required to calculate the Stokes number which was required to compare results with the results of other authors.

Experimental Errors

There are three main sources of experimental errors.

Inherent variability. Inherent variability in the experimental materials or conditions results in extraneous variations which are called errors. Such properties and conditions as variations in filter pore size, stearic acid aerosol particle size, settling chamber stagnation temperature, and the amount of stearic acid deposited on the sampling probe walls give rise to these errors. Such variations are not completely controllable or accountable but their effects can sometimes be minimized by careful selection of material and proper experimental design.

A variety of approaches were used to minimize these types of errors. Significant variations in filter pore size and filter collection efficiency were avoided by selecting polycarbonate membrane filters that have outstanding characteristics for uniform properties from membrane to membrane and a predictable collection efficiency. Confidence in the stability and reproducibility of the aerosol generator was gained by collecting 22 particle size samples regularly over the entire experiment, a period of several months. Variation in the settling chamber stagnation temperature occurred from run to run and within a run; the extreme range overall was 520-537R with an assumed average of 530R. As seen from

equation 9, for the worst case, this assumption resulted in a +/- 2% error in stagnation air density which translated to a similar error in isokinetic or subisokinetic sampling rates.

$$\rho t = (P_t \times MW) / (R_g \times T_t) \qquad (9)$$

Variation in orifice meter flowing air temperature, T_f, was also assumed negligible with T_f assumed to be 530R. As described in Appendix C, T_f actually ranged from 528R to 540R for the settling chamber sampling system orifice meter and from 528R to 549R for the free jet sampling system orifice meter. Since the standard volumetric flow rate, Q_b, through the orifice meter is inversly proportional to the square root of T_f, the maximum error in Q_b by assuming T_f = 530R is +/- 2%.

The amount of stearic acid deposited on the settling chamber sampling probe interior walls averaged 2% of the amount deposited on the filter; this was assumed negligible and was not accounted for in final calculations. For the free jet sampler, however, the probe wash averaged 12% of the filter weight gain and this average was added to the filter weight gain to determine the total weight of stearic acid collected on a given run. The actual range of probe wash results for 46 samples, was from 4% to 21% of the filter weight gain. Thus, the error in

determining the total weight of stearic acid collected on a single run due to variation in the amount deposited on the probe wall was +/- 9%.

Lack of Uniformity. Failure to standardize the procedure, or lack of uniformity, is the second source of experimental errors. For example, failure to wash the sampling probe with acetone between runs could result in this type of error. However, extreme care was taken in performing all procedures in as uniform a manner as possible. For example, all systems were operated using prepared check lists and data were recorded on standardized data sheets.

Bias Errors. Bias errors may also exist, such as consistently reading a scale too high or too low. Also, errors due to such things as flow leakage would result in measurements which were too high or too low. This type of error is more properly termed an accuracy rather than precision error and is usually simpler to locate and correct. For example, proper calibration (of both machine and operator) allowed the two errors mentioned above to be adequately accounted for or corrected.

For this study, it is noteworthy, that much of the critical procedure, such as determination of the stearic acid mass by gas chromatography or using the electron microscope for selecting the particle field to be counted for particle size determination, or calibration of the

settling chamber pressure gage, was done by operators other than the principal investigator. This independent analysis of key component data, reduced the opportunity for inadvertent compounded bias error of a single individual.

Another source of bias error is the judgment error associated with drawing best fit lines or curves between data points, not all of which fell on the line or curve. Examples for this experiment are the orifice meter calibration curves and the cumulative number distribution lines used to determine particle geometric mean size and geometric standard deviation. Since the scatter in these plots was small, it is estimated that the bias error that may have been introduced is less than +/- 2%.

Statistical Errors

Statistical errors involving significance testing are placed in two categories. Type I errors are usually the more serious and occur when the variations due to a specified factor are determined statistically to be significant when in fact they are not. In this experiment, there were no tests of this type. Type II errors are usually less serious and occur when a variation is not considered significant when in fact it is. For example, the t test was used to determine there was no significant difference at a significance level of 0.05, between gas chromatographic and gravimetric methods for

determining the weight of stearic acid collected on the membrane filters. If in fact, there is a difference, a type II error has occurred.

Finally, it should not be overlooked that a primary thrust of this experiment was, in fact, to determine an error; that is, the subisokinetic error associated with determining the mass concentration of small particles suspended in high speed jets of air. Fundamentally, the experimental challenge was to prevent the error of interest from being masked by other errors. Central to this task was calculation of aerosol concentration, that is, weight of stearic acid collected divided by the volume of air sampled. Considering all of the above discussion of error, aerosol concentration was measured to within +/- 10% of true value neglecting the subisokinetic error. Since the subisokinetic errors were generally an order of magnitude greater than the +/- 10% noise level, the basic experimental design objective was achieved.

SUMMARY AND RECOMMENDATIONS

Summary

The accurate measurement of aerosol mass concentration is frequently complicated by the nonideality of the aspiration process. It becomes particularly difficult to extract representative samples when the sampling velocity and ambient fluid velocity differ significantly. Under these conditions, inertial effects can cause particle trajectories to separate from fluid streamlines. Even isokinetic sampling can result in sampling biases when the probe is "thick walled."

An extensive literature exists on inertial sampling bias; both theoretical and experimental work are well represented. This work, however, is the pioneering experimental treatment of sampling bias for the case of submicrometer size particles suspended in near sonic and supersonic jets of air. Consideration of this regime was driven by practical interest in accurate determination of particle mass concentrations in gas turbine engine and rocket motor exhausts. Although all the characteristics of particle sampling in these real world environments were not simulated, the factors expected to have the most dominant effect on sampling bias were included. These factors were: (1) probe wall thickness, (2) sampling velocity ratio, (3) and shock front passage.

Probe wall thickness proved not to be important when the sampling velocity ratio was maintained at 1. The velocity ratio had a very significant effect on sampling bias; for velocity ratios approaching 0.1 the sampling error approached 300%. Most importantly, it was shown that when sampling in supersonic streams, it is not necessary to "swallow" the shock into the sampling probe in order to obtain a representative sample. In the supersonic cases, an isokinetic (i.e. representative) sample could be obtained by matching the sampling velocity with the subsonic velocity downstream of the probe bow-shock. This subsonic free stream velocity can be calculated using well established "normal" shock relationships for air. The practical significance of this finding is that real world sampling devices do not require the added complexity (i.e. probe design, pump capacity, etc.) necessary to achieve a "swallowed" shock.

Other experimental and theoretical studies of the effects of anisokinetic sampling show that the sampling bias is also strongly dependent on the Stokes number. In this work, Stokes number was essentially constant (i.e. 0.1 - 0.14) so a Stokes number functional relationship with the aspiration coefficient could not be developed.

It was also shown that for the free jet sampling system a significant amount (average of 12%) of the total

weight of collected sample was deposited on the interior walls of the sampling probe upstream of the collecting filter. Experimentally, it was easy to rinse the sampling probe and account for the deposited material. For real world sampling devices a similar procedure would be operationally very difficult.

Recommendations

Within the range of the experimental parameters, this work has shown that subisokinetic sampling errors for the extreme conditions of near sonic and supersonic free stream velocity and submicrometer particles can be well predicted with experimental correlations developed for more conventional particle sizes and free stream velocities. In essence, this work has extended the envelope for these experimental correlations. Although there are limited theoretical studies that consider sampling bias in supersonic streams, it is believed that additional experimental data are required to validate these approaches before the theoretical results are universally applied.

Accordingly, the following specific recommendations are made regarding future experimental work associated with this study.

1. Extend the Stokes number range to determine the dependence of the aspiration coefficient on Stokes

number. The Stokes number is most easily and significantly adjusted by changing particle size.

2. Perform probe wall effects studies with the sampling velocity ratio not equal to 1 and for a range of Stokes numbers.
3. Examine a variety of free jet sampling probe designs to minimize aerosol deposition on the interior walls.
4. Study superisokinetic effects.

BIBLIOGRAPHY

1. Environmental Protection Agency, "Control of air pollution from aircraft and aircraft engines," Federal Register 38 (136) part II, July 17, 1973 p. 19088-19103.

2. Society of Automotive Engineers, "Aircraft gas turbine engine exhaust smoke measurement," Aerospace Recommended Practice ARP 1179, May 4, 1970. 8 p.

3. Champagne, D. L., "Standard measurement of aircraft gas turbine engine exhaust smoke," American Society of Mechanical Engineers paper No. 71-GT-88, Gas Turbine Conference March 28 - April 1, Houston, Texas, 1971. 6 p.

4. Environmental Protection Agency, "National primary and secondary ambient air quality standards," Federal Register 36 (220) November 25, 1971. p. 22384-22409.

5. Finch, S. P. and Eyl, A. W., "Prediction of test cell visible emissions," Air Force Civil Engineering Center Technical Report, AFCEC-TR-76-47, December 1976. 41 p.

6. Johansen, K. M. and Kumm, E. L., "Determination of aircraft turbine engine particulates," Airesearch Manufacturing Company of Arizona, Inc., EPA report 650/2-75-055, May 1975. 77 p.

7. Coordinating Research Council, Inc., "1973 CRC aircraft engine exhaust particulate measurement tests," Aviation Fuel, Lubricant, and Equipment Research Committee CRC project No.CA-41-65 March 1977. 37 p.

8. Stockham, J. and Betz, H. "Study of visible exhaust smoke from aircraft jet engines," ITT Research Institute Report FAA-RD-71-22 (AD-726249) June 1971. 17 p.

9. Broderick, A. J., Scotto, M. J. and Sturm, J. C., "Particulates in jet aircraft exhaust: instrumentation and initial results," paper presented at the 65th Annual Meeting of the AIChE, November 1972. 7 p.

10. Dehne, H., "Design, development and fabrication of a prototype high volume particulate mass automatic-isokinetic jet engine sampling train," Fourth Monthly Progress Report, Aerotherm Acurex project 7125, U.S. Navy contract N00123-75-C-1075, June 1975. 15 p.

11. Los Angeles County Air Pollution Control District, "Study of jet aircraft emissions and air quality in the vicinity of the Los Angeles international airport," APTD -0662 (PB 198699) April 1971. 189 p.

12. Parts, L. and Ross, W. D., et al., "An assessment of instrumentation and monitoring needs for significant air pollutants emitted by Air Force operations and recommendations for future research on analysis of pollutants," Aerospace Research Laboratories Contract F 33615-72-C-1304, Monsanto Research Corp., ARL 74-0015, February 1974. 57 p.

13. Brady, W. and Touzalin, L. A., "The determination of dust in blast-furnace gas," J. Ind. Engr. Chem, 3 (9), 1911. p. 662-670.

14. Fenton, D. L., "Turbine engine particulate emission characterization," IIT Research Institute Report No. FAA-RD-76-141, September 1976. 67 p.

15. Parker, G. J., "Some factors governing the design of probes for sampling in particle- and drop-laden streams," Atmos. Environ 2 (5) 1968. p. 477-490.

16. Hemeon, W. C. L., and Haines, G. F., "The magnitude of errors in stack dust sampling," Air Repair, 4, (3), 1954. p. 159-164.

17. Whiteley, A. B. and Reed, L. E., "The effect of probe shape on the accuracy of sampling flue gases for dust content," Journal of the Institute of Fuel, 32, (222) 1959. p. 316-319.

18. Dennis, R. et al. "Isokinetic sampling probes," Industrial and Engineering Chemistry, 49, (2) 1957. p. 294-302.

19. American Society of Mechanical Engineers, "Determining dust concentration in a gas stream," Performance Test Code 27-1941, New York, New York, 1941. 11 p.

20. Devorkin, H., et al, "Source testing manual," Los Angeles County Air Pollution Control District, Los Angeles, California, 1965. 185 p.

21. Voloshchuck, V. M., and Levin, L. M., "Some theoretical aspects of aerosol aspiration." Izv. Akad Nauk. ser.Fisika Atm. Okeana, 4 (24) 1968. p. 241-249.

22. Fuchs, N. A., "Review papers-sampling of aerosols," Atmos. Environ 9, 1975. p. 697-707.

23. Belyaev, S. P. and Levin, L. M., "Techniques for collection of representative aerosol samples,: J. Aerosol Sci. 5, 1974. p. 325-338.

24. Rader, D. J. and Marple, V. A., "A study of the effects of anisokinetic sampling," Aerosol Science and Technology, 8, (3), 1988. p. 283-299.

25. Martone, J. A., Daley, P. S., and Boubel, R. W., "Sampling submicrometer particles suspended in near sonic and supersonic free jets," Journal of the Air Pollution Control Association, 30, (8), 1980. p. 898-903.

26. Badzioch, S., "Collection of gas-borne dust particles by means of an aspirated sampling nozzle," Br. J. Appl. Phys 10 (1), 1959. p. 26-32.

27. Watson, H. H., "Errors due to anisokinetic sampling of aerosols," Am. Ind. Hyg. Assoc Q. 15(1), 1954. p. 21-25.

28. Forney, L. J. and McGregor, W. K., "Particle sampling in supersonic streams with a thin-walled cylindrical probe," AIAA Journal, 25, (8), 1987. p. 1100-1104.

29. National Council for Air and Stream Improvement, "Manual for the sampling and analysis of Kraft mill recovery stack gases," Atmospheric Pollution Technical Bulletin No. 14, New York, New York, 1960. 65 p.

30. Cooper, H. B. H. and Rossano, A. T., Source testing for air pollution control, Environmental Research and Applications, Inc., 1971. 228 p.

31. Miller, A. M., Brown, J., et al., "Applied techniques of analyses of stack emissions," Presented at the West Coast Regional Meeting of the National Council for Air and Stream Improvement, Portland, Oregon, October 2, 1968. 11 p.

32. Stukel, J. J. and Soo, S. L., "Turbulent flow of a suspension into a channel," Powder Technology, 2 (1968/69), 1969. p. 278-289.

33. Hultbert, J. A. and Soo, S. L., "Two-phase flow through a nozzle," Astronautica Acta, 11 (3), 1965. p. 207-216.

34. Yong, N. L., and Soo, S. L., "A study of jets of electrically charged suspensions," Environ. Sci and Tech., 4 (8), 1970. p. 678-686.

35. Soo, S. L., "Gas dynamic processes involving suspended solids," A.I.Ch.E. Jour., 7 (3), 1961. p. 384-391.

36. Soo, S. L. and Tung, S. K., "Deposition and entrainment in pipe flow of a suspension," Powder Technology, 6 (1972), 1972. p. 283-294.

37. Soo, S. L., Professor of mechanical engineering, University of Illinois, personal communication, May, 1975.

38. Owczarek, J. A., Fundamentals of gas dynamics, International Textbook Company, Scranton, Pennsylvania, 1968. 648 p.

39. Hill, P. G., and Peterson, C. F., Mechanics and thermodynamics of propulsion, Addison-Wesley Pub. Co., Reading, Mass, 1965. 375 p.

40. Herman, R., Supersonic inlet diffusers and introduction to internal aerodynamics, Minneapolis-Honeywell Regulator Company, Minneapolis, Minnesota, 1956. 273 p.

41. Augustine, F. E., "Airborne sampling of particles emitted to the atmosphere from kraft paper mill processes and their characterization by electron microscopy," Ph.D. Dissertation, Oregon State University, 1974. 131 numb. leaves.

42. Nuclepore Corporation, "Specifications and physical properties," 7035 Commerce Circle, Pleasanton, California, Form SPP 10M 5/73, 1973. 12 p.

43. Davies, C. N., Department of Chemistry, University of Essex, Colchester, England, personal communication, April, 1975.

44. Cadle, R. D., National Center for Atmospheric Research, Boulder, Colorado, personal communication, March, 1975.

45. Fenton, D. L. and Knutson, E. O., Illinois Institute of Technology Research Institute, Chicago, Illinois, personal communication, April 1975.

46. Sinclair, D. and LaMer, V. K., "Measurement of particle size in aerosols," Chem. Rev., 44, 1949. p. 245-264.

47. Rapaport, E. and Weinstock, S. E., "A generator for homogeneous aerosols," Experimentia, 11 (9), 1955. p. 363-364.

48. Werle, D. K., et al., "High-volume condensation aerosol generator for research and testing," ITT Research Institute report prepared for submission to J. Aerosol Science, August, 1975. 10 p.

49. Tomaides, M., Liu, B.Y.H., and Whitby, K.T., "Evaluation of the condensation aerosol generator for producing monodispersed aerosols," J. Aerosol Science, 2 (39), 1971. p. 39-46.

50. Stahlhofen, W., et al, "Generation and properties of a condensation aerosol of di-2-ethylhexyl sebacate (DES)-1," J. Aerosol Science, 6, 1975. p. 161-167.

51. Preining, O., "Calibration of sizing devices for dust with grain sizes between 0.1 and 1 micrometer by means of test aerosols," Staub, 22 (11), 1962. p. 456-463.

52. Horvath, H., "A simple modification of the LaMer generator," Jour. of Colloid and Interface Sci., 29 (4), 1969. p. 733-735.

53. Fuchs, N. A. and Sutugin, A. G., "Coagulation rate of highly dispersed aerosols," Journal of Colloid Science, 20, 1965. p. 492-500.

54. Sehmel, G. A., "Errors in the subisokinetic sampling of an air stream," Ann. Occup. Hyg., 10, 1967. p. 73-82.

55. Sehmel, G. A., "Particle sampling bias introduced by anisokinetic sampling and deposition within the sampling line," Amer. Ind. Hyg. Jour., November-December, 1970. p. 758-771.

56. Ivie, J.J., Forney, L.J. and Rach, R.L., "Supersonic particle probes: measurement of internal wall losses," Arnold Engineering Development Center, AEDC-TR-88, November, 1988. 97 p.

57. Bean, H. S. (editor), Fluid meters their theory and application, Report of the ASME Research Committee on Fluid Meters, sixth ed., ASME, 1971. 315 p.

58. Sims, J. L., "Calculation of transonic nozzle flow," NASA TM X-53081, October 12, 1964. 20 p.

59. Cooper, D. W. and Reist, P. C., "Neutralizing charged aerosols with radioactive sources," Jour. of Colloid and Interface Sci., 45 (1), 1973. p. 17-26.

60. Boubel, R. W. and Ripperton, L. A., "Calibration of orifices in flow systems," American Industrial Hygiene Association Meeting, Cincinnati, Ohio, May, 1963. 9 p.

61. Ames Research Staff, "Equations, tables, and charts for compressible flow," NASA report TR-1135, (PB-115573) 1965. 69 p.

62. Pope, A. and Goin, K., High speed wind tunnel testing, John Wiley & Sons, Inc., New York, 1965. 217 p.

63. Wyler, J. S., "Probe blockage effects in free jets and closed tunnels," ASME Paper No. 74-WA/PTC-5, presented at the Winter Annual Meeting, New York, November, 1974. 6 p.

64. ASME Boiler and Pressure Vessel Code, Section VIII, "Pressure vessels," 1971. 67 p.

65. Broer, L. J. F. and Rietdijk, J. A., "Measurements on supersonic free jets," Appl. Sci. Res., Section A, 9, 1960. p. 465-477.

66. Jasper, T. M. and Sullivan, J. W., "The collapsing strength of steel tubes, ASME Transactions," 53, 1931. p. 567-571.

67. Moore, W. J., Physical chemistry, Prentice-Hall Inc., 3rd edition, 1962. p. 844.

68. Anderson, G. M., "Initial performance of rigid, porous sheets of sintered-polyethylene powder for filtering airborne sander dust," Ph.D. Dissertation, Oregon State University, 1974. 124 numb. leaves.

69. Volk, W., Applied statistics for engineers, 2nd Ed., McGraw-Hill, 1969. p. 415.

70. U.S. Dept. of Health Education and Welfare (NIOSH), The industrial environment - its evaluation and control, Cincinnati, OH, 1973. p. 719.

71. Perkins, H. C., Air pollution, McGraw-Hill, 1974. p. 407.

72. Forney, L. J., McGregor, W. K. and Van Dyke, D. B., "Computation of gas flowfields in supersonic particle probes," ASME Journal of Fluids Engineering, 76, (3), 1986. p. 76-81.

73. Williamson, R. C. and Stanforth, C. M., "The evaluation of factors which influence accuracy based upon experience in the measurement of aircraft exhaust emissions," General Electric Aircraft Engine Group Report No. R75-AEG-152, January 2, 1975. 26 p.

APPENDICES

APPENDIX A

SUPPLEMENTARY SYSTEM DESIGN INFORMATION

Free Jet Air Flow System

Figures A-1 through A-8 show details of the free jet air flow system. The comments which follow are intended to give an understanding of the design and function of each major component of the system. Most design criteria were based on recommendations made by Pope and Goin (62).

The sizing of the free jet apparatus was determined largely by the required area of the nozzle exit (i.e., test section). The flow area in the test section had to be large enough to completely submerge the sampling probe in the desired flow and to prevent flow blockage by the probe. Thus, the probe frontal area (i.e., the area normal to the flow) determined the nozzle exit diameter. The probe dimensions, in turn, were chosen to be representative of typical probes used in sampling gas turbine exhausts.

For solid models used in transonic wind tunnels with perforated test section walls, Pope and Goin (62) suggest a flow area 100 times the model area to completely neglect possible wall effects such as shock wave reflections which may disturb uniform flow. In the present case, the nozzle exit diameters were 5.08 cm (2 inches) providing a flow area of 20.26 cm^2 (3.14 in^2).

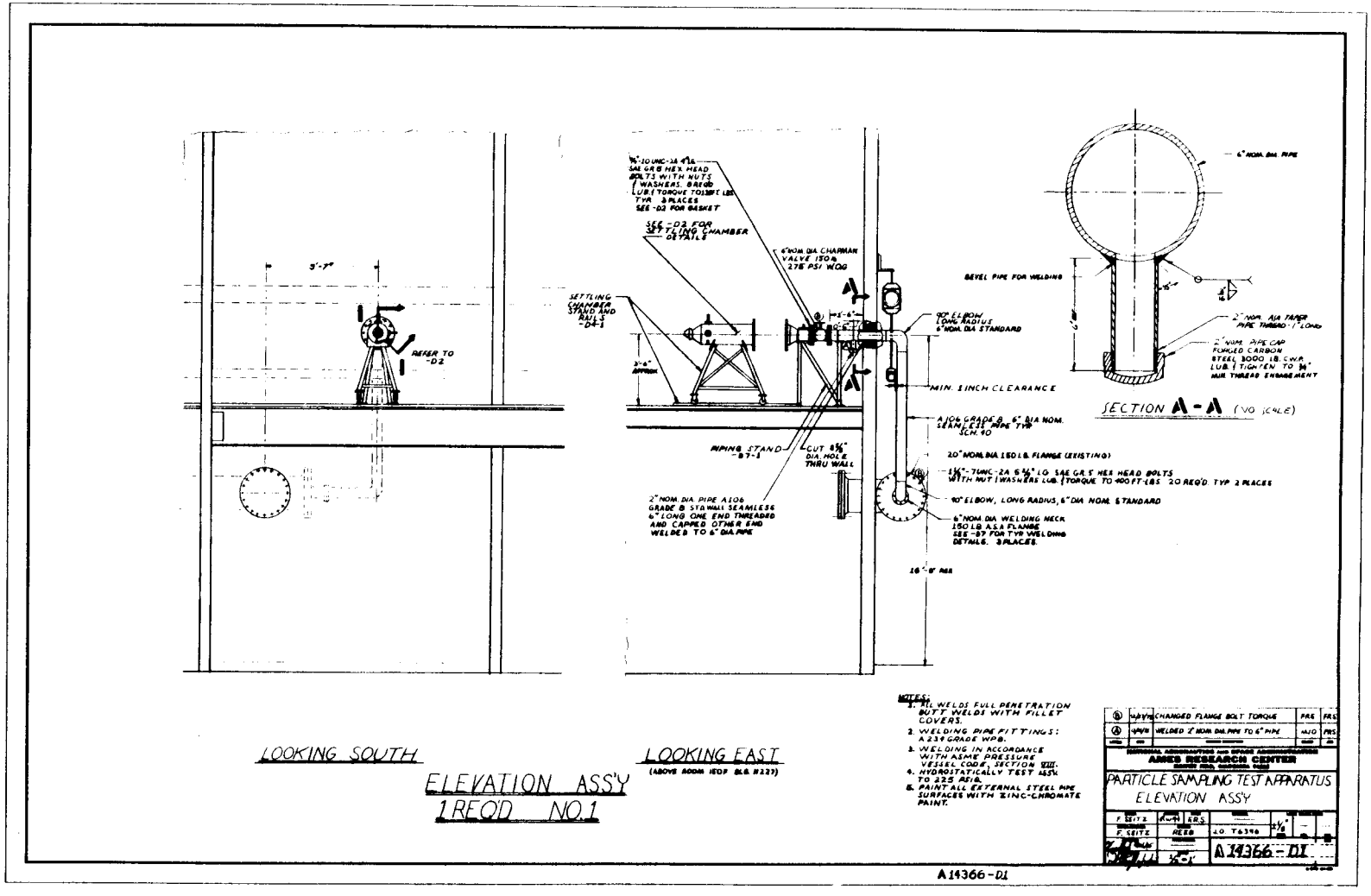

Figure A-1. Free jet system elevation assembly.

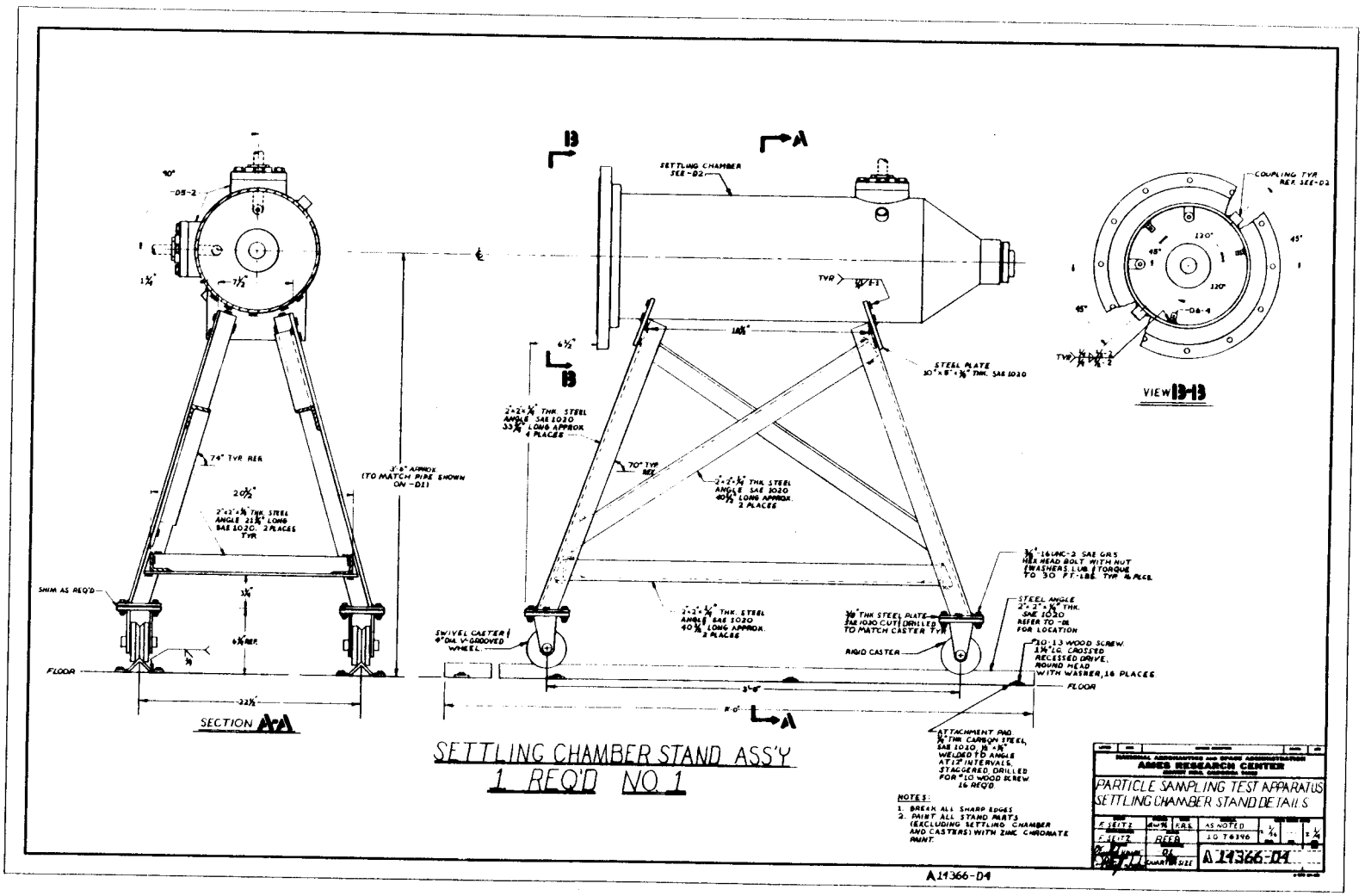

Figure A-2. Settling chamber stand.

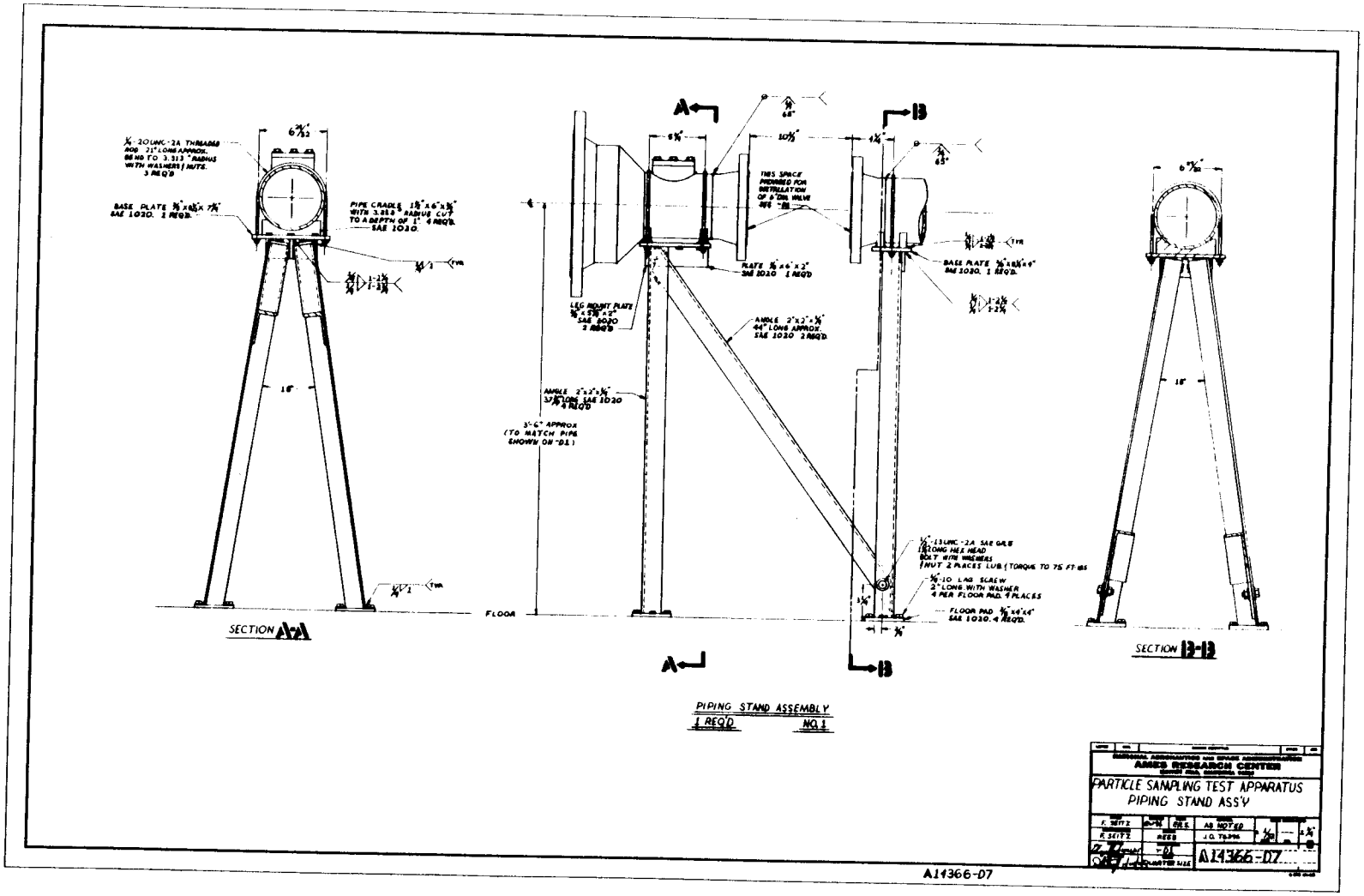

Figure A-3. Settling chamber piping stand assembly.

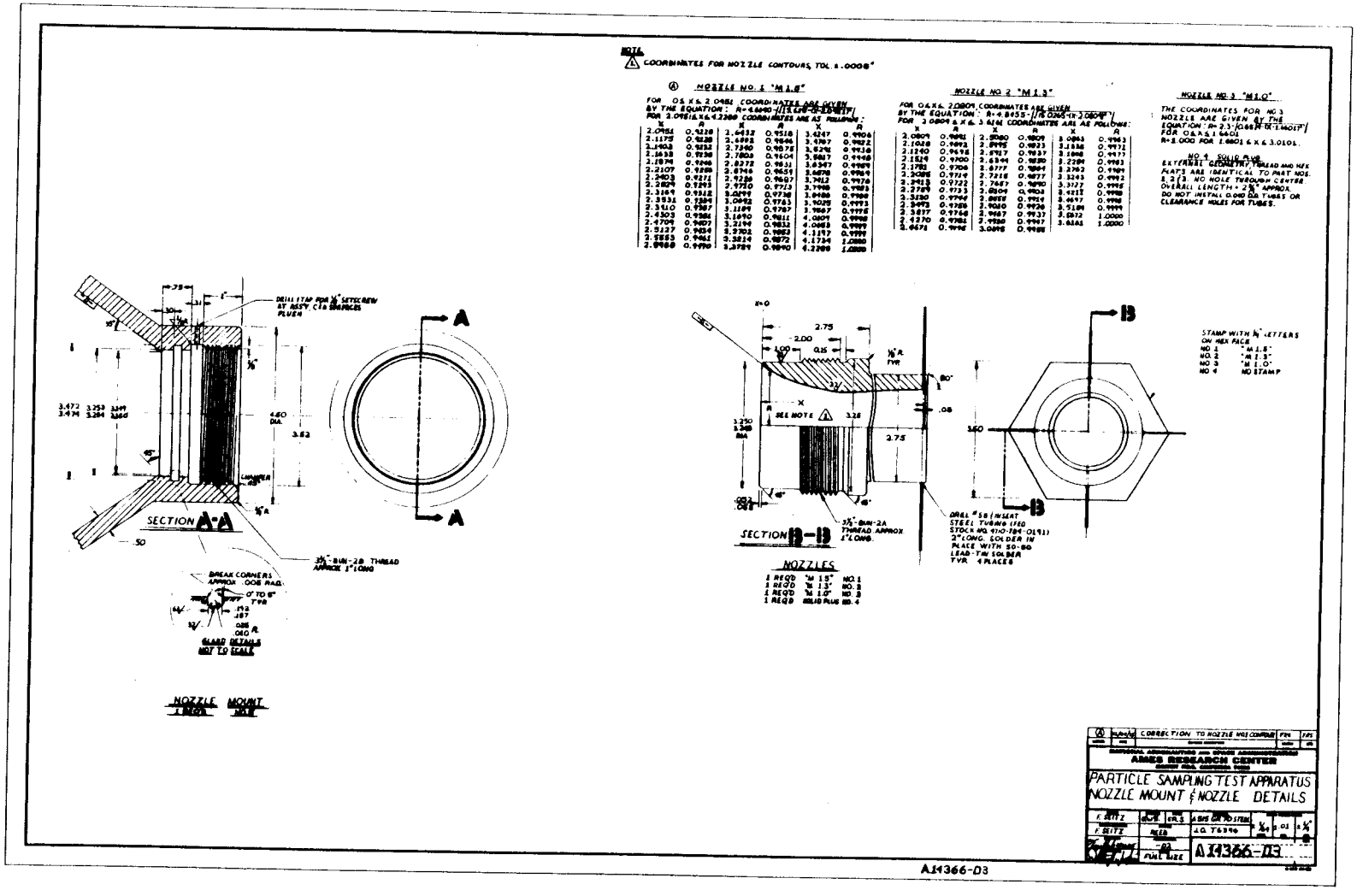

Figure A-4. Free jet nozzle mount and nozzle detail.

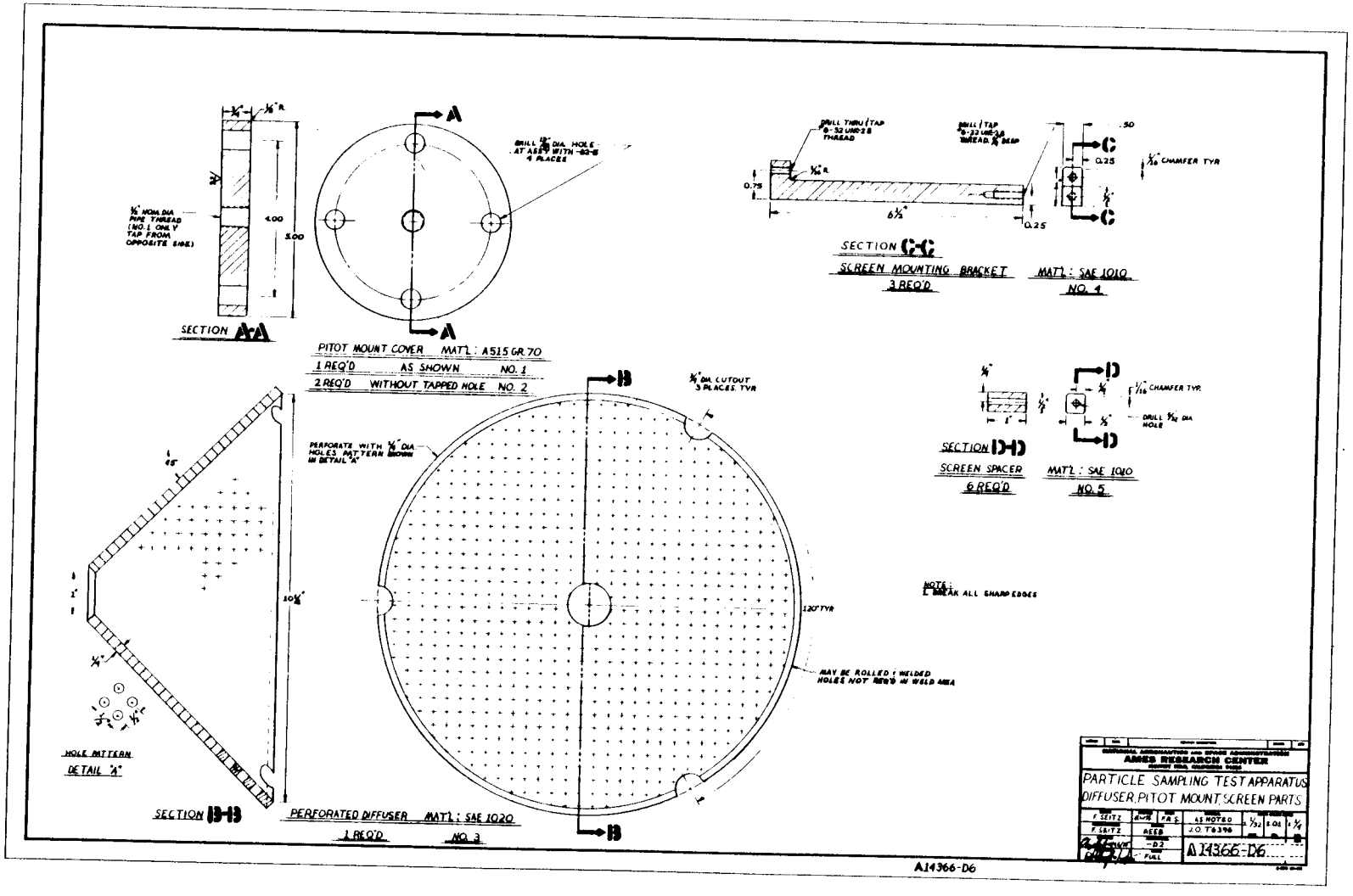

Figure A-5. Diffuser, pitot mount, and screen parts.

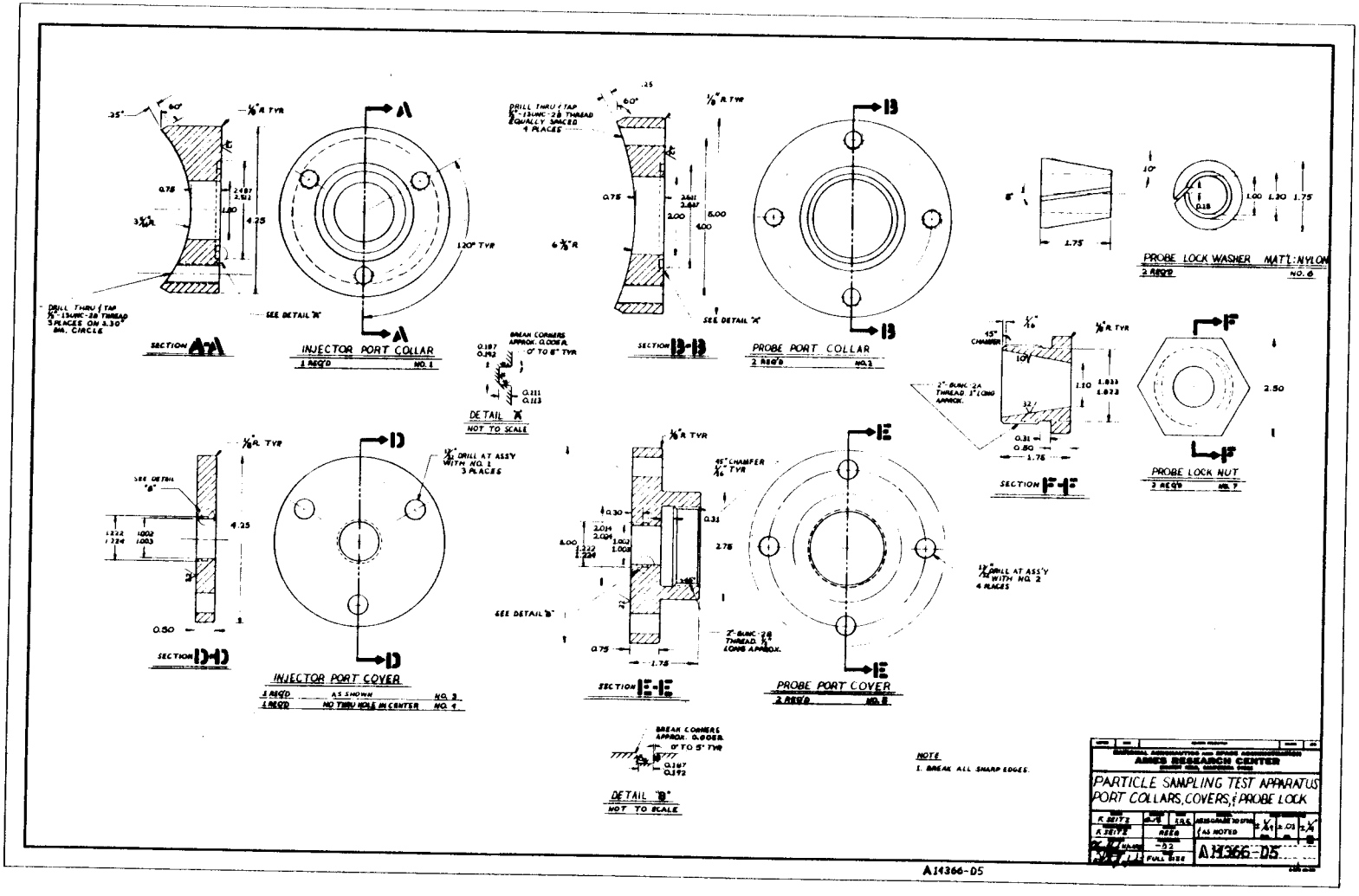

Figure A-6. Sampling port collars, covers, and probe lock.

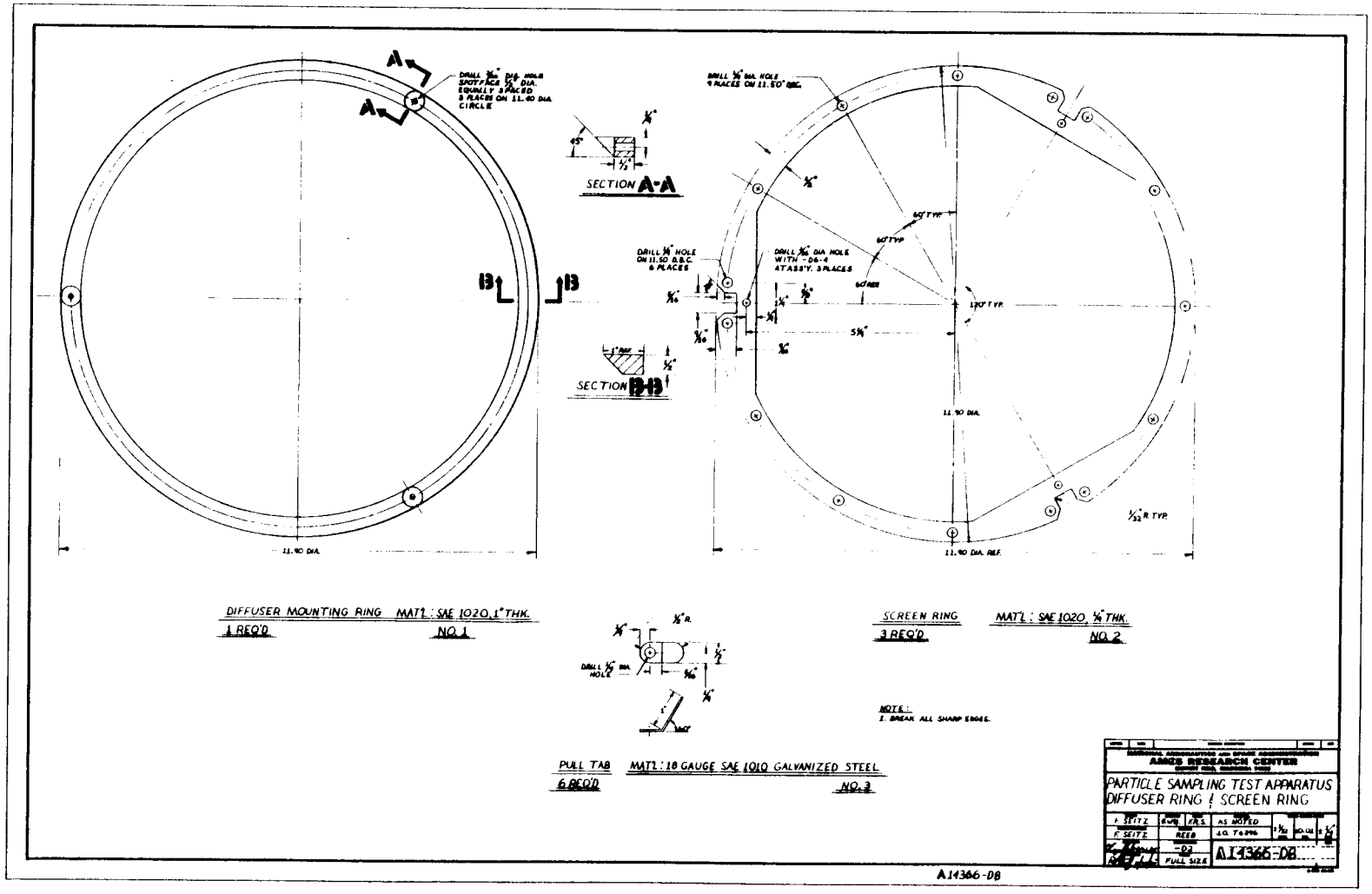

Figure A-7. Diffuser ring and screen ring.

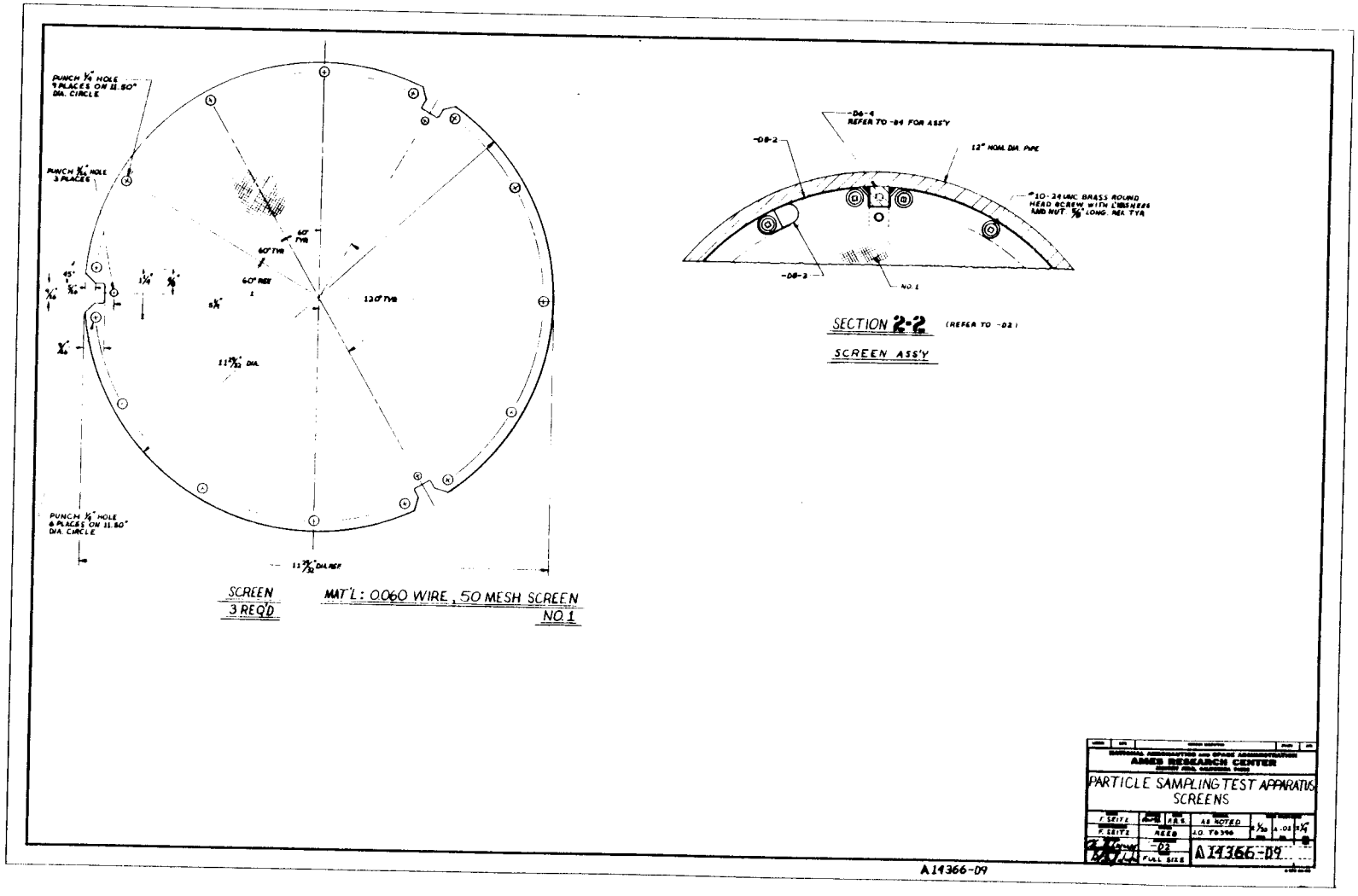

Figure A-8. Screens.

All the free jet sampling probe frontal areas (i.e., wall plus bore area) were 0.299 cm^2 (0.046 in^2) or less. Thus, the flow area was at least 68 times the total probe frontal area. If, however, only the probe wall thickness is considered to contribute to possible interference then the ratio of flow area to model area increases to 90 for the thickest walled probe and to 462 for the probe with the thinnest wall.

When considering the above discussion, it should be noted that in wind tunnel testing parlance the phenomenon generally called the probe blockage effect refers to the fact that large probes (i.e., usually pitot tubes not sampling probes) will noticeably influence the flow characteristics such that measurements (i.e., total and/or static pressure) will no longer indicate the correct flow parameters. The blockage effect can be looked upon as a perturbation of the velocity in the vicinity of the probe and, as such, is similar to the phenomenon which in this study is referred to as the probe wall effect. Therefore, the requirement for no flow blockage by the probe really applies to the case where the probe with the thinnest wall was used to sample the free jet isokinetically. As discussed above, the flow to probe area ratio in this case was 462. In other words, no probe wall effects would occur with the knife edged probe; a desireable situation.

As a final note on probe blockage effects, the recent experimental results of Wyler (63) should be mentioned. Two major conclusions were that the blockage effect in free jets was approximately the same magnitude as in closed tunnels and that the blockage effect is very important in the transonic flow regime, M = 0.9 to M = 1.2. The first result negates the customary argument that the effect of a disturbance on the flow properties of a free jet is negligible since the flow boundaries are free to adjust to any flow disturbance. These findings reinforced the need to include a wall effects study as part of this program.

Once the required size of the flow nozzles was determined, the sizing of the remaining system components was relatively straightforward. Referring to Figures 5 and 7, the major components of the air flow system include the wide angle diffuser, settling chamber, transition section, and the nozzles.

The purpose of the wide angle diffuser is to spread the flow from the 6-inch nominal diameter inlet pipe to the 12-inch nominal diameter settling chamber and to distribute the test particles as they are injected into the air stream. The perforations in the diffuser were designed with a sufficient flow area (about 700 1/4-inch diameter holes) to keep the average velocity through the perforations well below Mach 0.5 at the most severe

operating conditions. The spreader provided large scale turbulence to promote good mixing of the generated test particles and, because of its ventilated wall design, discourage turbulent deposition of particles on the diffuser surfaces.

The settling chamber was a cylindrical shell, more than one diameter long, which accepted aerosol from the wide angle diffuser, provided a length for settling to obtain uniform flow, provided screens for reducing turbulence, and then exhausted aerosol into the transition section. The concensus of wind tunnel engineers is that settling chamber velocities should be no greater than 80 to 100 ft/sec (62); in the present case, 12-inch pipe was available and its use meant that settling chamber velocities would be on the order of 20 ft/sec.

The purpose of the transition section was to give a smooth variation of Mach number with distance between the settling chamber and the minimum cross sectional area of the nozzle, A*. Typical recommended lengths for the entrance section are one or two test section heights. The large area contraction ratio (36 to 1) provided by the transition section contributes to low turbulence levels and uniform flow at the nozzle exit.

Three flow nozzles were designed and fabricated for this project; one subsonic nozzle and two supersonic

nozzles. The subsonic nozzle was a standard ASME long radius, low ratio type (57). The supersonic nozzle contours were generated at Ames by a computerized version of a design method due to Sims (58); exit Mach numbers of 1.3 and 1.5 were selected for design purposes. The measured exit Mach numbers were slightly less than design because the design method does not include a correction for boundary layer thickness in the computation of nozzle coordinates. In other words, the flow area at the nozzle exit will be somewhat less than the physical dimensions of the hardware because of a boundary layer close to the nozzle walls. Previous experience with the supersonic nozzle design method at Ames had proven it to be reliable for producing nozzles that provided the desired three dimensional parallel flow at the nozzle exit. Sims (58) method is based on an approximate solution of the transonic throat flow in a De Laval nozzle found by expanding the potential function in a power series about the critical line.

The air flow system was not provided with a blow off stack and safety disc. Thus, the system design pressure was the air supply line pressure, 150 psig. As a result, the system required a hydrostatic test at 150% of the design pressure (i.e. 225 psig) to meet the ASME Code for Unfired Pressure Vessels (64).

Several other features of the air flow system should

be noted. The settling chamber was on rollers to facilitate access to its interior for inspection, cleaning, and removal of screens, etc. Two sampling ports separated by 90^{o} were located on a settling chamber radius just upstream of the transition section. These ports could be fitted with a pitot tube for velocity measurements or a probe for particle sampling. When a pitot tube was used, differential pressures were determined by a 0-0.25 mm in H_2O Magnehelic gage equipped with a high pressure case that could accept total pressures up to 100 psig. The gage was protected by 50 psig cracking pressure check valves. A thermowell was provided for a thermometer to measure stagnation temperature and a pressure tap was fitted with a large dial calibrated pressure gage for the determination of stagnation pressure. Note that both of these fittings were located in a plane slightly downstream of the inlet of the sampling probe to avoid disturbance of the aerosol flow in the vicinity of the probe tip. Static pressure taps were also provided at the nozzle exit; the ratio of exit static pressure to total pressure was used to calculate the true exit Mach number.

As an experimental design consideration, it was considered necessary to perform all free jet aerosol sampling within the "potential core" of the jet to avoid the complication of expansion wave interactions. As an

apriori guideline, the data published by Broer and Rietdijk (65) was used to estimate the length, X_c, of the potential core of a fully expanded jet for the various nozzle exit Mach numbers (M_e) anticipated in the present study. Broer and Rietdijk (65) give experimentally derived values of X_c/D_e as a function of M_e, where D_e is the exit diameter of the nozzle, which for the present case was 5.08 cm. Table A-1 gives the resulting values of X_c.

Table A-1. Apriori estimates of potential core length.

Exit Mach Number (M_e)	X_c/D_e	X_c (cm)
0.2	2.8	14.2
0.6	3.5	17.8
0.8	4.0	20.3
1.3	6.0	30.5
1.5	7.0	35.6

Since the experimental sampling probe inlets were placed approximately 1.3 cm from the nozzle exit, they were, based on these predicted values of X_c, well within the potential core of the free jets. Subsequently, X-Y velocity traverses in the free jet, confirmed this prediction; these data are given in Appendix B.

Axisymmetric Flow Nozzle Design Equations

A. Subsonic nozzle (Figure A-4)

The subsonic nozzle coordinates were given by the equation:

$$R = 2.3 - \{0.65\ [4-(X-1.6601)^2]^{1/2}\} \qquad \text{(A-1)}$$

For $0 \leq X \leq 1.6601$ inches

and,

$R = 1.000$ inches

For $1.6601 \leq X \leq 3.0101$ inches

B. Supersonic nozzle with design exit Mach number of 1.3 (Figure A-4)

For $0 \leq X \leq 2.0809$ inches,

Coordinates were given by the equation:

$$R = 4.8455 - [15.0265 - (X-2.0809)^2]^{1/2} \qquad \text{(A-2)}$$

For $2.0809 \leq X \leq 3.6161$ inches, coordinates are given in Table A-2.

Table A-2. Nozzle contour coordinates for Mach 1.3 nozzle.

X	R	X	R	X	R
2.0809	0.9691	2.5080	0.9809	3.0863	0.9963
2.1028	0.9692	2.5495	0.9823	3,1335	0.9971
2.1240	0.9695	2.5917	0.9837	3,1808	0.9977
2.1514	0.9700	2.6344	0.9850	3.2284	0.9983
2.1781	0.9706	2.6777	0.9864	3,2762	0.9989
2.2085	0.9714	2.7215	0.9877	3.3243	0.9992
2.2413	0.9722	2.7657	0.9890	3.3727	0.9995
2.2759	0.9733	2.8104	0.9903	3.4211	0.9998
2.3120	0.9744	2.8555	0.9914	3.4697	0.9998
2.3493	0.9756	2.9010	0.9926	3.5184	0.9999
2.3877	0.9768	2.9467	0.9937	3.5672	1.0000
2.4270	0.9781	2.9930	0.9947	3.6161	1.0000
2.4671	0.9795	3.0395	0.9955		

C. Supersonic nozzle with design exit Mach number of 1.5 (Figure A-4)

For $0 \leq X \leq 2.0951$ inches,

Coordinates were given by the equation:

$$R = 4.6140 - [13.625 - (X-2.0951)^2]^{1/2} \quad \text{(A-3)}$$

For $2.0951 \leq X \leq 4.2288$ inches, coordinates are given in Table A-3.

Table A-3. Nozzle contour coordinates for Mach 1.5 nozzle.

X	R	X	R	X	R
2.0951	0.9228	2.6432	0.9518	3.4247	0.9906
2.1175	0.9228	2.6882	0.9546	3.4767	0.9922
2.1403	0.9232	2.7340	0.9575	3.5291	0.9936
2.1633	0.9238	2.7803	0.9604	3.5817	0.9948
2.1874	0.9246	2.8272	0.9631	3.6347	0.9959
2.2107	0.9256	2.8746	0.9659	3.6878	0.9969
2.2403	0.9271	2.9226	0.9687	3.7412	0.9976
2.2829	0.9293	2.9710	0.9713	3.7948	0.9983
2.3169	0.9312	3.0199	0.9738	3.8486	0.9988
2.3531	0.9334	3.0692	0.9763	3.9025	0.9993
2.3910	0.9357	3.1189	0.9787	3.9567	0.9995
2.4303	0.9381	3.1690	0.9811	4.0109	0.9998
2.4709	0.9407	3.2194	0.9832	4.0653	0.9999
2.5127	0.9434	3.2702	0.9853	4.1197	0.9999
2.5553	0.9461	3.3214	0.9872	4.1734	1.0000
2.5988	0.9490	3.3729	0.9890	4.2288	1.0000

Aerosol Generator

The aerosol generator employed in this program is shown in Figures A-9 and A-10. The sizing of the equipment was, for the most part, based on information received in communications with Donald Fenton and Earl O. Knutson of the Fine Particle Research Laboratory at IITRI (45). Stearic acid was selected as the aerosol material. Stearic acid has been used in condensation type aerosol generators by Werle et al. (48) and, in fact, was used in the original work of Sinclair and LaMer (46) and Rappaport and Weinstock (47). Stearic acid is a solid at room temperature but has a melting point of only 70 C. Liquid stearic acid particles retain a nearly

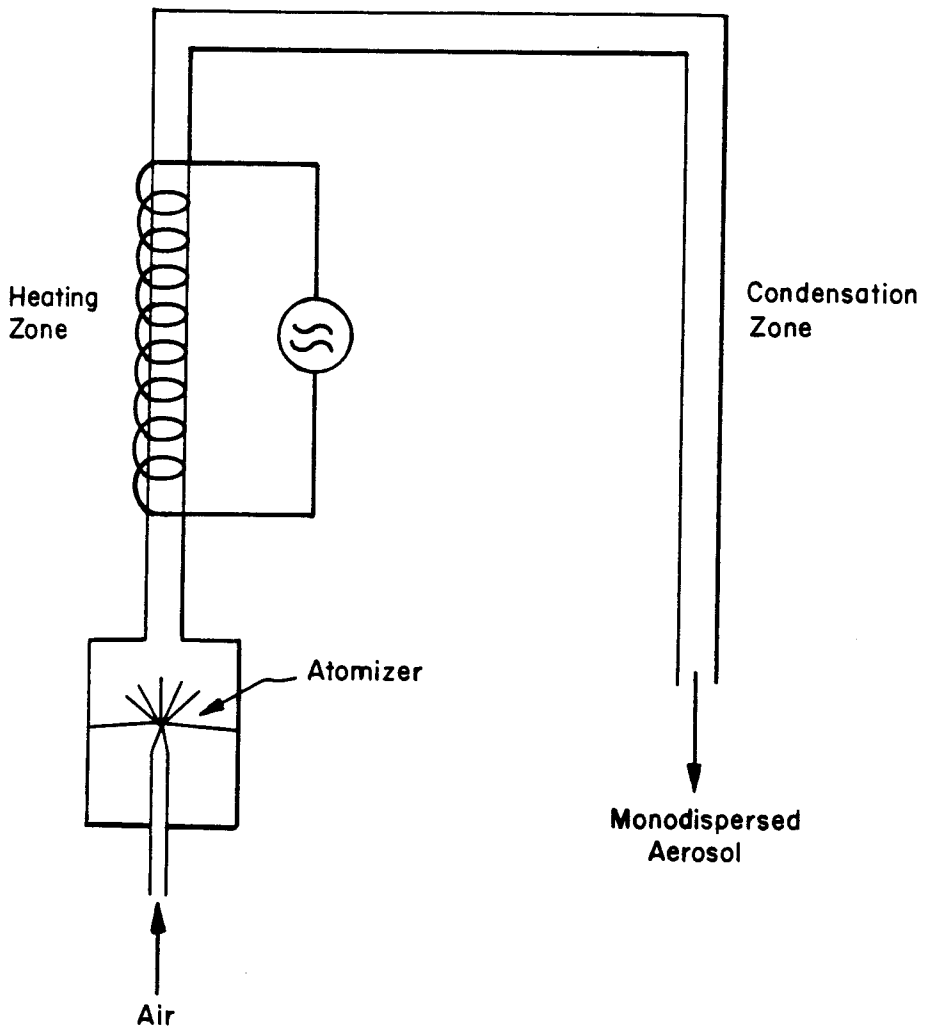

Figure A-9. Conceptual diagram of LaMer aerosol generator

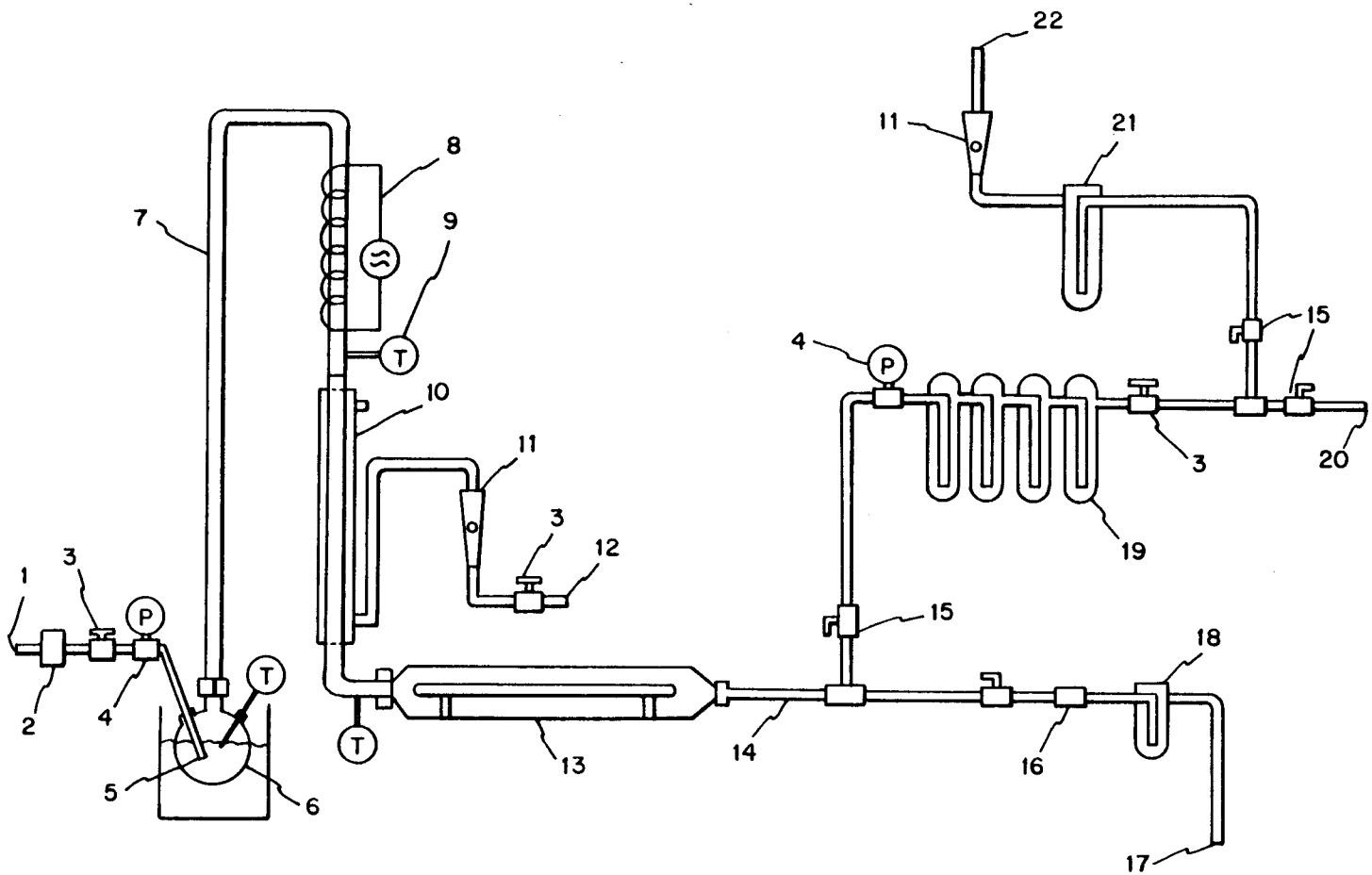

Figure A-10. Schematic diagram of aerosol generating system. Descriptions of these items appear in the pages following.

Key to Figure A-10

1. Regulated wind tunnel quality air inlet.
2. Royco Model 12 filter.
3. Metering valve.
4. Pressure gage.
5. Atomizer - 27 No. 81 holes drilled in 1/4" stainless steel tubing.
6. Stearic acid reservoir (approximate capacity 1000 ml) submerged in thermostatically controlled water bath, nominal temperature = 90C.
7. Stainless steel tubing, 1-1/2" OD.
8. Heating tape, heavy duty.
9. Thermometer.
10. Heat exchanger.
11. Rotameter.
12. Cooling water inlet.
13. Aerosol charge neutralizer.
14. Stainless steel tubing, 1/2" O.D.
15. Ball valves.
16. Check valve, 1/3 psi cracking pressure.
17. Aerosol discharge to settling chamber.
18. Simple U-tube trap.

19. Glass wool packed filters.
20. By-pass discharge line to room.
21. Norgren Ultra-air filter.
22. Discharge line to room.

spherical shape as they solidify and therefore result in a precisely sized, stable aerosol (48). Certain properties of stearic acid are presented in Appendix D.

There are a few differences between the generator constructed for this program and the high volume condensation generator used by IITRI (48). The first difference is in construction; the generator presently employed had to be hydrostatically tested at a pressure of 225 psig; accordingly, glass was not used as a construction material. The IITRI generator did not use a nucleating agent such as anthracene and, therefore, the requirement for uniform cooling of the condensing vapor stream was probably critical because the generator did not have the advantage of stable nuclei on which the vaporized material could recondense. The IITRI generator did not include an aerosol charge neutralizer.

When aerosol production from the LaMer generator (Figure A-10) was desired, the submerged orifice in the thermostatically controlled reservoir of molten stearic acid was pressurized, introducing a dense polydisperse spray ahead of the evaporator. The evaporator was located so that thermally degraded constituents formed in contact with the hot evaporator wall can not drain back into the reservoir with the molten stearic acid. The perforated plate at the inlet to the evaporator was intended to encourage flow distribution downstream of the

90° bend which was just ahead of the evaporator. The plate between the evaporator and condenser also promoted good flow distribution and a uniform temperature profile at the entrance to the condensing section. Temperatures of about 300 C were achieved in the evaporator.

The condenser was immediately below the evaporator and consisted simply of a counter current single pass shell and tube heat exchanger using water as the cooling liquid. After leaving the condenser, the generated aerosol passed through a charge neutralizer before delivery to the air flow system or to a series of glass wool packed traps which were used during the start-up and by-pass operation of the generator.

Because of the similarity between the IITRI generator and the one used in this study it was likely that their performance characteristics would be comparable. The IITRI generator reported an output of 0.3 gm/min consisting of 0.7 micrometer diameter particles at a concentration of about 10^6 particles/cm^3 with a geometric standard deviation typically less than 1.12 (45).

The generator flow rate was about 42 liters/min. (1.5 cfm) when a critical pressure drop was maintained across the atomizer nozzle submerged in the stearic acid reservoir. Since the air pressure delivered to the

generator could be increased to the line pressure (150 psig) it was possible to maintain a 30-40 liter/min flow rate through the generator even when the settling chamber pressures were increased to achieve the higher Mach numbers.

Based on an aerosol generator output of approximately 10^6 particles/cm^3 and a maximum air flow system dilution factor of 10^3, minimum aerosol concentrations on the order of 10^3 particles/cm^3 or 0.2 mg/m^3 were expected in the settling chamber and in the free jet. (Note: In actual practice, the lowest measured free stream aerosol concentration, C_o, was 1.5 mg/m^3.)

Aerosol Charge Neutralizer

In this study a 10 mCi ^{106}Ru-^{106}Rh beta radiation source was used in the aerosol charge neutralizer (Figure A-11). The neutralizer design was based on guidelines presented by Cooper and Reist (59). Basically, the particles are considered to have an initial charge at the Rayleigh limit (i.e. maximum charge before the particles become mechanically unstable) and the particle residence time in the neutralizer is selected to be approximately 30 times longer than the required time predicted from theory.

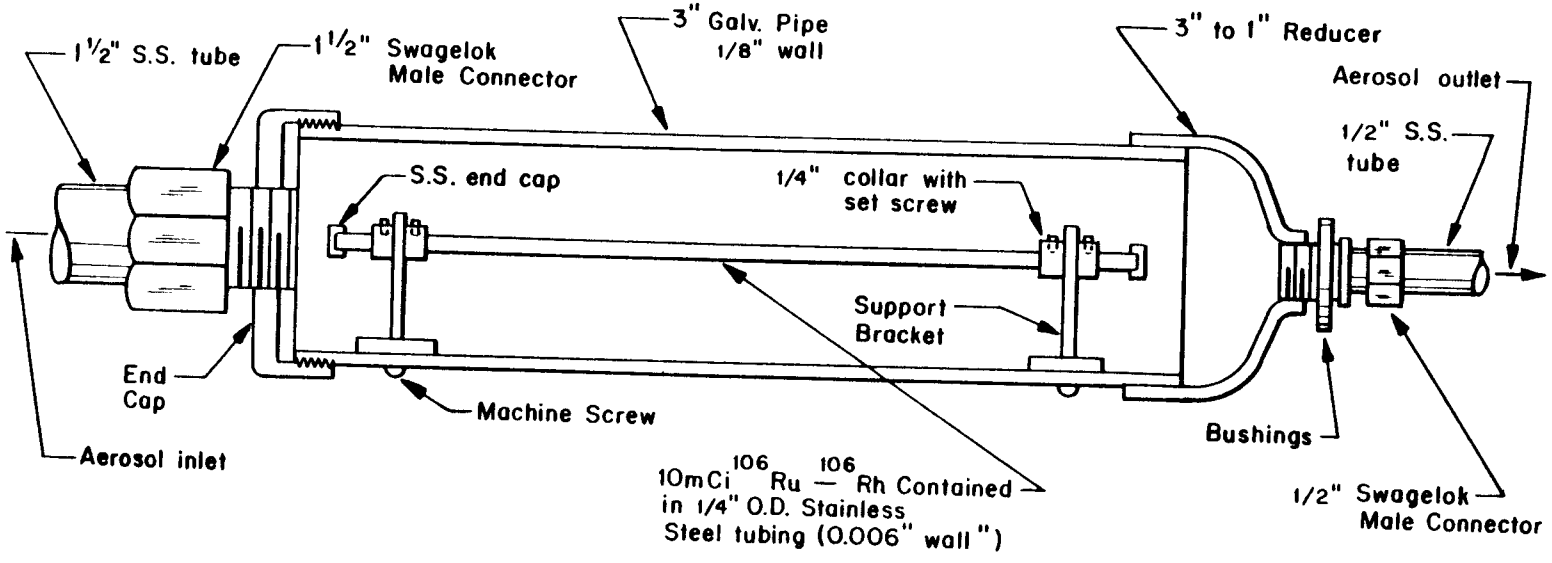

Figure A-11. Schematic diagram of aerosol charge neutralizer.

Aerosol Charge Neutralizer Design

A. Given:

1. Radioactive source is Ruthenium-106/Rhodium-106 (^{106}Ru-^{106}Rh) electrodeposited on a thin wire sealed in a thin waled (0.006 in) stainless steel 1/4 in OD tube.

Half-life:	1.0 year
ß-energy:	3.6 Mev (Max.)
γ - energies:	0.5 - 2.9 Mev

2. To achieve a Boltzmann charge equilibrium the aerosol must be in contact with a concentration of at least 10^6ions/cm^3 (n_∞) with the ratio (t*) of residence time t_{res}, to neutralization time τ, on the order of 30 (Cooper and Reist (59))

3. Assume an initial aerosol particle charge equal to the Rayleigh upper limit.

4. Outer cylinder of charge neutralizer is 3" carbon steel pipe (3.25" OD, 3" ID), approximately 20" long (L).

5. Assume maximum flow rate, Q_{max}, through neutralizer is 2 cfm.

B. Since the thin walled tube containing the radioactive source could possibly be exposed to positive pressure up to 150 psig, calculate collapsing pressure of the tube, P_C.

According to Jasper and Sullivan (66), the collapsing pressure, P_C, for a long thin-walled

commercial lap-welded steel tube is:

$$P_C = 50{,}200{,}000\left(\frac{t}{D}\right)^3 \qquad \text{(A-4)}$$

D = OD of tube, inches

t = wall thickness of tube, inches

P_C = collapsing pressure, psi

Equation (A-4) applies when D<40t

For the present case;

$$\frac{D}{t} = \frac{0.25}{0.006} = 41.6 \approx 40$$

$$P_C = 50{,}200{,}000\left(\frac{0.006}{0.25}\right)^3 = 693.9 \text{ psi}$$

and,

$$\text{Safety factor} = \frac{693.9}{150} = 4.6$$

C. Calculate linear absorption coefficients, in air, μ_{air}, and stainless steel, μ_{steel}, for source ß energy. In general, for ß emitters (59),

$$\mu = 17\rho E_{max}{}^{-1.14} \qquad \text{(A-5)}$$

where ρ = density of medium (gm/cm^3)

E_{max} = maximum ß energy (Mev)

$$\rho_{air} \approx 0.15 \frac{Lb}{ft^3} \times 454 \frac{gm}{Lb} \times \frac{1 ft^3}{28,317\ cm^3} = 0.0024 \frac{gm}{cm^3}$$

$$\rho_{steel} = 489 \frac{Lb}{ft^3} = 7.84 \frac{gm}{cm^3}$$

Therefore,

$$\mu_{air} = (17)\ (0.0024)\ (3.6)^{-1.14} = 0.00947\ cm^{-1}$$

$$\mu_{steel} = (17)\ (7.84)\ (3.6)^{-1.14} = 30.94\ cm^{-1}$$

D. Calculate specific ionization constant, k, ion pairs produced per cm per beta.

According to Cooper and Reist (59),

$$k = (17/3)\ \rho\ E_{max}^{-0.14} / (34\ ev/ion\ pair) \qquad (A\text{-}6)$$

Assume, ρ_{air} at ambient pressure (i.e., worst case) is $0.0012\ gm/cm^3$

or,

$$k_{air} = 167.17 \frac{ion\text{-}pairs}{cm\text{-}beta}$$

E. Calculate neutralization time, τ, and the required line source strength, S, in betas produced per second and millicuries (mCi)

We know,

$$V_{max} = \text{maximum aerosol velocity through neutralizer} = \frac{Qmax}{A} \qquad (A\text{-}7)$$

$$A = \text{flow area} = \pi r^2 = \frac{(3.14)\ (1.5)^2}{144} = 0.049\ ft^2$$

$$Q_{max} = \text{maximum volumetric aerosol flow rate through neutralizer} = 2 \frac{ft^3}{min}$$

Therefore;

$$V_{max} = \frac{2\ ft^3/min}{0.049\ ft^2} = 40.8\ ft/min$$

$$V_{max} = \frac{40.8\ ft/min}{60\ \frac{sec}{min}} = 0.68\ ft/sec$$

and,

$$\tau_{res} = \frac{L}{V_{max}} = \frac{20in \times \frac{1ft}{12in}}{0.68\ ft/sec} = 2.45\ sec \qquad (A-8)$$

Therefore,

$$\tau = \text{approximate neutralization time} = \frac{t_{res}}{t^*} \qquad (A-9)$$

$$\tau = \frac{2.45\ sec}{30} = 0.0816\ sec$$

According to Cooper and Reist (59);

$$n_\infty \approx 2\ [kS/(4r_o H\alpha)]^{1/2} \qquad (A-10)$$

where,

n_∞ = equilibrium ionic concentration (ions/cm^3)

As design guideline, select;

$n_\infty = 6 \times 10^6$ ions/cm^3 This corresponds to values of n_∞ for commercially available neutralizers (59)

k = specific ionization constant= 167.17 $\frac{\text{ion-pairs}}{\text{cm-beta}}$

r_o = radius of cylinder = 1.5 in = 3.81 cm

H = length of source = 20 in = 50.8 cm

α = recombination coefficient = 3×10^{-6} cm^3/sec

S = line source activity (betas/sec)

Solving for S,

$$n^2_\infty \approx 4kS/(4r_oH\alpha) \qquad \text{(A-11)}$$

or

$$S \approx \frac{r_oH\alpha n_\infty^2}{k} \qquad \text{(A-12)}$$

substituting,

$$S = \frac{(3.81\text{cm})\ (50.8\text{cm})\ (3\text{x}10^{-6}\ \text{cm}^3/\text{sec})(36\text{x}10^{12}\frac{\text{ions}}{\text{cm}^6})}{167.17\ \frac{\text{ion-pairs}}{\text{cm-beta}}}$$

$$S = 125 \times 10^6\ \frac{\text{betas}}{\text{sec}}$$

Since,

$$1\ \text{mCi} = 3.7 \times 10^7\ \text{betas/sec}$$

$$S = 125 \times 10^6\ \frac{\text{betas}}{\text{sec}} \times \frac{\text{mCi}}{3.7 \times 10^7\ \text{beta/sec}} = 3.37\ \text{mCi}$$

F. Calculate required source activity, S_o, if required line source strength, S = 3.37 mCi

This calculation accounts for fact that source, S_o, is contained in a stainless steel thin walled tube.

From Moore (67),

$$S = S_o \exp(-\mu_{steel}\ x_{steel}) \qquad \text{(A-13)}$$

μ_{steel} = absorbtion coefficient = 30.94 cm^{-1}

x_{steel} = wall thickness = 0.006 in = 0.0152 cm

Therefore,

$$\frac{S}{S_o} = \exp(-30.94 \times 0.0152)$$

$$\frac{S}{S_o} = \exp(-0.47) = 0.625$$

$S_o = S/0.625 = 5.39$ mCi

Since $^{106}Ru - ^{106}Rh$ has a 1 year half life and since the aerosol charge neutralizer would be required to be in use for up to 1 year, a 10mCi source was selected to insure sufficient activity throughout the experimental period.

Sampling Systems

There were two particle sampling systems constructed for use in this study. One system was used to sample the generated aerosol within the settling chamber just upstream of the sonic or supersonic nozzle. Since aerosol velocities in the settling chamber were expected on the order of only 20 ft/sec (less than Mach 0.05), it was assumed that correct isokinetic sampling procedures would give an accurate representation of the size distribution and mass concentration of the particles in the generated aerosol. The other sampling system used small bore probes to sample particles within the potential core of near sonic or supersonic free jets. Data from both systems were compared to determine the representativeness of the free jet sample.

Except for certain size differences, the two sampling systems were identical. For example, the settling chamber sampler had a probe with a 20.0 mm

(0.782 in) inlet diameter and a 1/2 hp vacuum pump (Gast model 0822) while the free jet sampler had a set of four probes with inlet diameters which ranged between 2.76 mm (0.109 in) and 5.15 mm (0.177 in) and a 3 hp vacuum pump (Gast model 5565). In both samplers the stearic acid particles were collected on 142 mm diameter, 0.4 micron pore size Nuclepore polycarbonate membrane filters. The filters were supported in double o-ring sealed stainless steel filter enclosures which were specially designed and constructed for tight positive pressure or vacuum operation (10)(See Figure A-12). From the probe inlet up to the filter housings both samplers employed stainless steel tubing and Swagelok or Brazetyte tube fittings; downstream of the filter housing 1/2" or 3/4" galvanized pipe fittings were employed.

Since both aerosol sampling systems had an orifice meter to measure the sampling flow rate located downstream of the vacuum pump, it was necessary to determine if pump leaks were significant relative to the total sampling rate. To determine pump leaks, the sampling probe inlet was blocked and the vacuum pump was operated such that outlet air was recycled to provide the pump inlet air; any overflow air (i.e. leaks) passed through a wet test meter or calibrated orifice meter. Pump vacuum was adjusted with a needle valve located between the pump inlet and outlet. The

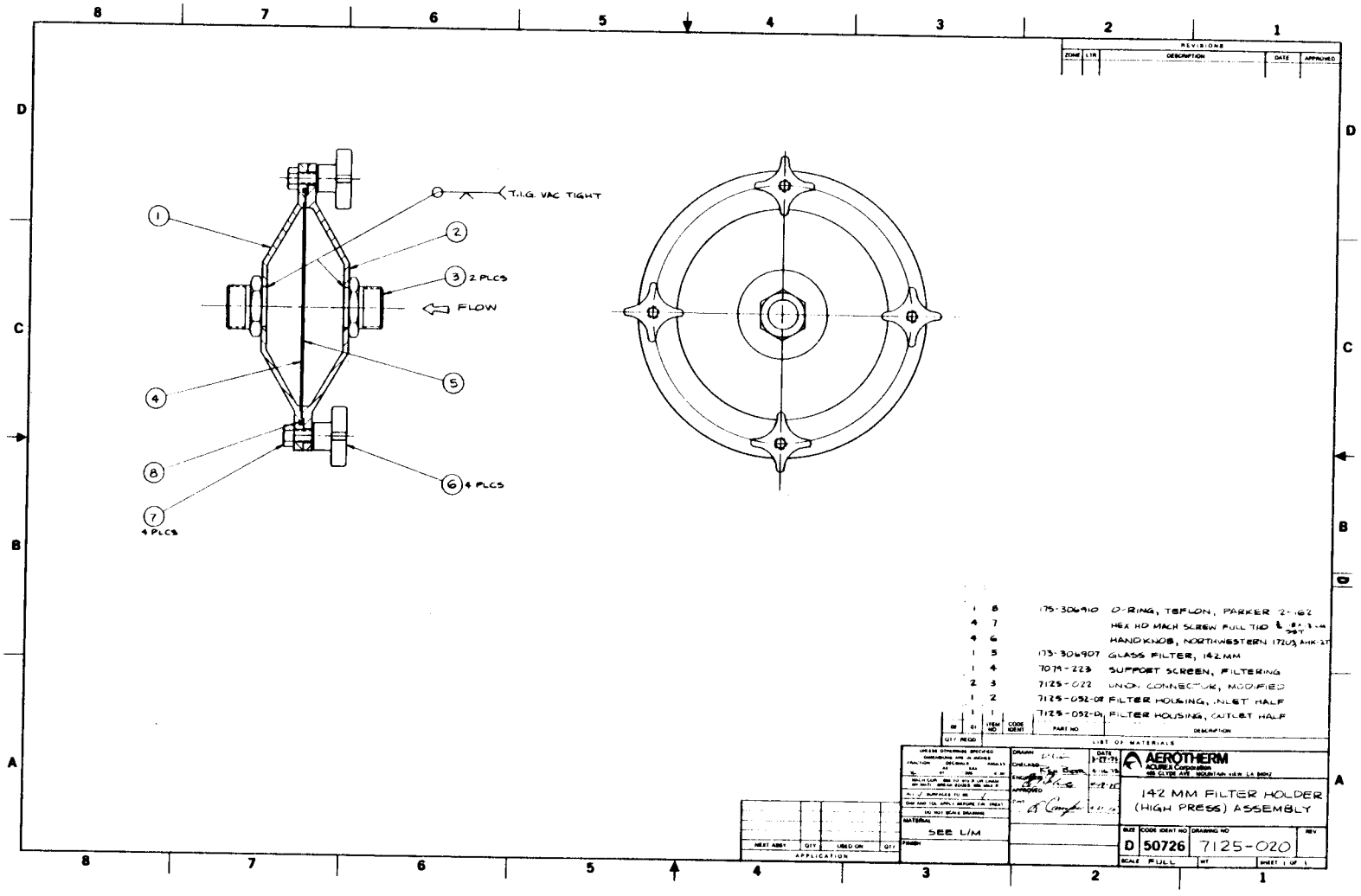

Figure A-12. Polycarbonate filter holder assembly.

settling chamber pump had a maximum inboard leak of 0.04 scfm at 10" Hg vacuum while the free jet pump had an outboard leak of 0.27 scfm at 13" Hg vacuum and an inboard leak of 0.55 scfm at 16" Hg vacuum. Since the settling chamber isokinetic sampling rates ranged from 4.88 to 12.41 scfm, the settling chamber pump leak rate was negligible. Free jet isokinetic sampling rates ranged from 7.0 to 19.9 scfm and, therefore, the pump leak constituted 3-4% of the total measured flow. Pump vacuum ranged from 13" Hg (for Me = 0.6, 0.8 and 1.47) to 16" Hg (for Me = 1.26) to achieve isokinetic sampling rates. It is important to note that except for sampling rates approaching isokinetic (i.e., $U/U_O > 0.8$), it was not necessary to use the free jet sampling pump to achieve the desired subisokinetic sampling rates in the free jet. The sampling system set points are discussed more thoroughly in Appendix C.

The set of free jet sampling probes consisted of three that were used to evaluate probe wall effects and one that was used to determine the effect of anisokinetic sampling in near sonic and supersonic free jets. The inlet dimensions of the probes were chosen to be representative of probe designs currently used in gas turbine exhaust sampling. The supersonic probe was designed and fabricated by Aerotherm Acurex Corporation. It is a reproduction of a probe inlet that Aerotherm used

in a prototype aircraft sampling system which they developed under contract with the Air Force and the Navy.(10).

The Aerotherm sampling probe, shown in Figures 12 and 13, is designed as a divergent supersonic inlet. For low supersonic Mach numbers (less than Mach 1.6) the divergent inlet portion should, with sufficiently low back pressure, accelerate the flow to the vicinity of Mach 2. The flow is decelerated in a shock pattern within the constant area cross section immediately downstream of the divergent inlet. The installation of the constant area cross section enhances the pressure recovery characteristics of the probe and also promotes flow uniformity because the non-uniform flow which occurs in the vicinity of the normal shock is not permittted to enter the subsonic divergent portion of the probe. It should be noted that the supersonic inlet portion of the sampling nozzle has an intentional surface roughness to reduce the tendency of the shock to move once it is swallowed by the probe.

The settling chamber sampling probe and a representative subsonic free jet sampling probe are shown in Figures A-13 and A-14. Excluding the vacuum pumps and components downstream of the pumps, both samplers were hydrostatically tested at a pressure of 225 psig.

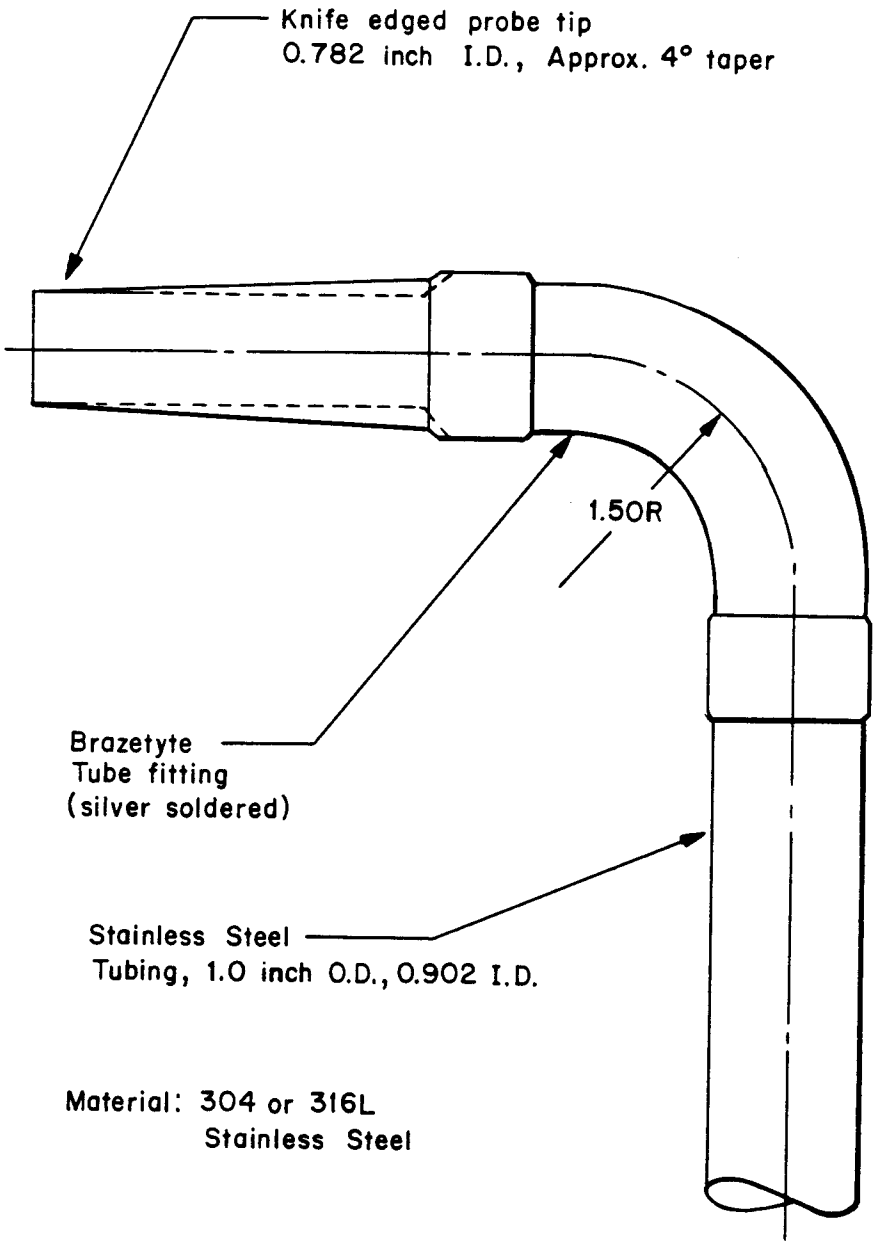

Figure A-13. Settling chamber sampling probe inlet.

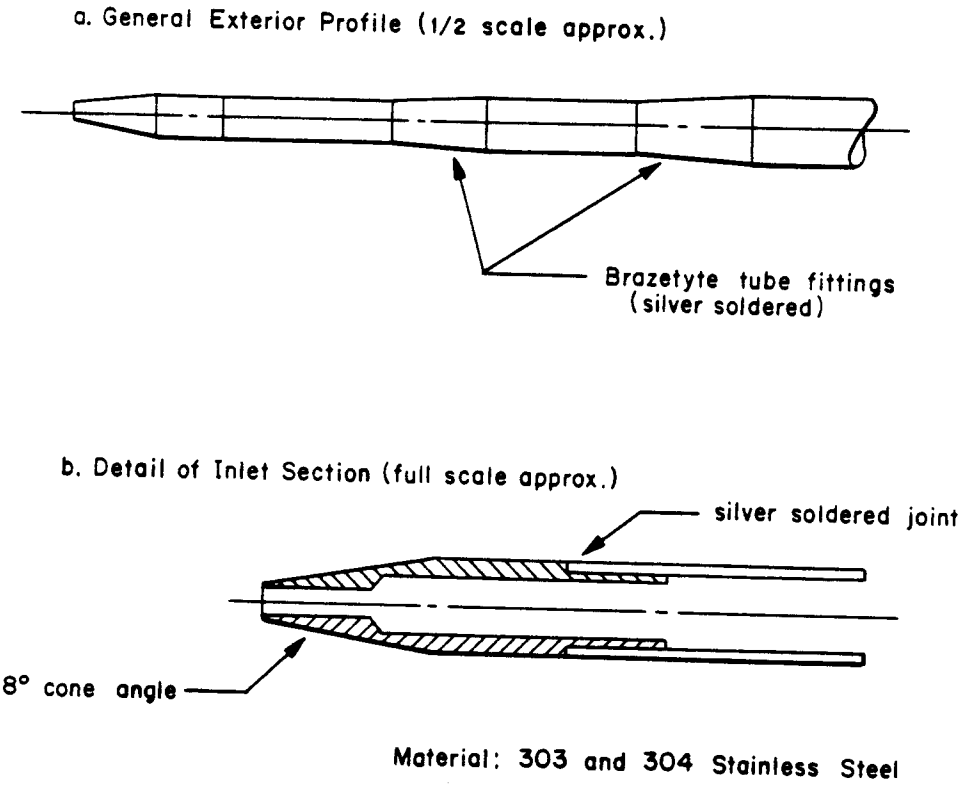

Figure A-14. Subsonic free jet sampling probe.

APPENDIX B

FREE JET AIR FLOW SYSTEM BASELINE DATA

A. Determination of true exit Mach number for supersonic flow nozzles.

The supersonic flow nozzles had design exit Mach numbers of 1.3 and 1.5. Initially, it was necessary to determine the true operating characteristics of these nozzles. This was accomplished by experimentally measuring the total or stagnation pressure, P_t, upstream of the nozzle when the free jet was properly expanded, that is, when the nozzle exit static pressure equalled ambient pressure. The true exit Mach number was determined from charts for compressible flow (61) based on the calculated ratio of exit static pressure to total pressure. The total pressure was measured in the settling chamber using a total pressure tube connected to a large dial calibrated pressure gage (Wallace and Tiernan Model FA234, S/N LL07542). Proper expansion of the supersonic jet was accomplished by connecting a static pressure tap located at the nozzle exit to a differential pressure gage (Dwyer Magnehelic gage, 0-25 in H_20 range) and adjusting P_t until the gage read zero (i.e., $P_{exit} - P_{amb} = 0$). Ambient pressure was measured with a laboratory quality mercury barometer.

Since each nozzle had multiple pressure taps located around the circumference of the nozzle exit, the procedure described above was repeated for four different pressure taps and the average P_t necessary to achieve proper expansion was used to calculate the ratio $\frac{P_{amb}}{P_t}$ and determine the exit Mach number, M_e from compressible flow charts.

For example:

For nozzles with design exit Mach numbers of 1.5 and 1.3 determine the true exit Mach numbers.

From barometer,

ambient pressure, P_{amb}, = 765.2 mmHg = 14.799 psia.

Establish properly expanded nozzle flow by adjusting P_t such that $P_{amb} - P_{exit} = 0$.

The following P_t's were measured when $P_{amb} - P_{exit} = 0$ at four different nozzle exit pressure taps.

Nozzle Exit Pressure Tap	Total Pressure, P_t M1.5 Nozzle (psia)	Total Pressure, P_t M1.3 Nozzle (psia)
1	51.4	38.4
2	52.0	38.6
3	52.0	38.4
4	52.2	39.4

For M1.5 nozzle,

$$P_{t_{ave}} = 51.9 \text{ psia}$$

and

$$\frac{P_{amb}}{P_{t_{ave}}} = \frac{14.8}{51.9} = 0.285$$

and from compressible flow chart for air,

$$Me = 1.47$$

For M1.3 nozzle,

$$P_{t_{ave}} = 38.7 \text{ psia}$$

and,

$$\frac{P_{amb}}{P_{t_{ave}}} = \frac{14.8}{38.7} = 0.382$$

and from compressible flow chart for air,

$$Me = 1.26$$

Calibration data for the large dial pressure gage used to measure P_t is given in Table B-1. Calibration was accomplished using a quartz gage standard at the NASA Ames Research Center calibration facility.

The subsonic flows, $M_e = 0.6$ and 0.8 were established by adjusting P_t to give the appropriate P_{amb}/P_t ratio as given in compressibility charts for subsonic flow. For $M_e = 0.6$, $P_{amb}/P_t = 0.784$ and for $M_e = 0.8$, $P_{amb}/P_t = 0.656$.

Table B-1. Pressure calibration for large dial pressure gage[1].

OBSERVED READING	STANDARD PRESSURE (psig)		
	RUN 1	RUN 2	RUN 3
0.00	0.00	0.00	0.00
5.00	5.12	5.04	5.08
10.00	10.12	10.08	10.13
15.00	15.10	15.12	15.09
20.00	20.13	20.10	20.09
25.00	25.00	24.97	24.99
30.00	30.10	29.96	30.01
35.00	35.09	34.90	35.00
40.00	40.06	39.82	39.86
45.00	45.01	44.85	44.83
50.00	50.02	49.85	49.98
55.00	55.02	54.89	54.88
60.00	60.05	59.97	60.05
65.00	65.01	64.84	64.90
70.00	70.00	69.82	69.96
75.00	75.00	74.86	74.95
80.00	79.84	79.79	79.91
85.00	84.80	84.75	84.86
90.00	89.82	89.82	89.91
95.00	94.84	94.80	94.90
100.00	99.79	99.82	99.88

[1] Wallace and Tierman Model FA234 S/N LL07542 Range 0-300 psig calibrated 10-16-75.

For day-to-day operation of the free jet system, the appropriate P_t was determined by measuring ambient atmospheric pressure, P_{amb}, in mm Hg and calculating the operating gage pressure, P'_t from the relationships given in Table B-2.

Table B-2. Settling chamber gage pressures for desired nozzle exit Mach numbers

Desired Nozzle Exit Mach Number (M_e)	Settling Chamber Pressure, P'_t (psig)
0.6	0.00533 P_{amb}[1]
0.8	0.0101 P_{amb}
1.26	0.0312 P_{amb}
1.47	0.0484 P_{amb}

1 ambient pressure measured in mm Hg.

B. Settling chamber velocity profiles

To determine the velocities required for eventual isokinetic sampling in the settling chamber, it was necessary to perform x-y velocity traverses. These were accomplished using a stainless steel pitot tube attached to a Dwyer Magnehlic gage (0-0.25 in H_20 range). Velocity pressures were measured at 1 inch intervals from

the chamber wall in the x and y orientation for a total of 22 points for each Me (i.e., 0.6, 0.8, 1.26, and 1.47) (Figure B-1). These traverses were repeated three times for Me = 0.6 and 0.8 and once for Me = 1.26 and 1.47. Air velocity was calculated by:

$$V \left(\frac{ft}{sec}\right) = 18.278 \left(\frac{h_v}{\rho}\right)^{1/2} \qquad \text{(B-1)}$$

where

ρ = air density = $1.325 \times \frac{P_t}{T_t} \quad \frac{lbs}{ft^3}$

P_t = stagnation pressure (in Hg)

T_t = absolute temperature (R)

h_v = velocity pressure in H_2O

Tables B-3 and B-4 give these data.

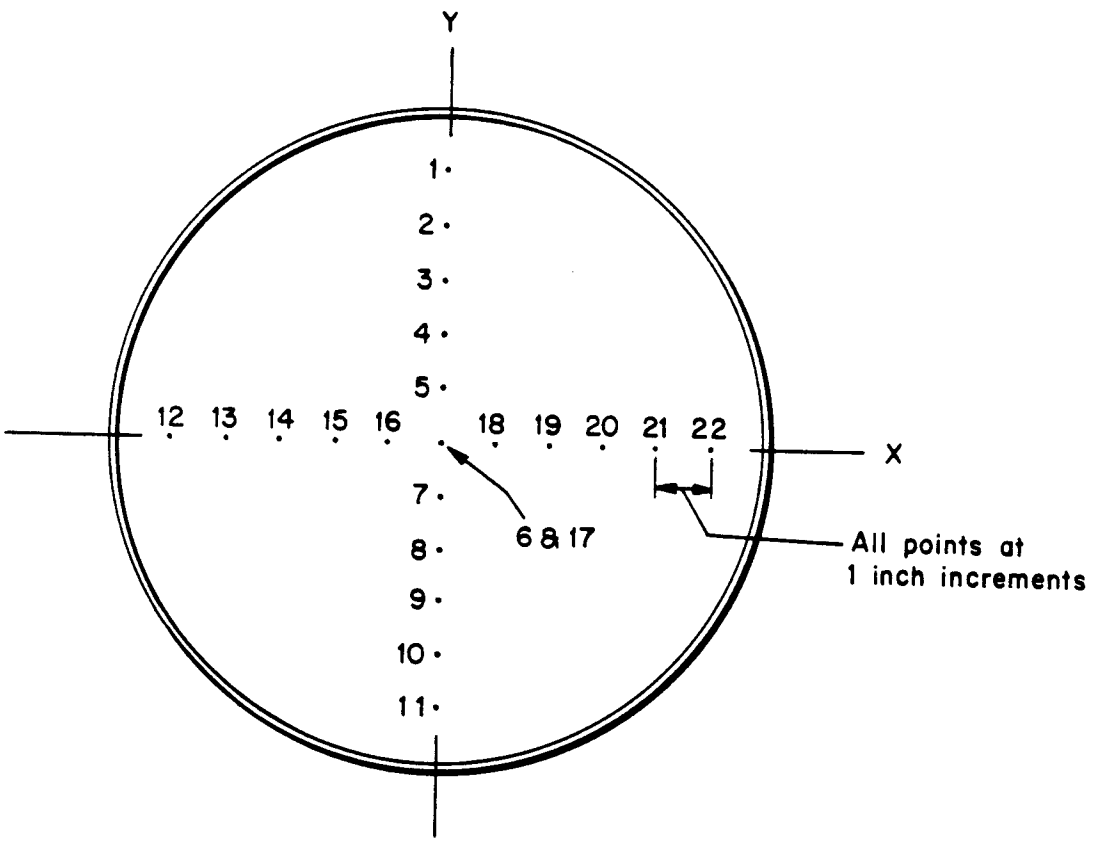

Figure B-1. Settling chamber air velocity measurement locations.

Table B-3. Settling chamber air velocity profiles.

Measurement Location	Nozzle exit Mach no. (M_e) 0.6 Velocity (ft/sec)			0.8 Velocity (ft/sec)			1.26 Velocity (ft/sec)	1.47 Velocity (ft/sec)
	Run 1	Run 2	Run 3	Run 1	Run 2	Run 3	Run 1	Run2
1	16.5	16.6	17.0	19.5	19.6	19.8	19.0	16.7
2	16.8	17.4	17.4	20.3	20.5	20.8	19.5	17.1
3	17.6	17.7	17.9	20.8	21.0	21.1	20.0	17.4
4	18.3	18.6	19.2	20.3	21.0	20.9	20.1	17.8
5	18.7	19.0	19.2	21.0	21.3	21.5	20.2	18.2
6	18.9	19.2	19.9	21.1	21.2	21.4	20.1	17.5
7	18.9	19.1	19.8	21.0	21.1	21.4	19.6	17.1
8	18.2	18.8	19.4	20.9	21.0	21.2	19.4	17.7
9	17.7	17.7	18.7	20.5	20.8	20.9	17.3	16.8
10	16.4	16.9	18.6	19.5	19.5	20.0	19.5	16.3
11	16.2	16.8	17.6	18.0	18.2	18.2	16.3	17.1
12	17.5	17.7	18.0	19.1	19.1	19.4	19.8	18.6
13	17.4	17.4	17.6	19.8	20.1	20.3	19.1	17.7
14	17.8	17.9	18.5	20.1	20.3	20.5	19.5	17.1
15	18.1	18.6	19.0	20.8	21.1	21.1	19.9	17.6
16	18.8	19.0	19.4	21.2	21.2	21.3	20.4	18.0
17	19.2	19.7	20.0	21.5	21.6	21.6	20.5	18.5
18	18.3	18.6	19.0	21.2	21.8	21.8	20.3	18.2
19	18.5	18.5	19.0	20.5	20.9	21.1	18.7	18.1
20	18.1	18.3	19.0	20.8	21.0	21.0	19.3	17.9
21	18.2	18.3	19.1	20.8	21.0	21.1	19.6	17.8
22	18.1	18.1	18.9	21.2	21.2	21.4	19.9	18.2
Average	17.9	18.2	18.7	20.5	20.7	20.8	19.5	17.6

Table B-4. Settling chamber air velocity profile summary.

	Nozzle exit Mach no. (M_e)			
	0.6	0.8	1.26	1.47
(1) Average velocity (ft/sec)	18.3	20.7	19.5	17.6
Average velocity (m/sec)	5.6	6.3	5.9	5.4
(2) Average centerline velocity (ft/sec)	19.5	21.4	20.1	18.0
Average centerline velocity (m/sec)	5.9	6.5	6.1	5.5
$\frac{(2) - (1)}{(2)} \times 100$ (%)	5.1	3.0	3.2	1.8
Maximum difference (%) between (2) and lowest measured velocity	14.4	15.4	16.4	9.4

C. Nozzle exit velocity profiles.

To avoid shock wave interaction effects, it was desirable to locate the free jet sampling proble within the potential core where the jet velocity is equal to the nozzle exit velocity. Fourteen point velocity traverses were made in the free jet 1.3 cm downsteam of the nozzle exit to confirm that this location was in the potential core. Total pressure was measured across the 5.08 cm (2 inch) diameter nozzle in 0.63 cm (0.25 inch) increments. Total pressure measurements were made using a total pressure tube connected to a calibrated transducer (0-100 psi range) equipped with a digital display. The transducer was calibrated immediately before and after each set of pressure measurements using a calibrated large dial pressure gage (Table B-1). Figure B-2 shows the measurement locations. Mach number was determined by calculating the ratio of static pressure, P_1, (i.e., ambient pressure) to the measured total pressure, P_t and then using this ratio to interpolate compressibility tables for air (61). Table B-5 gives these data.

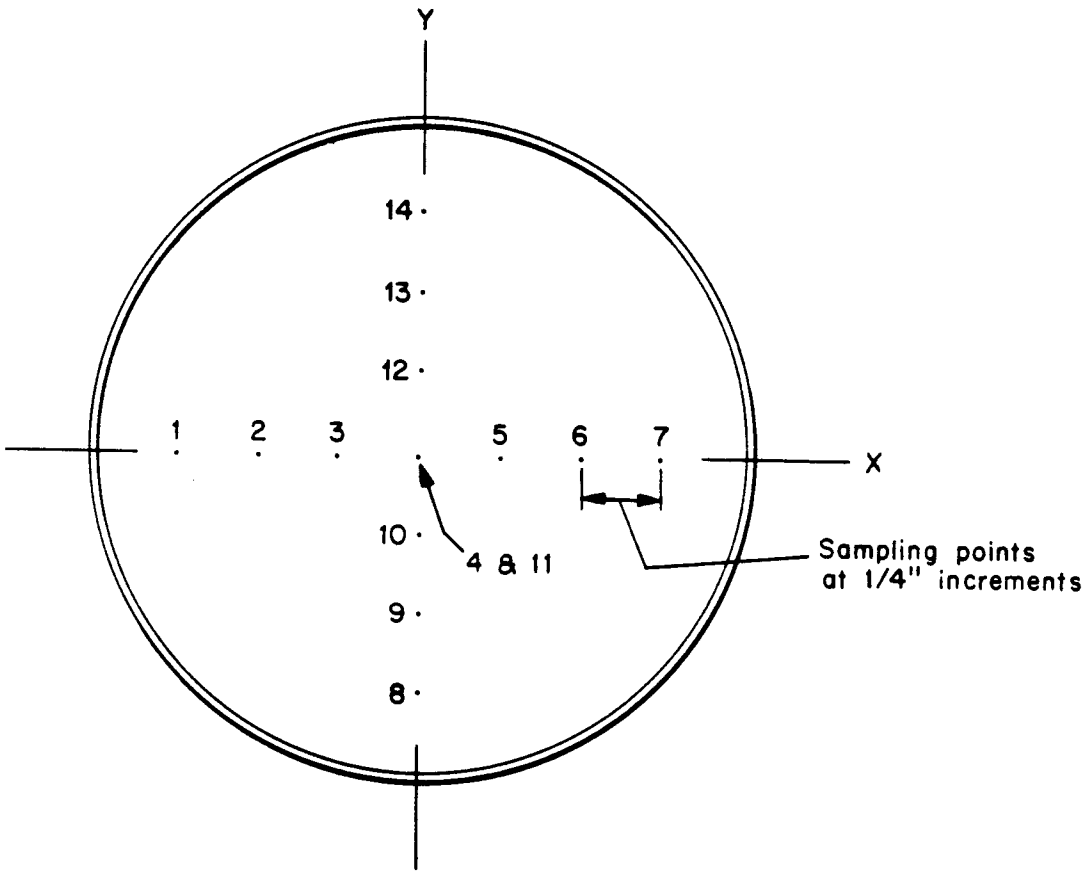

Figure B-2. Free jet air velocity measurement locations.

Table B-5. Free jet velocity profiles downstream of nozzle exit.

	Nozzle exit Mach no. (M_e) 0.6			0.8		
Measurement Location[1]	P_t(psia)	P_1/P_t	M	P_t(psia)	P_1/P_t	M
1	18.95	0.7810	0.605	22.48	0.6584	0.796
2	18.98	0.7798	0.607	22.43	0.6598	0.794
3	18.95	0.7798	0.607	22.50	0.6577	0.797
4	18.98	0.780	0.606	22.48	0.6584	0.796
5	18.93	0.7818	0.603	22.45	0.6592	0.795
6	18.90	0.783	0.601	22.48	0.6584	0.796
7	18.93	0.7818	0.603	22.45	0.6592	0.795
8	18.93	0.7818	0.603	22.45	0.6592	0.795
9	18.95	0.7810	0.605	22.45	0.6592	0.795
10	18.95	0.7810	0.605	22.41	0.6604	0.793
11	18.95	0.7810	0.605	22.45	0.6592	0.795
12	18.93	0.7818	0.603	22.45	0.6592	0.795
13	18.98	0.7798	0.607	22.48	0.6584	0.796
14	18.95	0.7810	0.605	22.43	0.6598	0.794
Average M			0.605			0.795

1 All measurements were made 1.3 cm downstream of nozzle exit.

Table B-5. (Continued)

	Nozzle exit Mach no. (M_e) 1.26			1.47		
Measurement Location[1]	P_t(psia)	P_1/P_t	M	P_t(psia)	P_1/P_t	M
1	38.25	0.3869	1.259	48.4	0.3058	1.462
2	38.25	0.3869	1.259	48.1	0.3077	1.456
3	38.35	0.3859	1.261	48.2	0.3071	1.458
4	38.25	0.3869	1.259	48.2	0.3071	1.458
5	37.90	0.3905	1.259	48.1	0.3071	1.458
6	38.25	0.3869	1.259	47.8	0.3096	1.451
7	38.25	0.3869	1.259	48.1	0.3077	1.456
8	38.25	0.3869	1.259	48.6	0.3045	1.465
9	38.25	0.3869	1.259	48.7	0.3039	1.467
10	38.15	0.3879	1.257	48.5	0.3052	1.463
11	38.25	0.3869	1.259	48.5	0.3052	1.463
12	38.00	0.3895	1.253	48.2	0.3071	1.458
13	38.25	0.3869	1.259	48.7	0.3039	1.467
14	38.25	0.3869	1.259	48.7	0.3039	1.467
Average M			1.258			1.461

1 All measurements were made 1.3 cm downstream of nozzle exit.

D. Free jet system flow parameters.

Table B-6 gives the nominal isentropic flow and normal shock parameters for the free jet airflow system. The basic assumptions for these data are:

1. Ratio of specific heats for air = γ = 1.4
2. Total temperature, T_t, in settling chamber = 530R.
3. Ideal gas behavior
4. Nozzle exit static pressure, P_{exit} = 14.7 psia

In actual practice, T_t ranged from 520 - 537R and P_{exit} from 14.7 to 14.9 psia. The parameter ratios given in Table B-6 are from standard compressible flow tables. The mass flow, G, was calculated using equation B-2 for the subsonic Mach numbers and equation B-3 for the supersonic Mach numbers.

$$G = AP_t \sqrt{\frac{2g\gamma}{(\gamma-1)\ R_g T_t} \left[\left(\frac{P}{P_t}\right)^{2/\gamma} - \left(\frac{P}{P_t}\right)^{(\gamma+1)/\gamma}\right]} \qquad \text{(B-2)}$$

$$G = A^* P_t \sqrt{\frac{g\gamma}{R_g T_t} \left(\frac{2}{\gamma + 1}\right)^{\frac{\gamma + 1}{\gamma - 1}}} \qquad \text{(B-3)}$$

In Table B-6, subscript 1 refers to conditions just upstream of a normal shock and subscript 2 just downstream of a normal shock.

Table B-6. Nominal isentropic flow and normal shock data for free jet system.

Nozzle exit Mach no. (Me)	0.6	0.8	1.26	1.47
Pressure ratio, P_{exit}/P_t	0.784	0.656	0.381	0.285
Settling chamber stagnation pressure, P_t(psia)	18.75	22.40	38.59	51.67
Nozzle exit area to throat area ratio, A/A*	1.0	1.0	1.050	1.156
Nozzle temperature ratio, $\frac{T_{exit}}{T_t}$	0.933	0.886	0.759	0.698
T_{exit}, (R)	494	470	402	370
Stagnation air density, ρ_t (lbs/ft^3)	0.0954	0.1141	0.196	0.263
Nozzle air density ratio, $\frac{\rho_{exit}}{\rho_t}$ (lbs/ft^3)	0.84	0.74	0.50	0.41
Nozzle exit air density, ρ_{exit} (lbs/ft^1)	0.080	0.084	0.098	0.107
Air mass flow, G (lbs/sec)	1.14	1.57	2.66	3.24
M_2	-	-	0.81	0.71
$P2/P_1$	-	-	1.69	2.35
$\rho 2/\rho 1$	-	-	1.45	1.81
T_2/T_1	-	-	1.17	1.30

APPENDIX C

ORIFICE METER CALIBRATION

AND

SAMPLING SYSTEM SET POINTS

A. Orifice meter calibration.

A set of three sharp-edged orifice flow meters were used to determine the air flow rates through the particle sampling systems. The orifice meters were located in the sampling systems according to accepted practice; approximately 50 pipe diameters downstream and 10 pipe diameters upstream of any flow obstruction. Flow calibration of each orifice was accomplished by a method involving the use of a saran or plastic bag, with a known (calibrated) volume (60); bags with a volume of 10.9 ft^3 and 20.7 ft^3 were used. After the bag was evacuated and connected to the orifice exhaust, a pump was turned on and the time for the bag to fill was recorded. The bag was considered full when a differential pressure gage connected between the bag and ambient indicated 0.15 in H_2O. For each calibration run the following information was recorded:

1. Run number
2. Orifice pressure drop
3. Elapsed time to fill bag
4. Ambient pressure
5. Pressure drop between the downstream orifice tap and ambient.
6. Orifice temperature

7. Ambient temperature

8. Bag temperature

Differential pressures were measured using Dwyer Magnehelic differential pressure gages (accuracy is within 2% of full scale) and temperatures were measured using mercury in glass thermometers.

The basic flow equation for a sharp-edged orifice is (68):

$$Q_m = C' \, [h_w P_f]^{1/2} \qquad \text{(C-1)}$$

where:

Q_m = Volumetric flow rate at desired conditions (ft^3/min)

h_w = Orifice pressure differential (in H_2O)

P_f = Flowing pressure (absolute pressure at downstream orifice tap) (Lbs_f/in^2)

$[h_w P_f]^{\frac{1}{2}}$ = Pressure extension

C' = "Constant"

$$= F_b \cdot F_{pb} \cdot F_{tb} \cdot Fg \cdot F_{tf} \cdot F_r \cdot Y \cdot F_{pv} \cdot F_m \qquad \text{(C-2)}$$

where:

F_b = Basic orifice factor (unknown)

F_{pb} = Pressure base factor = $14.73/P_b$

F_{tb} = Temperature base factor = $(460+T_b)/520$

F_g = Specific gravity factor = 1

F_{tf} = Flowing temperature factor = $[520/(460+T_f)]^{1/2}$

F_r = Reynolds number factor = $1 + [b/(h_w P_f)^{1/2}]$

F_{pv} = Supercompressibility factor = 1

F_m = Manometer factor = 1

Y = Expansion factor = 1

P_b = Base pressure (pressure at which Q_m is determined (Lb_f/in^2)

T_b = Flowing temperature (temperature at downstream orifice tap) (F)

b = Unknown constant [(in H_2O x $Lb_f/in^2)^{1/2}$]

Thus,

$$C' = F_b \left[\frac{14.73}{P_b}\right] \left[\frac{460+T_b}{520}\right] \left[\frac{520}{460+T_f}\right]^{1/2} \left[1 + \frac{b}{(h_w P_f)^{1/2}}\right] \quad \text{(C-3)}$$

In general, base conditions may be selected arbitrarily at the values for the desired flow conditions. This allows determination of the flow rate at desired conditions rather than at existing actual conditions. However, for calibration purposes, the measured volume is at some actual condition of temperature and pressure. Therefore, in this case, T_b and P_b must refer to actual bag conditions if the actual bag volume is to be used.

In the present case, each data point was converted to represent the values which would have existed if the

bag had been at standard conditions (i.e., P_b = 14.7 psi and T_b = 60F = 520F). This was accomplished as follows. Define a new "constant".

$$C = F_b \left[1 + \frac{b}{(h_w P_f)^{1/2}}\right] \qquad \text{(C-4)}$$

So that,

$$Q_m = C\left[\frac{14.7}{P_b}\right]\left[\frac{460+T_b}{520}\right]\left[\frac{520}{460 + T_f}\right]^{1/2}[h_w P_f]^{1/2} \qquad \text{(C-5)}$$

$$Q_m = C.x.y.z.[h_w P_f]^{1/2}$$

or,

$$C = \frac{Q_m}{x.y.z.[h_w P_f]^{1/2}} \qquad \text{(C-6)}$$

The value of C was determined for each data point in the calculation. That is, setting,

Q_m = Bag volume/time to fill

P_b = Actual bag pressure = barometric pressure

T_f = Actual flowing temperature

T_b = Actual bag temperature =

$$\frac{\text{ambient temperature + flowing temperature}}{2}$$

h_w = Actual orifice differential pressure

P_f = Actual flowing pressure

Then, for each point,

$$Q_b = C \left[\frac{520}{460 + T_f}\right]^{1/2} [h_w P_f]^{1/2} \qquad \text{(C-7)}$$

where Q_b is the volumetric flow rate at standard conditions.

Figures C-1 through C-7 give calibration data for all three orifice flow meters. Orifice meter number 1 had an ID of 0.4 inch; number 2, 0.5 inch; and number 3, 0.7 inch. Figure C-8 shows the relationship between pressure extension, $(h_w P_f)^{1/2}$, and orifice pressure drop, h_w.

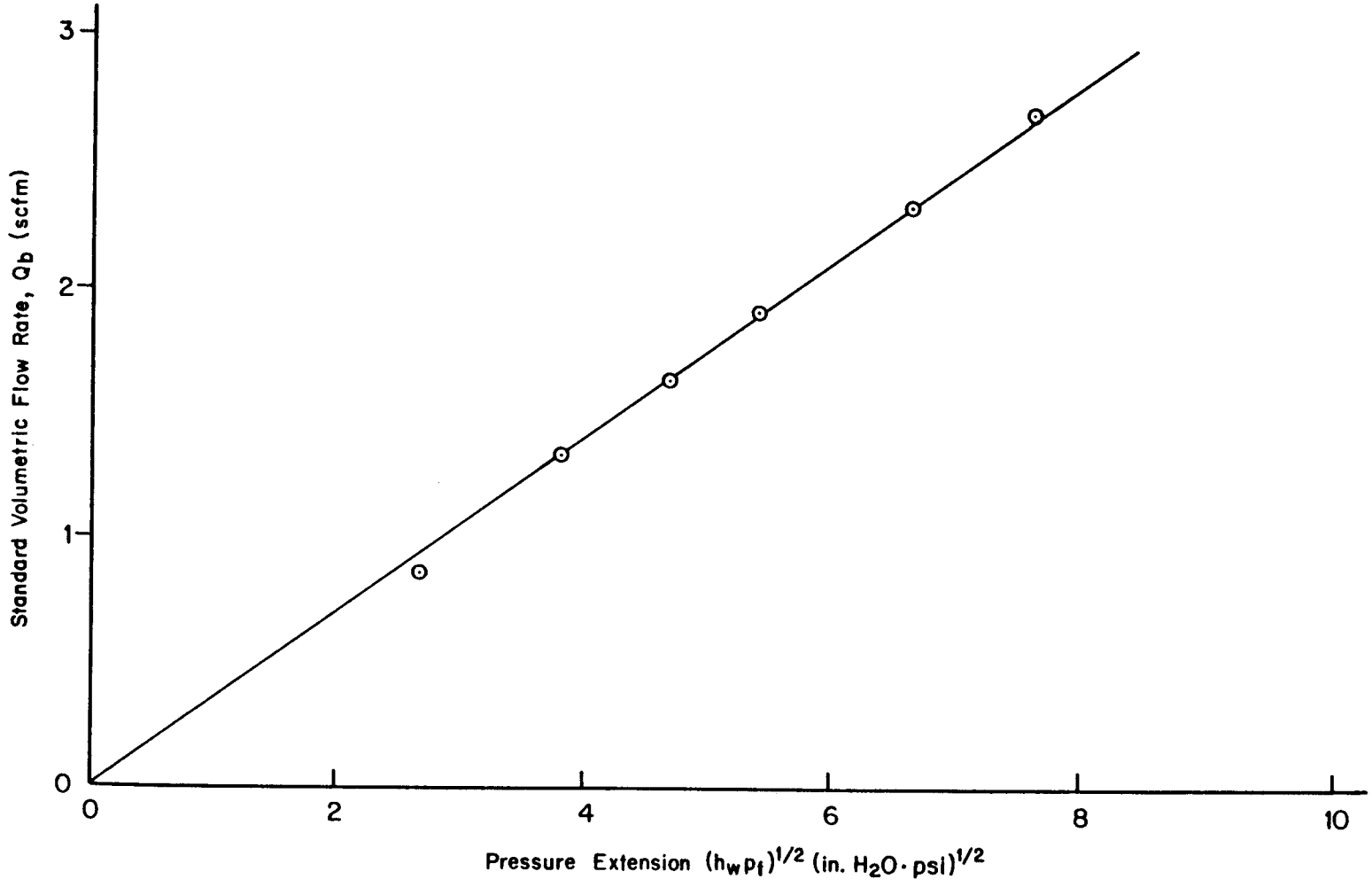

Figure C-1. Calibration data for orifice meter number one.

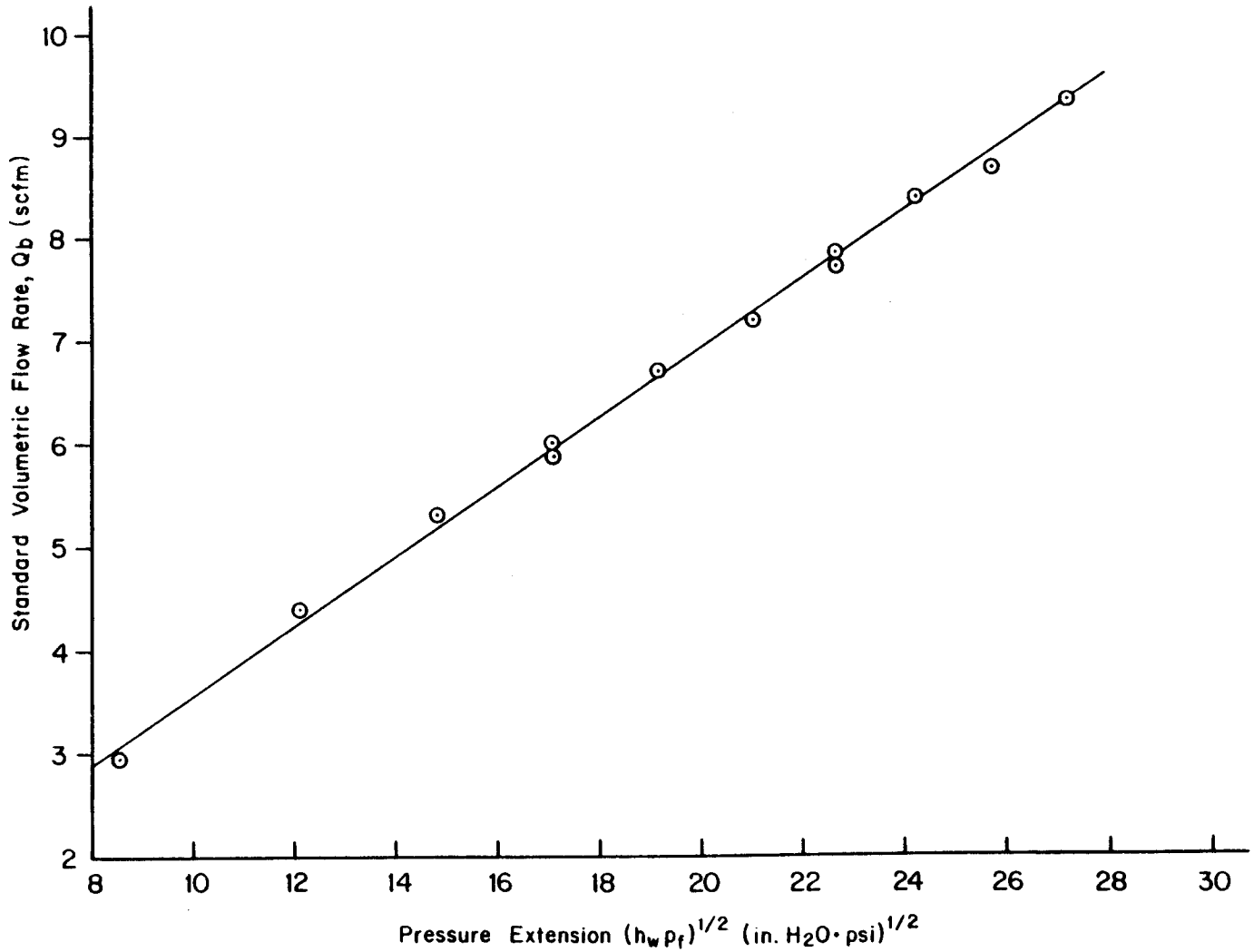

Figure C-2. Calibration data for orifice meter number one.

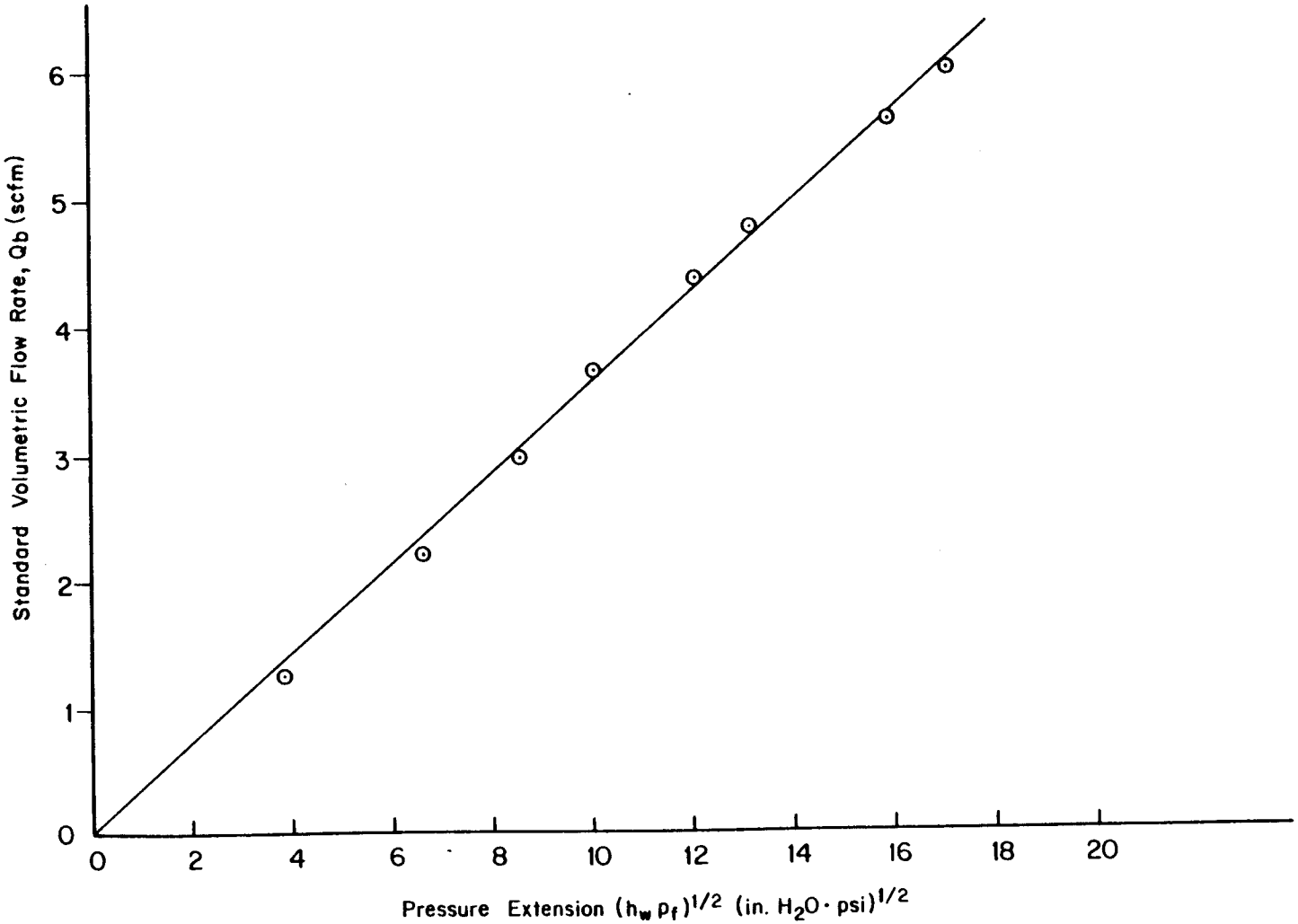

Figure C-3. Calibration data for orifice meter number one.

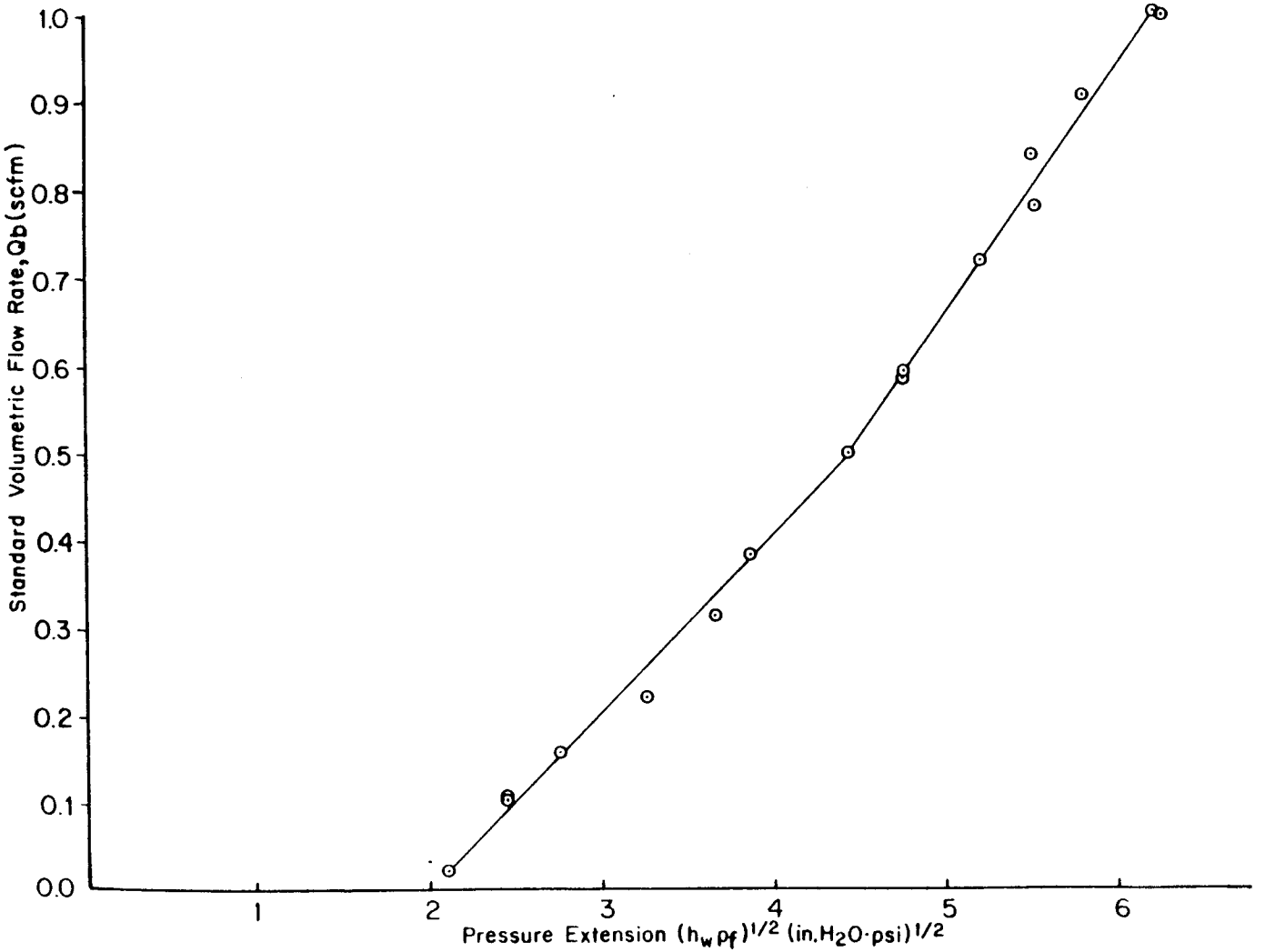

Figure C-4. Calibration data for orifice meter number one.

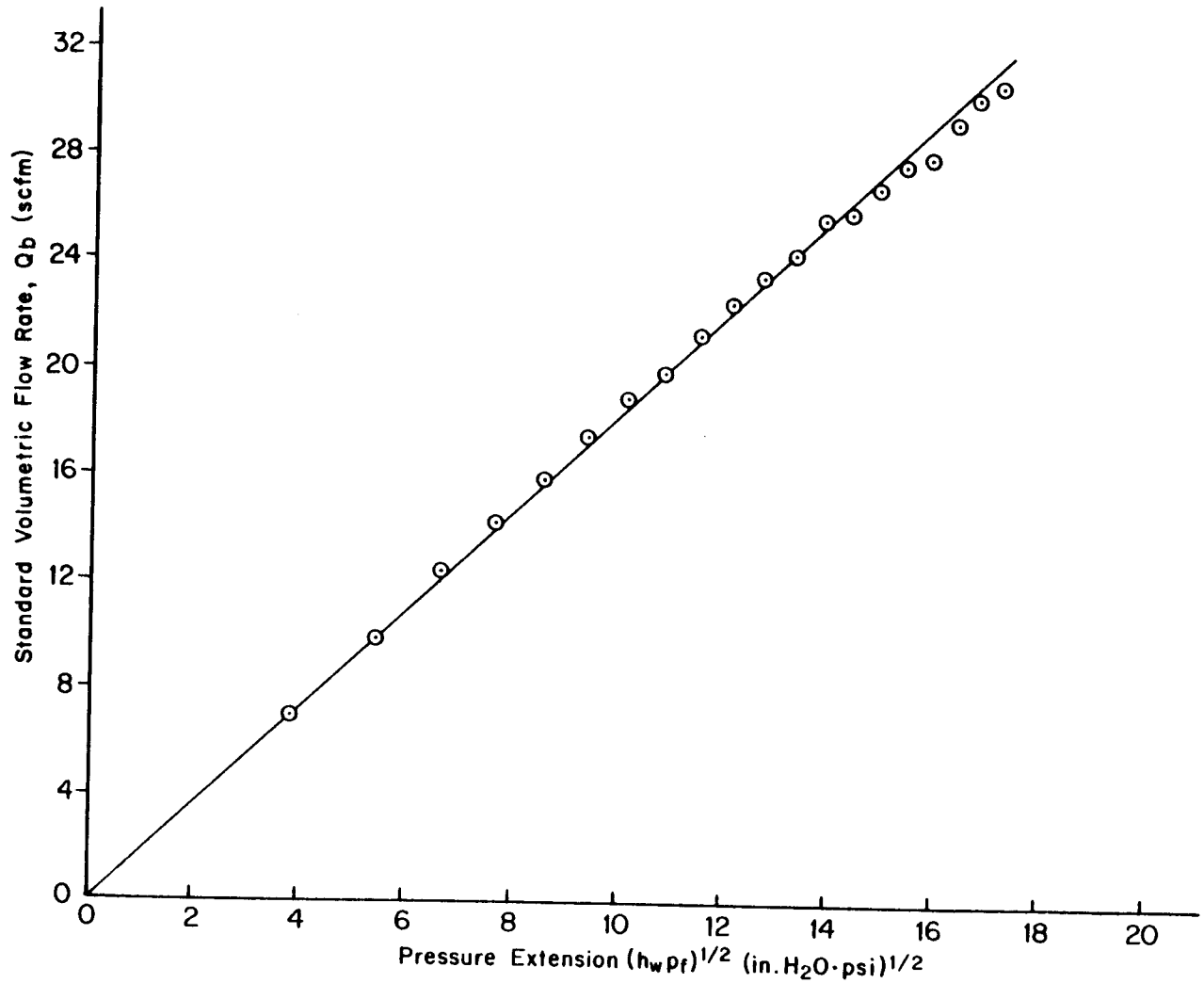

Figure C-5. Calibration data for orifice meter number two.

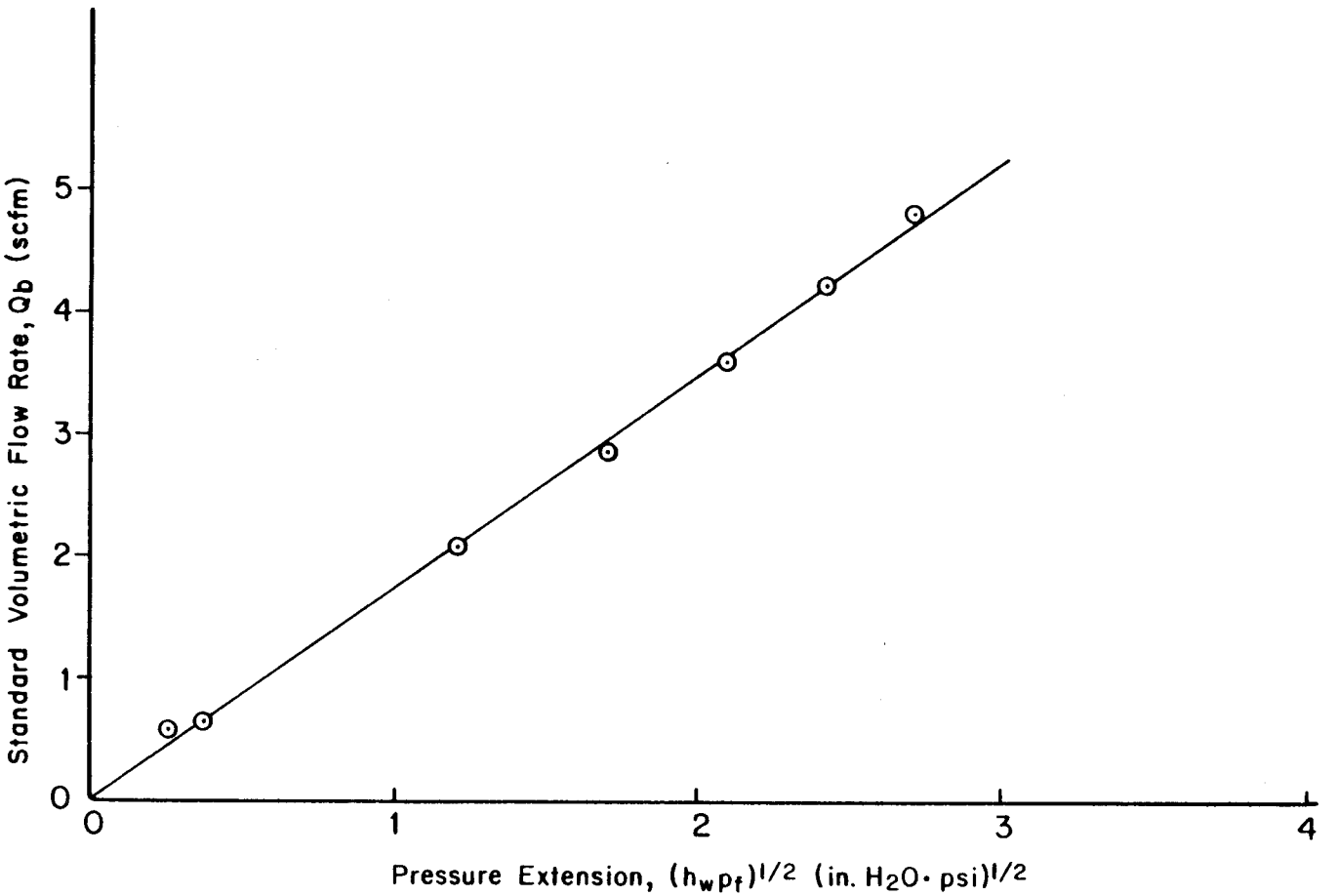

Figure C-6. Calibration data for orifice meter number two.

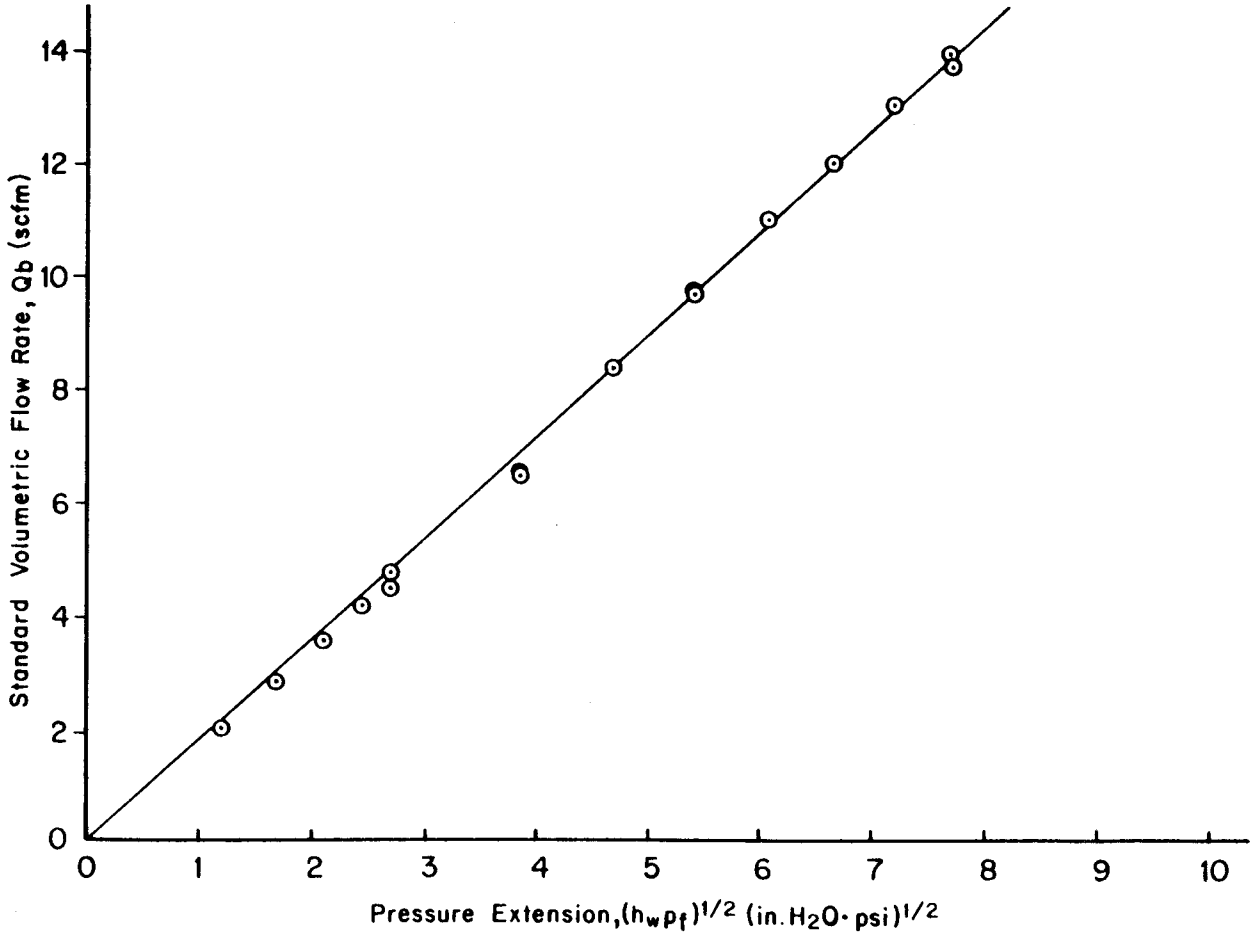

Figure C-7. Calibration data for orifice meter number three.

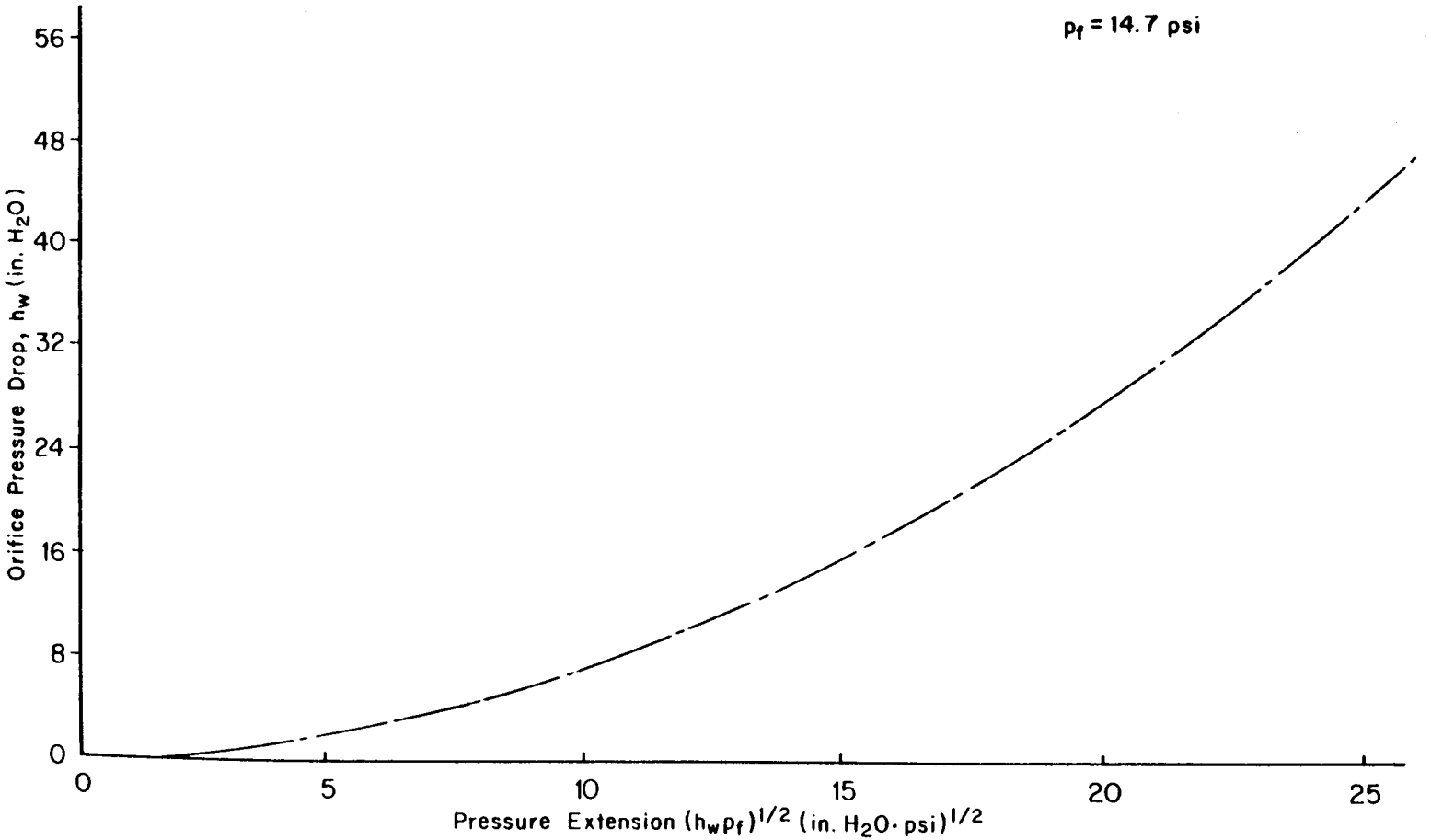

Figure C-8. Pressure extension versus orifice pressure drop.

B. Isokinetic sampling conditions for the settling chamber.

The following example calculations illustrate the methodology for achieving isokinetic sampling in the settling chamber. Table C-1 gives the sampling parameters assuming T_t = 530R. Since the sampling location for the purpose of determining C_o was on the centerline of the settling chamber, the average measured centerline velocities were used to determine the appropriate sampling rate.

For Table C-1,

$$Q_A = V\ A_p\ \left(\frac{60\ sec}{min}\right) \qquad (C\text{-}8)$$

and,

$$Q = Q_A\ \frac{\rho t}{\rho std} \qquad (C\text{-}9)$$

where,

A_p = inlet area of settling chamber sampling probe

= 0.00334 ft^2

ρstd = density of air at standard conditions

= 0.076 Lb/ft^3

Note that the orifice meter calibration curves (Figures C-1 to C-7) are drawn for T_f = 530F and P_f = 14.7 psia. For actual experimental conditions T_f for the

Table C-1. Isokinetic sampling conditions for settling chamber.

Nozzle Exit Mach No. (Me)	Average Centerline Velocity, V (ft/sec)	Stagnation Air Density, ρ_t (lbs/ft^3)	Actual Volumetric Isokinetic Sampling Rate, Q_A (acfm)	Standard Volumetric Isokinetic Sampling Rate, Q (scfm)	Flow Orifice (No.)	Isokinetic Pressure Extension, $(h_w P_f)^{1/2}$	Isokinetic Pressure Differential h_w (in H_2O)
0.6	19.5	0.0954	3.91	4.88	1	13.7	12.8
0.8	21.4	0.114	4.29	6.39	1	18.9	24.4
1.26	20.1	0.196	4.03	10.33	2	5.7	2.2
1.47	18.0	0.263	3.61	12.41	2	7.0	3.3

settling chamber sampling system orifice meter ranged from 528 - 540R and P_f from 14.7 - 14.9 psia.

C. Sampling flowrate conditions for the free jet.

The following example calculations illustrate the methodology for establishing the desired sampling velocity, U, for the sampling probes used for sampling in the free jet. The illustration is based on T_t = 530R. In actual experiments, T_t ranged from 520-537R.

For sampling probe number 4, the area of the probe inlet, A_b, was 1.71 x 10^{-4} ft^2. The isokinetic sampling velocity, U_o, is given by:

$$U_o = M(\gamma R_g T)^{1/2} \qquad \text{(C-10)}$$

where,

$$R = 1716 \ \frac{ft^2}{sec^2 R} \text{ for air}$$

γ = 1.4 = ratio of specific heats

For M_e = 0.8, $\frac{T_{exit}}{T_t}$ = 0.8865 and T_{exit} = 470R

From equation C-10,

$$U_o = 850.1 \ \frac{ft}{sec}$$

For M_e = 0.8, ρ_{exit} = 0.084 Lbs/ft^3

Therefore, the mass flow through the probe, G, for

isokinetic sampling with probe number 4 is:

$$G = \rho_{exit}\, U_o\, A_b \qquad \text{(C-11)}$$

$$G = 0.0122 \text{ Lb/sec}$$

The required volumetric sampling rate at standard conditions, Q, is given by:

$$G = \frac{G}{\rho_{std}} \times 60 \frac{\text{sec}}{\text{min}} \qquad \text{(C-12)}$$

For the example,

$$Q = \frac{0.0122 \frac{\text{Lb}}{\text{sec}}}{0.0764 \frac{\text{Lbs}}{\text{ft}^3}} \times 60 \text{ sec} = 9.57 \text{ scfm}$$

From the calibration curve for orifice meter number 2, for Q = 9.57 scfm,

$$(h_w P_f)^{1/2} = 5.6 \quad \text{and} \quad h_w = 2.1\text{"}H_2O$$

Note that orifice meter calibration curves are drawn for T_f = 530R and P_f = 14.7 psia. In actual experiments T_f, for the free jet orifice meters, ranged from 528-549F and P_f from 14.7 - 14.9 psia.

Table C-2 summarizes the sampling flowrate conditions for the free jet. The data in Table C-2 were calculated using the approach outlined for probe number 4 and M_e = 0.8. The following probe inlet areas were

used:

$$A_b \text{ (probe 1)} = 6.48 \times 10^{-5} \text{ ft}^2$$

$$A_b \text{ (probe 2)} = 1.33 \times 10^{-4} \text{ ft}^2$$

$$A_b \text{ (probe 3)} = 2.25 \times 10^{-4} \text{ ft}^2$$

In Table C-2, the orifice meter information is illustrative. Generally, the orifice meters were interchangeable and were selected for a specific experiment to yield measurable pressure differentials. For example, for M_e at 0.6 or 0.8 with $U/U_o = 0.1$ or 0.2, orifice meter no 1 was used so that h_w was in the range of 1-2 in H_20.

For the supersonic cases, equation C-10 becomes,

$$U_o' = M_1 (\gamma R_g T_1)^{1/2} \qquad \text{(C-13)}$$

and,

$$U_o = M_2 (\gamma R_g T_2)^{1/2} \qquad \text{(C-14)}$$

For these cases, Table C-2 includes values of $\frac{U}{U_o'}$ and $\frac{U}{U_o}$.

For example, where $M_e = M_1 = 1.26$

$$U'_o = 1.26 (1.4 \times 1716 \times 402)^{1/2}$$

$$U'_o = 1238 \text{ ft/sec}$$

and since, $T_2/T_1 = 1.17$ $T_2 = 470R$ and $M_2 = 0.81$

$$U_o = 0.81 (1.4 \times 1716 \times 470)^{1/2}$$

$$U_o = 856 \frac{\text{ft}}{\text{sec}}$$

Table C-2. Summary of sampling flowrate conditions for free jet.

Probe No.	Exit Mach No. M_e	$\frac{U}{U_o}$	$\frac{U}{U'_o}$	U $\frac{ft}{sec}$	Sampling Probe Mass flow, G(Lbs/sec) ($\times 10^3$)
1	0.8	1	-	850	4.63
2	0.8	1	-	850	9.48
3	0.8	1	-	850	16.1
4	0.6	1	-	654	8.94
4	0.8	1	-	850	12.2
4	1.26	1	1	1238	20.8
4	1.47	1	1	1386	25.4
4	0.6	0.1	-	65.4	0.89
4	0.6	0.3	-	196	2.68
4	0.6	0.5	-	327	4.47
4	0.6	0.7	-	458	6.26
4	0.6	0.9	-	589	8.05
4	0.8	0.1	-	85.0	1.22
4	0.8	0.3	-	255	3.66
4	0.8	0.5	-	425	6.10
4	0.8	0.7	-	595	8.54
4	0.8	0.9	-	765	11.0
4	1.26	0.14	0.1	124	2.08
4	1.26	0.43	0.3	371	6.24
4	1.26	0.72	0.5	619	10.4
4	1.26	1.01	0.7	867	14.6
4	1.26	1.30	0.9	1114	18.7
4	1.47	0.18	0.1	139	2.54
4	1.47	0.54	0.3	416	7.61
4	1.47	0.91	0.5	693	12.7
4	1.47	1.27	0.7	970	17.8
4	1.47	1.63	0.9	1247	22.8

Table C-2. (Continued)

Probe No.	Exit Mach No. M_e	Standard Volumetric Probe Flow, Q (scfm)	Orifice Meter No.	Orifice Meter Pressure Extension $(h_w P_f)^{\frac{1}{2}}$	Orifice Meter Pressure Differential, h_w (in H_2O)
1	0.8	3.63	2	2.14	0.32
2	0.8	7.44	2	4.33	1.28
3	0.8	12.6	2	7.30	3.65
4	0.6	7.01	2	4.08	1.14
4	0.8	9.57	2	5.55	2.10
4	1.26	16.3	3	9.20	5.75
4	1.47	19.9	3	11.1	8.30
4	0.6	0.70	2	0.40	0.01
4	0.6	2.10	2	1.23	0.11
4	0.6	3.51	2	2.05	0.29
4	0.6	4.91	2	2.88	0.57
4	0.6	6.31	2	3.70	0.94
4	0.8	0.957	2	0.53	0.02
4	0.8	2.87	2	1.68	0.19
4	0.8	4.78	2	2.82	0.54
4	0.8	6.70	2	3.90	1.03
4	0.8	8.61	2	5.00	1.70
4	1.26	1.63	3	0.92	0.06
4	1.26	4.89	3	2.70	0.5
4	1.26	8.16	3	4.50	1.40
4	1.26	11.4	3	6.30	2.70
4	1.26	14.7	3	8.15	4.50
4	1.47	1.99	3	1.12	0.09
4	1.47	5.97	3	3.31	0.75
4	1.47	9.94	3	5.55	2.10
4	1.47	14.0	3	7.74	4.08
4	1.47	17.9	3	9.90	6.68

APPENDIX D

DETERMINATION OF STEARIC ACID RESIDUES BY GAS-LIQUID CHROMATOGRAPHY (GLC)

Part A of this appendix was prepared by Stoner Laboratories Inc., Santa Clara, California. It was designated Technical Report number 50637.

A. Methodology

1. Scope

This method is designed for the determination of stearic acid that is (1) retained on 142 mm diameter Nuclepore polycarbonate membrane filters and (2) present in acetone solutions.

2. Principle

The principle of this procedure is the conversion of stearic acid and heptadecanoic acid (internal standard) to the corresponding methyl esters and their subsequent identification and quantitation by gas-liquid chromatography.

3. Experimental

Reagents

a. Stearic acid, Emersol 153 95

b. n-Heptadecanoic acid (97%), Aldrich Chemical Company, Inc., Milwaukee, Wisconsin

c. Diethyl ether, nanograde reagent

d. Acetone, distilled

e. Diazomethane ethereal solution. Made from "Diazald", according to the direction of the manufacturer (Aldrich Chemical Company, Inc., Milwaukee, Wisconsin)

Apparatus

a. Laboratory shaker

b. Water bath

c. Gas chromatographs

-- Tracor, Model MT-220, equipped with a flame ionization detector and U-shaped glass columns containing either 3% OV-1 or 3% OV-17.

-- Hewlett-Packard, Model 5730A, equipped with a flame ionization detector and spiral glass column containing 2% OV-101 on Gas Chrom Q.

GLC Operating Conditions

a. Column oven: operated isothermally between 190-210C

b. Inlet, 250C

c. Detector, 300C

d. Carrier gas, purified N_2

e. Recorder, 1 mv

f. Chart speed, 15 inches per hour

Procedure

Analysis of Nuclepore Polycarbonate Filters

a. Filters are transferred carefully into 25 x 200 culture tubes. Twenty milliliters of diethyl ether

is added to each tube. To the resulting solutions is added a known quantity of heptadecanoic acid (internal standard). The tubes are tightly capped and shaken mechanically for ten minutes.

b. The extracts are then decanted into 50 ml bottles.

c. An aliquot (1-2 ml) of each sample is placed into individual 15 ml centrifuge tubes and methylated with ethereal diazomethane, allowing each tube to stand for a minimum of ten minutes.

d. The samples are diluted to an appropriate volume with acetone. Quantitative determination of the methyl esters is made by GLC using a flame ionization detector.

Analysis of Acetone Solutions

a. A known quantity of heptadecanoic acid (internal standard) is added to each acetone solution.

b. The solutions are evaporated in a water bath to approximately two milliliters and cooled.

c. The remaining concentrates are methylated with ethereal diazomethane, and allowed to stand for a minimum of ten minutes.

d. Quantitative determination of the methyl esters is made by GLC, using a flame ionization detector.

Preparation of Standard Ratios

a. Ten milligrams n-heptadecanoic acid (internal standard) is combined with standards of five and ten milligrams stearic acid. Each mixture is methylated as described in the previous sections.

b. Determination of the ratio of peak heights of n-heptadecanoic acid (internal standard) and stearic acid in each standard is made by GLC, using a flame ionization detector.

Fortification and Analysis of Nuclepore Polycarbonate Membrane Filters

a. A series of untreated Nuclepore polycarbonate membrane filters is fortified with stearic acid at various concentrations and stored at room temperature up to seven days (Table D-1).

b. Following timed storage, the filters are analyzed as described previously.

Fortification and Analysis of Acetone Solutions

a. A series of untreated acetone solutions is fortified with stearic acid at various concentrations and stored at room temperature up to seven days (Table D-2).

b. Following storage, the solutions are analyzed as described previously.

4. Results and discussion

Stearic acid cannot be directly gas chromatographed. Consequently, the analytical procedure is based on the measurement of the corresponding methyl ester. The ester is easily formed by treatment with ethereal diazomethane.

Table D-1. Fortification and storage of Nuclepore polycarbonate filters.

Sample Code	Level of Fortification Stearic Acid (mg)	Storage Interval (Days)
A-1	0	0
A-2	0	2
A-3	0	4
A-4	0	7
B-1	2	0
B-2	2	2
B-3	2	4
B-4	2	7
C-1	5	0
C-2	5	2
C-3	5	4
C-4	5	7
D-1	10	0
D-2	10	2
D-3	10	4
D-4	10	7

To eliminate any errors due to incomplete esterification, spillage, or volatization of the esters, all determinations are based on an internal standard (the methyl ester of n-heptadecanoic acid). The typical ratios between stearic acid and n-heptadecanoic acid are

given in Table D-3.

The applicability of this gas chromatographic method for determining residues of stearic acid was demonstrated on a number of Nuclepore polycarbonate filters and acetone solutions. Recovery of stearic acid added to untreated filters and acetone solutions averaged 101% and 102%, respectively, over the range of one to ten milligrams (Tables D-4 and D-5).

Table D-2. Fortification and storage of acetone solutions.

Sample Code	Level of Fortification Stearic Acid (mg)	Storage Interval (Days)
A'-1	0.5	0
A'-2	0.5	3
A'-3	0.5	7
B'-1	1.0	0
B'-2	1.0	3
B'-3	1.0	7
C'-1	5.0	0
C'-2	5.0	3
C'-3	5.0	7
D'-1	0.0	0
D'-2	0.0	3
D'-3	0.0	7

Table D-3. Standard ratios between stearic acid and n-heptadecanoic acid.

Standard	Ratio
5. mg stearic acid/10. mg n-heptadecanoic acid	0.33
10. mg stearic acid/10. mg n-heptadecanoic acid	0.67

Table D-4. Recovery of Stearic acid from Nuclepore polycarbonate filters.

Sample Code	Recovery mg	Recovery %
A-1	nd	
A-2	nd	
A-3	nd	
A-4	nd	
B-1	2.0	100
B-2	1.9	95
B-3	1.9	95
B-4	2.0	100
C-1	5.2	104
C-2	5.4	108
C-3	5.1	102
C-4	4.9	98
D-1	10.7	107
D-2	10.3	103
D-3	10.0	100
D-4	10.0	100

nd = none detected

Table D-5. Recovery of stearic acid from acetone solutions.

Sample Code	Recovery mg	Recovery %
A'-1	0.50	100
A'-2	0.50	100
A'-3	0.52	104
B'-1	1.0	100
B'-2	0.94	94
B'-3	1.0	100
C'-1	5.4	108
C'-2	5.4	108
C'-3	5.3	106
D'-1	nd	
D'-2	nd	
D'-3	nd	

nd = none detected

B. Stearic Acid Analysis

The stearic acid used in this study was provided by Emery Industries, Inc., San Francisco, California. The product designation was Emersol 153 Stearic Acid 95 having a nominal composition of 95% stearic acid (C_{18} H_{36} O_2) and 5% palmitic acid (C_{16} H_{32} O_2) by gas liquid chromatographic analysis. The lot number was 0610. An analysis of this lot by Stoner Laboratories gave the following composition:

Constituent	Composition (wt%)
C_{18}	94.3
C_{12}	0.51
C_{14}	0.62
C_{16}	3.01
C_{17}	0.25
C_{20}	0.67

Early in the study it was discovered that standard laboratory sources of stearic acid (i.e., Mallinckrodt) typically contained up to 50% palmitic acid (C_{16}) making it unsuitable for this experiment. Important physical properties of stearic acid are given below:

melting point	69C
boiling point	370C
molecular weight	284.48
density	0.847 gm/ml at 69C
index of refraction	1.4299

APPENDIX E

COMPARISON OF GRAVIMETRIC AND GAS CHROMATOGRAPHIC DETERMINATION OF STEARIC ACID

The mass of stearic acid collected on the polycarbonate membrane filters used in both aerosol sampling systems was determined gravimetrically with pre and post test filter weighings on an analytical balance (Mettler Model H54). The same filters were submitted for gas chromatographic analysis using the method described in Apppendix D. In this way, gravimetric and gas chromatographic results were available for the same samples. Table E-1 lists these paired results and data for calculation of the t statistic. The clean filters weighed approximately 150 mg; sample weight gains, excluding blanks, ranged from 0.75 to 16.0 mg.

Table E-1. Comparison of gravimetric and gas chromotographic (GC) determinations of stearic acid collected on polycarbonate filters.

Sample No.	GC Result (mg) (X_1)	Gravimetric Result (mg) (X_2)	y' (X_1-X_2)	Y ($10y'$)	y^2
1	2.5	2.8	-0.3	-3	9
2	4.2	4.4	-0.2	-2	4
3	8.4	8.6	-0.2	-2	4
4	14.9	15.7	-0.8	-8	64
5	4.0	5.6	-1.6	-16	256
6	7.3	6.9	+0.4	+4	16
7	4.3	4.9	-0.6	-6	36
8	7.8	7.4	+0.4	+4	16
9	4.3	4.6	-0.3	-3	9
10	8.2	7.8	+0.4	+4	16
11	4.9	5.2	-0.3	-3	9
12	9.4	9.4	+0	+0	0
13	4.5	4.8	-0.3	-3	9
14	7.9	8.3	-0.4	-4	16
15	5.9	5.1	+0.8	+8	64
16	11.0	10.3	+0.7	+7	49
17	5.7	4.9	+0.8	+8	64
18	11.0	10.6	+0.4	+4	16
19	5.8	6.8	-1.0	-10	100
20	11.0	11.2	-0.2	-2	4

Table E-1. (Continued).

Sample No.	GC Result (mg) (X_1)	Gravimetric Result (mg) (X_2)	y' (X_1-X_2)	y, ($10y'$)	y^2
21	5.9	7.0	-1.1	-11	121
22	12.0	10.9	+1.1	+11	121
23	5.7	6.0	-0.3	-3	9
24	12.0	12.6	-0.6	-6	36
25	4.3	4.0	+0.3	+3	9
26	7.5	7.0	+0.5	+5	25
27	4.6	4.3	+0.3	+3	9
28	8.2	8.0	+0.2	+2	4
29	4.4	3.5	+0.9	+9	81
30	8.5	8.0	+0.5	+5	25
31	5.1	4.4	+0.7	+7	49
32	9.7	9.9	-0.2	-2	4
33	4.7	4.0	+0.7	+7	49
34	9.3	8.2	+1.1	+11	121
35	5.8	5.8	0	0	0
36	7.3	7.6	-0.3	-3	9
37	8.9	8.7	+0.2	+2	4
38	5.9	6.0	-0.1	-1	1
39	7.6	7.4	+0.2	+2	4
40	5.5	5.3	+0.2	+2	4
41	4.8	4.5	+0.3	+3	9

Table E-1. (Continued).

Sample No.	GC Result (mg) (X_1)	Gravimetric Result (mg) (X_2)	y' (X_1-X_2)	y, ($10y'$)	y^2
42	4.6	4.4	+0.2	+2	4
43	7.9	7.3	+0.6	+6	36
44	4.5	3.4	+1.1	+11	121
45	11.0	10.2	+0.8	+8	64
46	6.0	5.6	+0.4	+4	16
47	11.0	10.1	+0.9	+9	81
48	4.8	5.0	-0.2	-2	4
49	5.8	5.6	+0.2	+2	4
50	3.6	3.8	-0.2	-2	4
51	5.7	5.8	-0.1	-1	1
52	7.8	7.6	+0.2	+2	4
53	5.6	5.6	0	0	0
54	9.1	8.9	+0.2	+2	4
55	4.9	4.8	+0.1	+1	1
56	5.8	5.8	0	0	0
57	3.7	3.8	-0.1	-1	1
58	9.3	9.6	-0.3	-3	9
59	4.6	4.6	0	0	0
60	8.2	8.2	0	0	0
61	5.0	5.1	-0.1	-1	1
62	9.4	9.0	+0.4	+4	16

Table E-1. (Continued).

Sample No.	GC Result (mg) (X_1)	Gravimetric Result (mg) (X_2)	y' (X_1-X_2)	y, ($10y'$)	y^2
63	5.3	5.7	-0.4	-4	16
64	11.0	10.4	+0.6	+6	36
65	6.6	4.8	-1.8	-18	324
66	7.9	8.0	-0.1	-1	1
67	4.6	5.9	-1.3	-13	169
68	8.9	8.9	0	0	0
69	3.6	2.8	+0.8	+8	64
70	7.8	8.4	-0.6	-6	36
71	5.2	4.4	+0.8	+8	64
72	9.4	8.1	+1.3	+13	169
73	4.5	4.4	+0.1	+1	1
74	8.1	8.6	-0.5	-5	25
75	4.7	5.0	-0.3	-3	9
76	9.1	9.0	+0.1	+1	1
77	6.7	5.8	+0.9	+9	81
78	14.0	12.7	+1.3	+13	169
79	5.0	5.1	-0.1	-1	1
80	15.0	14.4	+0.6	+6	36
81	15.0	15.3	-0.3	-3	9
82	16.0	15.8	+0.2	+2	4
83	5.4	5.1	+0.3	+3	9

Table E-1. (Continued).

Sample No.	GC Result (mg) (X_1)	Gravimetric Result (mg) (X_2)	y' (X_1-X_2)	y, ($10y'$)	y^2
84	5.8	5.6	+0.2	+2	4
85	8.7	8.7	0	0	0
86	13.0	13.2	-0.2	-2	4
87	5.8	6.0	-0.2	-2	4
88	5.3	5.4	-0.1	-1	1
89	5.8	5.8	0	0	0
90	5.8	5.8	0	0	0
91	7.3	7.6	-0.3	-3	9
92	8.9	8.7	+0.2	+2	4
93	5.9	6.0	-0.1	-1	1
94	7.6	7.4	+0.2	+2	4
95	5.5	5.3	+0.2	+2	4
96	4.8	4.5	+0.3	+3	9
97	4.6	4.4	+0.2	+2	4
98	8.4	7.3	+1.1	+11	121
99	4.5	3.7	+0.8	+8	64
100	11.0	10.2	+0.8	+8	64
101	6.0	5.6	+0.4	+4	16
102	11.0	10.1	+0.9	+9	81
103	4.8	5.0	-0.2	-2	4
104	5.8	5.6	+0.2	+2	4

Table E-1. (Continued).

Sample No.	GC Result (mg) (X_1)	Gravimetric Result (mg) (X_2)	y' (X_1-X_2)	y, ($10y'$)	y^2
105	3.6	3.8	-0.2	-2	4
106	5.7	5.8	-0.1	-1	1
107	7.8	7.6	+0.2	+2	4
108	5.6	5.6	0	0	0
109	9.1	8.9	+0.2	+2	4
110	4.9	4.8	+0.1	+1	1
111	5.8	5.8	0	0	0
112	3.7	3.8	-0.1	-1	1
113	6.1	6.1	0	0	0
114	3.3	3.4	-0.1	-1	1
115	5.8	6.6	+0.8	+8	64
116	5.7	5.7	0	0	0
117	4.8	5.0	-0.2	-2	4
118	2.2	2.2	0	0	0
119	5.5	5.9	-0.4	-4	64
120	9.0	9.3	-0.3	-3	9
121	5.9	6.4	-0.5	-5	25
122	12.0	11.9	-0.1	-1	1
123	5.5	5.6	-0.1	-1	1
124	6.4	6.8	-0.4	-4	16
125	9.9	10.4	-0.5	-5	25

Table E-1. (Continued).

Sample No.	GC Result (mg) (X_1)	Gravimetric Result (mg) (X_2)	y' (X_1-X_2)	y, ($10y'$)	y^2
126	4.8	4.9	-0.1	-1	1
127	6.2	6.7	-0.5	-5	25
128	5.0	5.1	-0.1	-1	1
129	7.9	7.8	-0.1	-1	1
130	5.8	5.1	-0.7	-7	49
131	8.7	8.4	+0.3	+3	9
132	3.5	3.2	+0.3	+3	9
133	5.0	5.1	-0.1	-1	1
134	5.8	5.6	+0.2	+2	4
135	7.7	7.4	+0.3	+3	9
136	8.5	8.4	+0.1	+1	1
137	10.0	10.1	-0.1	-1	1
138	3.3	3.2	+0.1	+1	1
139	4.8	4.6	+0.2	+2	4
140	5.2	5.1	+0.1	+1	1
141	6.1	6.1	0	0	0
142	6.5	6.4	+0.1	+1	1
143	8.2	8.2	0	0	0
144	4.1	1.8	0	0	0
145	4.1	3.7	+0.4	+4	16
146	4.7	4.3	+0.4	+4	16

Table E-1. (Continued).

Sample No.	GC Result (mg) (X_1)	Gravimetric Result (mg) (X_2)	y' (X_1-X_2)	y, ($10y'$)	y^2
147	5.4	5.3	+0.1	+1	1
148	6.9	6.7	+0.2	+2	4
149	7.1	7.0	+0.1	+1	1
150	8.1	7.9	+0.2	+2	4
151	8.5	9.1	-0.6	-6	36
152	9.7	10.2	-0.5	-5	25
153	12.0	12.5	-0.5	-5	25
154	3.5	3.3	+0.2	+2	4
155	4.3	4.6	-0.3	-3	9
156	4.7	4.3	+0.4	+4	16
157	5.6	4.9	+0.7	+7	49
158	5.6	5.5	+0.1	+1	1
159	6.0	6.2	-0.2	-2	4
160	6.8	6.8	0	0	0
161	6.0	6.5	-0.5	-5	25
162	7.2	7.4	-0.2	-2	4
163	8.8	9.2	-0.4	-4	16
164	7.4	8.1	-0.7	-7	49
165	3.7	4.2	-0.5	-5	25
166	7.2	7.9	-0.7	-7	49
167	3.8	4.1	-0.3	-3	9

Table E-1. (Continued).

Sample No.	GC Result (mg) (X_1)	Gravimetric Result (mg) (X_2)	y' (X_1-X_2)	y, ($10y'$)	y^2
168	7.1	7.9	-0.8	-8	64
169	4.3	3.9	+0.4	+4	16
170	7.2	8.0	-0.8	-8	64
171	3.8	4.0	-0.2	-2	4
172	7.2	8.1	-0.9	-9	81
173	3.2	3.6	-0.4	-4	16
174	6.6	7.8	-1.2	-12	144
175	3.3	3.7	-0.4	-4	16
176	6.6	7.1	-0.5	-5	25
177	4.1	4.3	-0.2	-2	4
178	7.5	7.8	-0.3	-3	9
179	4.0	4.2	-0.2	-2	4
180	7.8	8.2	-0.4	-4	16
181	4.3	4.3	0	0	0
182	7.9	7.7	+0.2	+2	4
183	4.4	4.6	-0.2	-2	4
184	7.9	8.5	-0.6	-6	36
185	1.8	1.8	0	0	0
186	3.5	3.6	-0.1	-1	1
187	1.5	1.7	-0.2	-2	4
188	2.7	3.2	-0.4	-4	16

Table E-1. (Continued).

Sample No.	GC Result (mg) (X_1)	Gravimetric Result (mg) (X_2)	y' (X_1-X_2)	y ($10y'$)	y^2
189	1.8	2.0	-0.2	-2	4
190	1.5	1.5	0	0	0
191	1.5	1.6	-0.1	-1	1
192	1.5	1.6	-0.1	-1	1
193	1.1	1.3	-0.2	-2	4
194	1.5	1.9	-0.4	-4	16
195	0.96	1.0	-0.04	-0.4	0.16
196	1.9	1.8	+0.1	+1	1
197	0.75	0.55	+0.2	+2	4
198	1.0	0.93	+0.07	+0.7	0.49
199	1.6	1.5	+0.1	+1	1
200	1.2	1.1	+0.1	+1	1
201	1.5	1.4	+0.1	+1	1
202	2.1	1.9	+0.2	+2	4
203	1.8	1.7	+0.1	+1	1
204	2.4	2.6	-0.2	-2	4
205	2.5	3.0	-0.5	-5	25
206	2.7	3.0	-0.3	-3	9
207	2.7	2.9	-0.2	-2	4
208	4.6	5.4	-0.8	-8	64
209	2.5	2.7	-0.2	-2	4

Table E-1. (Continued).

Sample No.	GC Result (mg) (X_1)	Gravimetric Result (mg) (X_2)	y' (X_1-X_2)	y, ($10y'$)	y^2
210	5.2	5.5	-0.3	-3	9
211	2.7	2.9	-0.2	-2	4
212	5.7	5.9	-0.2	-2	4
213	2.4	2.7	-0.3	-3	9
214	3.0	3.1	-0.1	-1	1
215	1.3	1.2	+0.1	+1	1
216	1.9	1.8	+0.1	+1	1
217	2.4	2.4	0	0	0
218	3.0	3.3	-0.3	-3	9
219	3.1	3.3	-0.2	-2	4
220	4.5	4.1	+0.4	+4	16
221	4.0	4.9	-0.9	-9	81
222	5.1	5.6	-0.5	-5	25
223	5.8	6.2	-0.4	-4	16

The t test was used to determine whether there was a significant difference between the gas chromatographic and gravimetric methods. The t test for this circumstance is to determine whether the true mean, μ, of the difference between the methods is zero. That is:

$$H_o;\ \mu = 0$$

If y is the difference within pairs of measurements, t is calculated as follows:

$$t = \frac{|\bar{y} - 0|}{S(\bar{y})} \qquad \text{(E-1)}$$

where $S(\bar{y})$ is the estimated standard deviation of the mean.

For this case, the pertinent parameters are:

$$n = 223 \qquad \Sigma y = -40.7 \qquad \bar{y} = \frac{\Sigma y}{n} = -0.183$$

$$\Sigma y^2 = 5041 \qquad \Sigma' y^2 = \Sigma y^2 - \bar{y}\Sigma y = 5034$$

$$S^2(y) = \frac{\Sigma' y^2}{n-1} = 22.7 \qquad S^2(\bar{y}) = \frac{S^2(y)}{n} = 0.102$$

$$S(\bar{y}) = 0.319$$

and,

$$t = \frac{|\bar{y} - 0|}{S(\bar{y})} = \frac{|-0.183|}{0.319} = 0.574$$

from statistical tables (69)

$$t_{0.05,\infty} = 1.960$$

Since the calculated t value is less than the critical value for infinite degrees of freedom, the hypothesis, that there is no difference between the analytical methods, is accepted.

APPENDIX F

AEROSOL CONCENTRATION PROFILES

Tables F-1 and F-2 give all data points for the measurement of aerosol concentration profiles in the settling chamber and free jet for each exit Mach number, M_e, 0.6, 0.8, 1.26 and 1.47. All of these samples were obtained using isokinetic sampling. The free jet samples were extracted using sampling probe number 4 which had a knife edged, divergent supersonic inlet. Figures F-1 and F-2 show the settling chamber and free jet sampling locations. These data are summarized in Chapter III, "Experimental Program."

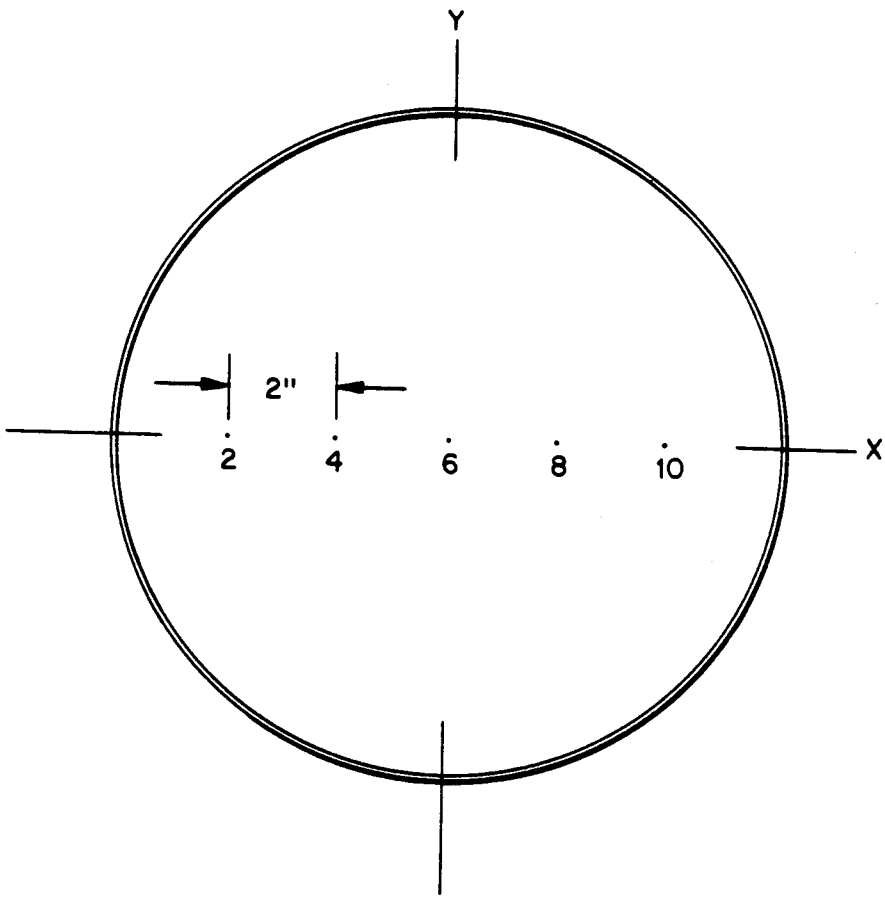

Figure F-1. Settling chamber sampling locations for aerosol concentration profiles.

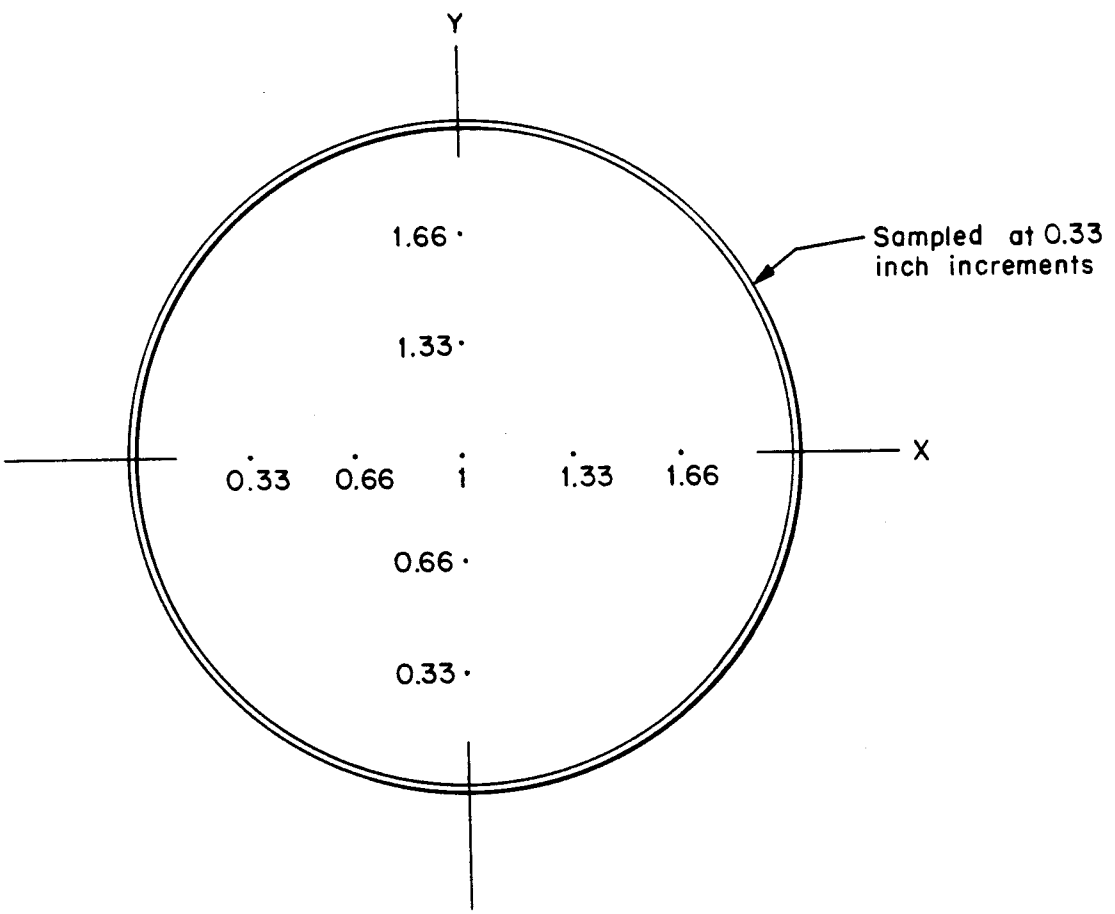

Figure F-2. Free jet sampling locations for aerosol concentratin profiles.

Table F-1. Settling chamber aerosol concentration profiles.

Sample Number	Sample Location	Aerosol Concentration (mg/m^3) for Specified M_e			
		M_e = 0.6	M_e = 0.8	M_e = 1.26	M_e = 1.47
1	2	11.3	6.3	3.3	
2	2	7.9	6.7	2.5	
3	4	7.7	4.5	2.5	
4	4	8.1	6.5	2.9	
5	6	7.4	6.2	2.4	1.9
6	6	7.9	5.8	2.8	1.7
7	6	7.6	6.3	2.9	1.6
8	6	8.8	6.3		1.7
9	6	8.1	7.4		1.8
10	8	7.9	8.3	3.1	
11	8	8.2	6.3	3.1	
12	10	7.9	7.2	3.4	
13	10	7.7	6.9	3.3	
14	2		6.5		
15	6		7.2		
16	6		7.3		
17	6		7.3		
18	6		7.2		
19	10		7.2		
Mean		8.2	6.7	2.9	1.7
Std Dev		1.0	0.82	0.34	0.11

Table F-2. Free jet aerosol concentration profiles.

Sample Number	Sample Location	Aerosol Concentration (mg/m^3) for Specified M_e			
		M_e = 0.6	M_e = 0.8	M_e = 1.26	M_e = 1.47
1	0.33x	9.0	6.9	3.1	
2	0.66x	8.0	8.1	3.1	
3	1.0x	7.6	6.4		
4	1.0x	8.3	6.3	3.2	1.8
5	1.0x	8.6	6.6	3.1	2.0
6	1.0x	9.8	7.0	3.1	2.3
7	1.0x	9.4	8.1		
8	1.33x	9.2	5.7	2.9	
9	1.66x	8.2	6.9	2.9	
10	0.33y	7.7	10.3	3.3	
11	0.66y	8.3	6.8	3.4	
12	1.33y	8.0	8.1	3.4	
13	1.66y	7.9	8.1	3.4	
14	0.33x		6.8		
15	1.0x		8.1		
16	1.0x		8.1		
17	1.0x		8.8		
18	1.0x		8.8		
19	0.66x		8.0		
Mean		8.5	7.6	3.2	2.0
Std Dev		0.70	1.1	0.20	0.21

APPENDIX G

PARTICLE SIZE DATA

The size distribution of stearic acid particles was intended to be constant for all experiments. To confirm that this was the case, samples were collected for particle size determination at various locations (i.e., settling chamber, free jet, etc.) and at various experimental set points throughout the experimental period. The sampling time for a particle size sample was 10-15 seconds compared with 5 minute samples used for aerosol mass determinations. This procedure avoided excessive numbers of particles in the counting field. The 10-15 second sampling period for particle sizing was approximately at the mid-point of the 5 minute period of system operation used for a mass determination. Table G-1 summarizes the particle size data.

Table G-1. Aerosol size distribution summary.

Sample Number	Date Sample Taken	Description of Sample Location And Experimental Conditions	Geometric Mean Particle Size (μm)	Geometric Standard Deviation (σ_g)
1	10 Aug 76	Discharge of aerosol neutralizer	0.80	1.27
2	20 Aug 76	Free Jet (FJ) M_e = 0.8	0.84	1.23
3	20 Aug 76	Settling Chamber (SC) M_e = 0.8	0.85	1.25
4	29 Oct 76	SC M_e = 0.8	0.79	1.27
5	29 Oct 76	FJ M_e = 0.8	0.80	1.31
6	29 Oct 76	SC M_e = 0.6	0.74	1.32
7	2 Oct 76	FJ M_e = 0.6	0.76	1.32
8	5 Nov 76	SC M_e = 0.6	0.81	1.33
9	5 Nov 76	FJ M_e = 0.6	0.83	1.31
10	12 Nov 76	SC M_e = 0.6	0.86	1.27
11	19 Nov 76	SC M_e = 1.26	0.78	1.26
12	28 Nov 76	FJ M_e = 1.26	0.74	1.37
13	3 Dec 76	SC M_e = 1.26	0.69	1.27
14	3 Dec 76	FJ M_e = 1.26	0.73	1.26
15	7 Dec 76	SC M_e = 1.26	0.70	1.21
16	7 Dec 76	FJ M_e = 1.26 40% isokinetic	0.65	1.30
17	14 Dec 76	SC M_e = 1.47	0.82	1.32
18	14 Dec 76	FJ M_e = 1.47	0.80	1.27
19	14 Dec 76	SC M_e = 1.47	0.79	1.28
20	12 Aug 76	Discharge of charge neutralizer	0.71	1.24
21	12 Aug 76	Discharge of charge neutralizer	0.81	1.25
22	13 Aug 76	FJ M_e = 0	0.77	1.26
			Ave = 0.78 μm (std dev 0.06)	Ave = 1.28 (std dev 0.04)

Particle geometric mean size and geometric standard deviation (σ_g) were determined by direct counting of the particle images (minimum of 100 particles counted per sample) on SEM micrographs and plotting the resulting cumulative number distribution on log probability paper. Since these plots were straight lines, the aerosol was log normally distributed.

The geometric standard deviation, σ_g, of a log-normal distribution is defined as the ratio of the particle size at the 84.1% point on the cumulative distribution curve divided by the size at the 50% point. It is a measure of the particle size distribution range of an aerosol sample.

The geometric mean diameter by count can be converted to a geometric mean diameter by weight using the equation (70):

$$\ln M_g' = \ln M_g + 3 (\ln \sigma_g)^2 \qquad \text{(G-1)}$$

M_g' = geometric mean diameter by weight

M_g = geometric mean diameter by count

σ_g = geometric standard deviation

Table G-2 is a typical particle size count and Table G-3 the resulting cumulative number distribution which is plotted in Figure G-1.

Since the experimental aerosol was practically

monodisperse (i.e., a perfectly monodispersed aerosol would have a geometric standard deviation of 1.0), M'g is practically the same as M_g. Using the averaged aerosol values, $M_g = 0.78$ and $\sigma_g = 1.28$, we have from equation G-1:

$$\ln M'_g = \ln M_g + 3 (\ln \sigma_g)^2$$

$$\ln M'_g = \ln 0.78 + 3 (\ln 1.28)^2$$

$$M'_g = 0.94 \ \mu m.$$

Table G-2. Particle sizing data sheet.

Part No.	Particle Size on Micrograph (mm)	Actual Particle Size (μm)	Part No.	Particle Size on Micrograph (mm)	Actual Particle Size (μm)
1	2.4	0.8	26	2.1	0.70
2	2.7	0.9	27	3.3	1.10
3	3.0	1.0	28	4.2	1.40
4	4.3	1.43	29	2.0	0.67
5	2.0	0.67	30	1.4	0.47
6	3.0	1.00	31	2.8	0.93
7	2.1	0.70	32	2.8	0.93
8	4.0	1.33	33	3.1	1.03
9	4.0	1.33	34	3.3	1.10
10	2.4	0.80	35	2.2	0.73
11	1.9	0.63	36	2.4	0.80
12	1.8	0.60	37	2.4	0.80
13	1.3	0.43	38	1.4	0.47
14	2.0	0.67	39	2.5	0.83
15	2.1	0.70	40	1.9	0.63
16	3.1	1.03	41	2.9	0.97
17	3.0	1.00	42	3.4	1.13
18	2.9	0.97	43	3.1	1.03
19	2.0	0.67	44	2.5	0.83
20	4.0	1.33	45	2.1	0.70
21	1.5	0.50	46	6.9	3.00
22	2.0	0.67	47	1.9	0.63
23	2.2	0.73	48	3.0	1.00
24	2.5	0.83	49	2.1	0.70
25	2.8	0.93	50	2.2	0.73

Table G-2. (Continued).

Part No.	Particle Size on Micrograph (mm)	Actual Particle Size (μm)	Part No.	Particle Size on Micrograph (mm)	Actual Particle Size (μm)
51	1.5	0.50	76	2.3	0.77
52	2.0	0.67	77	1.9	0.63
53	2.5	0.83	78	2.4	0.80
54	2.7	0.90	79	3.0	1.00
55	2.7	0.90	80	2.9	0.97
56	2.0	0.67	81	2.1	0.70
57	3.0	1.00	82	2.6	0.87
58	2.8	0.93	83	2.4	0.80
59	2.8	0.93	84	1.9	0.63
60	2.3	0.77	85	4.1	1.37
61	2.2	0.73	86	2.8	0.93
62	2.4	0.80	87	2.4	0.80
63	3.1	1.03	88	2.3	0.77
64	2.8	0.93	89	2.1	0.70
65	3.0	1.00	90	3.7	1.23
66	2.0	0.63	91	2.3	0.77
67	2.3	0.77	92	2.3	0.77
68	2.4	0.80	93	2.3	0.77
69	2.4	0.80	94	4.1	1.37
70	2.0	0.67	95	2.7	0.90
71	1.8	0.60	96	2.5	0.83
72	2.5	0.83	97	2.1	0.70
73	2.1	0.70	98	2.1	0.70
74	4.0	1.33	99	2.2	0.73
75	4.3	1.43	100	3.3	1.10

Table G-3. Typical particle cumulative size distribution by count.

Groups	Tally	Midpoint	Total	Cumulative Number (%)
0.3 - 0.399		0.35		
0.4 - 0.499	///	0.45	3	3
0.5 - 0.599	//	0.55	2	5
0.6 - 0.699	𝍸 𝍸 𝍸 /	0.65	16	21
0.7 - 0.799	𝍸 𝍸 𝍸 𝍸 //	0.75	22	43
0.8 - 0.899	𝍸 𝍸 𝍸 //	0.85	17	60
0.9 - 0.999	𝍸 𝍸 ////	0.95	14	74
1.0 - 1.099	𝍸 𝍸 /	1.05	11	85
1.1 - 1.199	////	1.15	4	89
1.2 - 1.299	/	1.25	1	90
1.3 - 1.399	𝍸 /	1.35	6	96
1.4 - 1.499	///	1.45	3	99
1.5 - 1.599		1.55		
1.6 - 1.699		1.65		
1.7 - 1.799		1.75		
1.8 - 1.899		1.85		
1.9 - 1.999		1.95		
2.0 - 2.099		2.05		
3.0	/	3.05	1	100

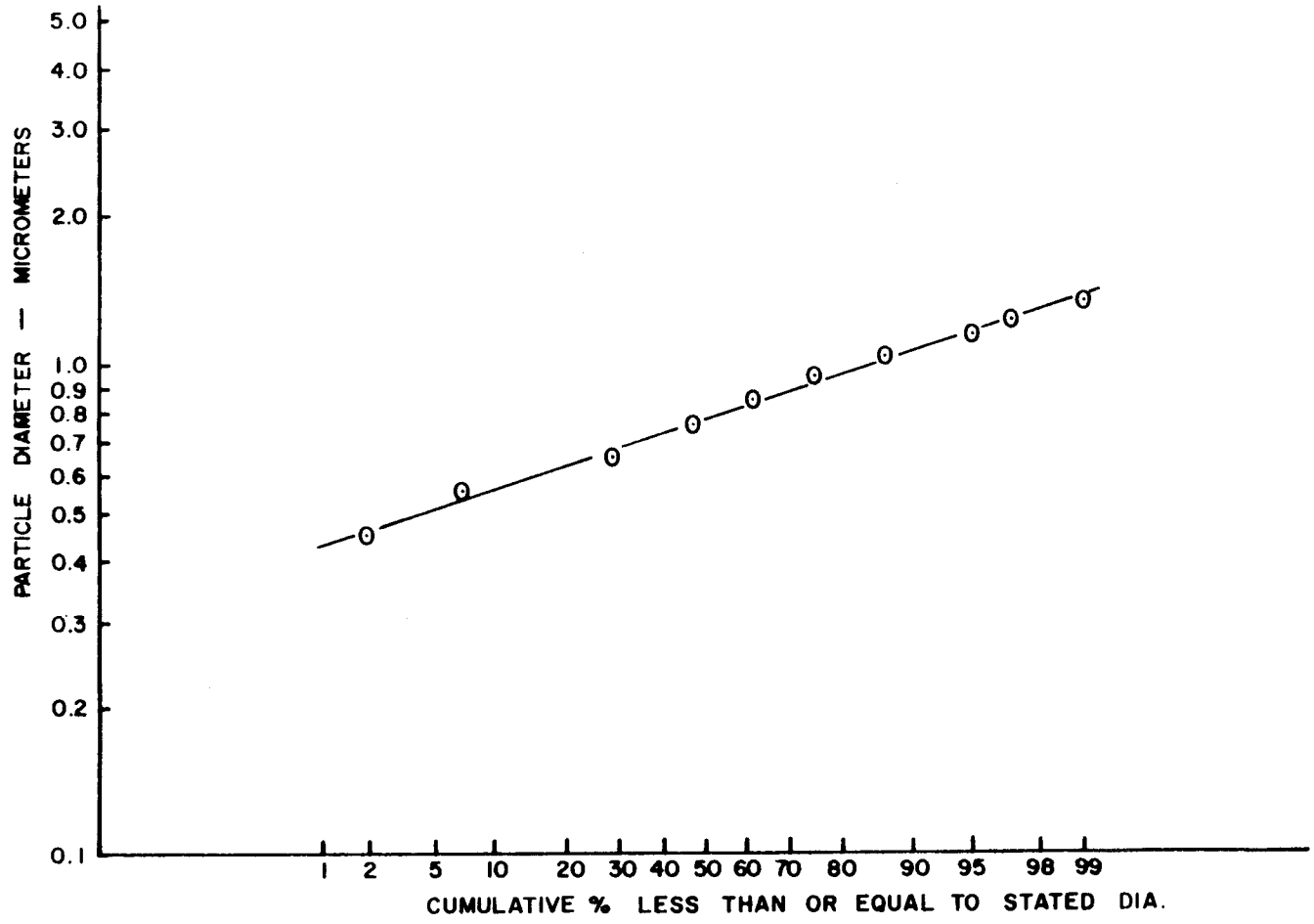

Figure G-1. Typical particle size distribution.

APPENDIX H

BLANK SAMPLE AND PROBE WASH DATA

Tables H-1 to H-5 give blank sample and probe wash data. These data are discussed in Chapter III, "Experimental Program."

Table H-1. Background levels of stearic acid on unused (blank) polycarbonate filters.

Sample Number	Stearic Acid (mg)
1	0.19
2	0.045
3	0.23
4	0.05
5	0.05
6	0.02
7	<0.01
8	<0.01
9	0.02
10	0.03
Average	0.07

From Table H-1, the average background level of stearic acid on unused filters was 0.07 mg.

Since the minimum sample weight gain was 0.75 mg (Appendix E), the maximum error due to background stearic

acid levels is:

$$\frac{0.07}{0.75} \times 100 \approx 9\%$$

Also, in over 90% of the samples (205 out of 223) the sample weight gain was greater than 2mg, therefore the "blank" error was generally about 3%.

Table H-2. Background concentrations of stearic acid in settling chamber and free jet air stream with aerosol generator not operating.

Sample No.	Free Jet (FJ) or Settling Chamber (SC)	Exit Mach No. (M_e)	Stearic Acid Concentration (mg/m^3)
1	FJ	0.6	0.25
2	FJ	0.6	0.57
3	FJ	0.6	0.05
4	FJ	0.8	0.07
5	FJ	0.8	0.19
6	FJ	0.8	0.02
7	FJ	0.8	0.47
8	FJ	1.26	0.03
9	FJ	1.26	0.04
10	FJ	1.26	0.02
11	FJ	1.47	0.01
12	SC	0.6	0.13
13	SC	0.6	0.15
14	SC	0.8	0.11
15	SC	0.8	0.24
16	SC	0.8	0.06
17	SC	0.8	0.10
18	SC	0.8	0.11
19	SC	1.26	0.08
20	SC	1.26	0.07
21	SC	1.26	0.03
22	SC	1.47	0.01

Table H-3. Comparison of average stearic acid concentration in settling chamber and free jet airstream with and without aerosol generator in operation.

Exit Mach No. (M_e)	Free Jet (FJ) or Settling Chamber (SC)	Stearic Acid[1] Concentration (Generator On) C_o (mg/m^3)	Stearic Acid[2] Concentration (Generator Off) C'_o (mg/m^3)	Difference $\frac{C'_o}{C_o} \times 100$ (%)
0.6	FJ	8.7	0.3	3.4
0.8	FJ	7.6	0.2	2.6
1.26	FJ	3.1	0.03	1.0
1.47	FJ	2.0	0.01	0.5
0.6	SC	7.9	0.1	1.3
0.8	SC	6.8	0.1	1.5
1.26	SC	2.7	0.06	2.2
1.47	SC	1.7	0.01	0.6

[1] Average centerline concentration (from Table 4)

[2] Average centerline concentration (from Table H-2)

The amount of stearic acid aerosol that was deposited on the interior surface of sampling probes during a sampling period is given in Table H-4 for the settling chamber probe and in Table H-5 for the free jet probes. In some cases, the acetone probe wash solution was reused for several rinses of sampling probes to yield a composite wash that represented the wall losses for several samples. There was no (i.e., <0.004 mg) stearic acid detected in four unused samples of the acetone rinse solution. Except as noted, the supersonic inlet probe was used to sample free jet aerosol for the probe washes shown in Table H-5.

Table H-4. Stearic acid aerosol deposited on settling chamber sampling probe interior wall.

Probe Wash No.	No. of Aerosol Samples Represented	Stearic Acid In Probe Wash (mg) (A)	Stearic Acid Collected On Filter(s) (mg) (B)	$\frac{A}{B} \times 100$ (%)
1	1	0.15	2.5	6.0
2	1	0.11	8.4	1.3
3	1	0.08	4.0	2.0
4	1	0.08	4.3	1.9
5	1	0.15	4.3	3.5
6	1	0.15	5.9	2.5
7	1	0.13	5.7	2.3
8	1	0.10	5.8	1.7
9	1	0.13	5.9	2.2
10	1	0.14	5.7	2.5
11	3	0.16	13.3	1.2
12	2	0.17	9.8	1.7
13	6	0.37	30.3	1.2
14	7	0.27	25.4	1.1
15	4	0.37	22.1	1.7
16	4	0.42	23.1	1.8
17	4	0.37	22.3	1.7
18	5	0.27	22.9	0.9
19	4	0.35	25.5	1.4
20	5	0.18	18.4	1.0
21	3	0.12	10.6	1.1
22	5	0.16	12.6	1.5
23	3	0.08	5.7	1.4
24	3	0.11	7.9	1.4
25	1	0.11	3.0	3.7
26	1	0.11	2.8	3.9

Table H-5. Stearic acid aerosol deposited on free jet sampling probe interior wall.

Probe Wash No.	No. of Aerosol Samples Represented	Stearic Acid In Probe Wash (mg) (A)	Stearic Acid Collected On Filter(s) (mg) (B)	$\frac{A}{B} \times 100$ (%)
1	5	4.5	36.4	12.4
2	5	3.8	29.7	12.8
3	12	7.1	74.6	9.5
4	1	0.63	4.7	13.4
5	1	0.97	5.4	18.0
6	1	1.3	8.1	16.0
7	1	0.54	3.5	15.4
8	1	0.56	4.3	13.0
9	1	0.69	5.6	12.3
10	1	0.81	5.6	14.5
11	1	1.0	6.8	14.7
12	1	0.41	7.1	5.8
13	1	0.37	7.2	5.1
14	1	0.31	7.2	4.3
15	1	0.38	1.8	21.0
16	1	0.29	1.5	19.3
17	1	0.22	1.1	20.0
18	1	0.47	4.2	11.2
19	1	1.1	14.9	7.4
20	1	0.67	7.3	9.2
21	1	0.68	7.8	8.7
22	1	0.68	8.2	8.3
23	1	0.97	11.0	8.8
24	1	0.83	11.0	7.5
25	1	0.91	11.0	8.3
26	1	0.83	12.0	6.9

Table H-5. (Continued).

Probe Wash No.	No. of Aerosol Samples Represented	Stearic Acid In Probe Wash (mg) (A)	Stearic Acid Collected On Filter(s) (mg) (B)	$\frac{A}{B} \times 100$ (%)
27	1	0.83	12.0	6.9
28	3	3.8	24.2	15.7
29	2	2.4	19.0	12.6
30	6	6.0	54.4	11.0
31	5	3.9	48.7	8.0
32	5	4.6	45.3	10.2
33	4 (Probe 1)	4.0	18.0	18.2
34	4 (Probe 2)	3.4	34.0	10.0
35	4 (Probe 3)	9.8	59.0	16.6
36	1	0.32	1.5	21.3
37	1	0.37	1.8	20.5
38	1	0.24	2.5	9.4
39	1	0.32	4.6	6.9
40	1	0.21	5.2	4.0
41	1	0.27	5.7	4.8
42	1	0.27	1.4	19.3
43	1	0.51	2.4	21.3
44	1	0.52	3.0	17.4
45	1	0.54	4.5	12.0
46	1	0.28	5.1	5.5

APPENDIX I

PROBE WALL THICKNESS EFFECTS

Table I-1 gives all sampling results for the probe wall effects study. The true value of the aerosol concentration, C_o, was assumed to be the average of 12 samples using probe number 4 (i.e., knife edge) to sample aerosol in the Mach 0.8 free jet. Considering the wall to bore ratio as an independent variable, x, and the relative error as a dependent variable, y, the linear correlation coefficient, r, for 15 data points (11 points for probes 1-3, and 4 points for probe 4) was calculated as follows:

$$N = 15 \quad \Sigma x = 19.8 \quad \Sigma y = 129 \quad \Sigma x^2 = 51.4$$

$$\Sigma y^2 = 2841 \quad \Sigma xy = 244$$

$$\Sigma' x^2 = \Sigma x^2 - \frac{(\Sigma x)^2}{N} = 25.3$$

$$\Sigma' y^2 = \Sigma y^2 - \frac{(\Sigma y)^2}{N} = 1732$$

$$\Sigma' xy = \Sigma xy - \frac{\Sigma x \Sigma y}{N} = 73.7$$

$$r = \frac{\Sigma' xy}{(\Sigma' x^2 \Sigma' y^2)^{1/2}} = 0.35$$

From statistical tables for the correlation coefficient, r, for N-2 degrees of freedom (69), there is no significant correlation unless the value of r is at least 0.44 at the 0.1 probability level.

Table I-1. Aerosol concentration in a Mach 0.8 free jet determined by different sampling probes.

Probe No.	Wall to Bore Area Ratio A_w/A_b	Aerosol Concentration C (mg/m^3)		Relative Error $\left(\frac{C-C_o}{C_o}\right) \times 100$
1	3.77	8.5		6.3
1	3.77	8.7		8.8
1	3.77	10.7		33.8
2	1.39	7.5		-6.3
2	1.39	8.8		10.0
2	1.39	9.0		12.5
2	1.39	8.5		6.3
3	0.44	8.4		5.0
3	0.44	9.5		18.8
3	0.44	9.4		17.5
3	0.44	9.9		23.7
4	0.28	8.1		-
4	0.28	6.8		-
4	0.28	8.2		-
4	0.28	8.2		-
4	0.28	8.2		-
4	0.28	8.4	Ave = 8.0	-
4	0.28	8.2		-
4	0.28	8.0		-
4	0.28	8.2		-
4	0.28	7.6		-
4	0.28	7.7		-
4	0.28	8.2		-

APPENDIX J

ANISOKINETIC SAMPLING RESULTS

Table J-1 lists all anisokinetic data. Note that for the supersonic exit Mach numbers, M_e = 1.26 and M_e = 1.47, values of U_o, U/U_o, and U/U'_o are listed where $U'_o = M_e$ and U_o = actual Mach no upstream of the sampling probe inlet when a bow shock exists in front of the sampling probe. For M_e = 1.26, the Mach number ratio across a normal shock will be 1.56, or U_o = Mach 0.81. For M_e = 1.47, the Mach number ratio across a normal shock will be 2.06, or U_o = Mach 0.71. In all cases U = velocity at sampling probe inlet. For isokinetic sampling conditions in the supersonic free jets there is no bow shock upstream of the sampling probe (i.e., shock is swallowed) and for these sampling points, $M_e = U'_o = U_o$.

Figures J-1 through J-4 show the data plotted as the relative % error, $\left[\frac{(C - C_o)}{C_o} \times 100\right]$, versus the sampling rate expressed as the % of isokinetic, $(\frac{U}{U_o} \times 100)$.

Because all of the error curves displayed a similar form, it was convenient to display all of the data on a single plot shown in Figure 15. Note that in Figure 15, the data for $M_e = 1.26$ and 1.47 are displayed in terms of the values of U/U_o derived from the Mach number ratio across the bow shock just upstream of the probe inlet as illustrated in Figure 16.

Initially, all the data in Figure 15 were subject to a linear regression of the form:

$$y = A + B/x \qquad \text{(J-1)}$$

where $y = C/C_o$ and $x = U/U_o$

The best linearized fit of the data gave:

$$\frac{C}{C_o} = 0.28 \frac{U_o}{U} + 0.81 \qquad \text{(J-2)}$$

with a correlation coefficient, $r = 0.94$.

A non-linear regression of the form:

$$y = N + \frac{(1-N)}{x} \qquad \text{(J-3)}$$

where $y = \frac{C}{C_o}$ and $x = \frac{U}{U_o}$

gave,

$$\frac{C}{C_o} = 0.69 + 0.31 \frac{U_o}{U} \qquad (J-4)$$

with an average relative deviation of $\pm$ 11.8%.

These regression analyses were performed using standard programs available for a programmable Hewlet-Packard scientific calculator.

Table J-1. Free jet anisokinetic sampling data.

Sample No.	Free Jet Mach No. (M_e or U'_o)	Free Stream Velocity, U_o (ft/sec)	Sampling Velocity, U (ft/sec)	$\frac{U}{U_o}$	True Aerosol Conc, C_o (mg/m^3)	Measured Aerosol Conc, C (mg/m^3)	$\frac{C}{C_o}$	$\frac{U}{U'_o}$
1	0.6	654	58.8	0.09	10.4	41.5	3.99	-
2	0.6	654	92.2	0.14	10.4	38.8	3.73	-
3	0.6	654	92.2	0.14	10.4	41.7	4.00	-
4	0.6	654	201	0.31	10.4	22.4	2.15	-
5	0.6	654	256	0.39	10.4	18.8	1.81	-
6	0.6	654	331	0.51	10.4	18.3	1.76	-
7	0.6	654	58.8	0.09	10.4	28.1	2.70	-
8	0.6	654	201	0.31	10.4	17.8	1.71	-
9	0.6	654	331	0.51	10.4	13.7	1.32	-
10	0.6	654	466	0.71	10.4	12.4	1.19	-
11	0.6	654	560	0.86	10.4	11.3	1.09	-
12	0.6	654	65.4	0.10	10.4	39.3	3.79	-
13	0.6	654	131	0.20	10.4	24.2	2.33	-
14	0.6	654	131	0.20	10.4	26.8	2.58	-
15	0.6	654	196	0.30	10.4	21.2	2.04	-
16	0.6	654	261	0.40	10.4	15.9	1.53	-
17	0.6	654	327	0.50	10.4	13.5	1.30	-
18	0.6	654	392	0.60	10.4	12.8	1.23	-
19	0.6	654	392	0.60	10.4	11.2	1.08	-

Table J-1. (Continued).

Sample No.	Free Jet Mach No. (M_e or U'_o)	Free Stream Velocity, U_o (ft/sec)	Sampling Velocity, U (ft/sec)	$\frac{U}{U_o}$	True Aerosol Conc, C_o (mg/m^3)	Measured Aerosol Conc, C (mg/m^3)	$\frac{C}{C_o}$	$\frac{U}{U'_o}$
20	0.6	654	458	0.70	10.4	11.6	1.12	-
21	0.6	654	654	1.0	10.4	9.9	0.95	-
22	0.8	850	64.6	0.076	9.2	35.9	3.90	-
23	0.8	850	258	0.30	9.2	15.6	1.70	-
24	0.8	850	435	0.51	9.2	9.9	1.08	-
25	0.8	850	621	0.73	9.2	9.5	1.03	-
26	0.8	850	791	0.93	9.2	9.5	1.03	-
27	0.8	850	64.6	0.076	9.2	37.9	4.12	-
28	0.8	850	146	0.17	9.2	23.9	2.60	-
29	0.8	850	146	0.17	9.2	27.8	3.02	-
30	0.8	850	258	0.30	9.2	20.7	2.25	-
31	0.8	850	329	0.39	9.2	17.7	1.92	-
32	0.8	850	435	0.51	9.2	15.3	1.66	-
33	0.8	850	85	0.10	9.2	33.8	3.67	-
34	0.8	850	170	0.20	9.2	19.6	2.13	-
35	0.8	850	255	0.30	9.2	14.8	1.61	-
36	0.8	850	340	0.40	9.2	14.2	1.54	-
37	0.8	850	340	0.40	9.2	14.8	1.61	-
38	0.8	850	425	0.50	9.2	13.4	1.46	-

Table J-1. (Continued).

Sample No.	Free Jet Mach No. (M_e or U'_o)	Free Stream Velocity, U_o (ft/sec)	Sampling Velocity, U (ft/sec)	$\frac{U}{U_o}$	True Aerosol Conc, C_o (mg/m^3)	Measured Aerosol Conc, C (mg/m^3)	$\frac{C}{C_o}$	$\frac{U}{U'_o}$
39	0.8	850	510	0.60	9.2	11.7	1.27	-
40	0.8	850	595	0.70	9.2	11.5	1.25	-
41	0.8	850	850	1.0	9.2	9.9	1.08	-
42	1.26	1238	1238	1.0	1.5	1.7	1.13	1.0
43	1.26	856	991	1.16	1.5	1.6	1.07	0.8
44	1.26	856	743	0.87	1.5	1.4	0.93	0.6
45	1.26	856	495	0.58	1.5	1.8	1.20	0.4
46	1.26	856	248	0.29	1.5	2.6	1.73	0.2
47	1.26	856	124	0.14	1.5	4.8	3.25	0.1
49	1.26	856	186	0.22	1.5	3.5	2.33	0.15
50	1.26	856	248	0.29	1.5	2.8	1.87	0.2
51	1.26	856	372	0.43	1.5	2.5	1.67	0.3
52	1.26	856	495	0.58	1.5	2.6	1.73	0.4
53	1.26	856	619	0.72	1.5	1.7	1.13	0.5
54	1.26	856	867	1.01	1.5	1.7	1.13	0.7
55	1.26	856	1114	1.30	1.5	1.4	0.93	0.9
56	1.26	1238	1238	1.0	1.5	1.3	0.87	1.0
57	1.47	765	139	0.18	2.1	5.3	2.52	0.1

Table J-1. (Continued).

Sample No.	Free Jet Mach No. (M_e or U'_o)	Free Stream Velocity, U_o (ft/sec)	Sampling Velocity, U (ft/sec)	$\frac{U}{U_o}$	True Aerosol Conc, C_o (mg/m^3)	Measured Aerosol Conc, C (mg/m^3)	$\frac{C}{C_o}$	$\frac{U}{U'_o}$
58	1.47	765	208	0.27	2.1	5.2	2.48	0.15
59	1.47	765	277	0.36	2.1	3.8	1.81	0.2
60	1.47	765	416	0.54	2.1	3.2	1.52	0.3
61	1.47	765	554	0.72	2.1	3.0	1.43	0.4
62	1.47	765	693	0.91	2.1	2.5	1.19	0.5
63	1.47	765	832	1.09	2.1	3.0	1.43	0.6
64	1.47	765	970	1.27	2.1	2.3	1.10	0.7
65	1.47	765	1109	1.45	2.1	2.5	1.19	0.8
66	1.47	765	1247	1.63	2.1	2.6	1.24	0.9
67	1.47	1386	1386	1.0	2.1	1.8	0.86	1.0
68	1.47	1386	1386	1.0	2.1	2.1	1.00	1.0
69	1.47	1386	1386	1.0	2.1	2.2	1.05	1.0
70	1.26	1238	1238	1.0	3.6	3.6	1.00	1.0
71	1.26	1238	1238	1.0	3.6	3.5	0.97	1.0
72	1.26	1238	1238	1.0	3.6	3.5	0.97	1.0
73	1.26	1238	1238	1.0	3.6	3.5	0.97	1.0
74	1.26	1238	1238	1.0	3.6	3.5	0.97	1.0
75	1.26	1238	1238	1.0	3.6	3.2	0.89	1.0
76	1.26	1238	1238	1.0	3.6	3.2	0.89	1.0

Table J-1. (Continued).

Sample No.	Free Jet Mach No. (M_e or U'_o)	Free Stream Velocity, U_o (ft/sec)	Sampling Velocity, U (ft/sec)	$\frac{U}{U_o}$	True Aerosol Conc, C_o (mg/m^3)	Measured Aerosol Conc, C (mg/m^3)	$\frac{C}{C_o}$	$\frac{U}{U'_o}$
77	1.26	1238	1238	1.0	3.6	3.7	1.03	1.0
78	1.26	1238	1238	1.0	3.6	3.8	1.06	1.0
79	1.26	1238	1238	1.0	3.6	3.8	1.06	1.0
80	1.26	1238	1238	1.0	3.6	3.8	1.06	1.0
81	0.8	850	850	1.0	8.5	7.6	0.89	-
82	0.8	850	850	1.0	8.5	7.7	0.91	-
83	0.8	850	850	1.0	8.5	9.0	1.06	-
84	0.8	850	850	1.0	8.5	7.1	0.84	-
85	0.8	850	850	1.0	8.5	7.0	0.82	-
86	0.8	850	850	1.0	8.5	7.4	0.87	-
87	0.8	850	850	1.0	8.5	7.8	0.92	-
88	0.8	850	850	1.0	8.5	9.0	1.06	-
89	0.8	850	850	1.0	8.5	9.0	1.06	-
90	0.8	850	850	1.0	8.5	9.0	1.06	-
91	0.8	850	850	1.0	8.5	9.9	1.16	-
92	0.8	850	850	1.0	8.5	9.9	1.16	-
93	0.8	850	850	1.0	8.5	6.4	0.75	
94	0.8	850	850	1.0	8.5	7.7	0.91	-
95	0.8	850	850	1.0	8.5	9.0	1.06	-

Table J-1. (Continued).

Sample No.	Free Jet Mach No. (M_e or U'_o)	Free Stream Velocity, U_o (ft/sec)	Sampling Velocity, U (ft/sec)	$\frac{U}{U_o}$	True Aerosol Conc, C_o (mg/m^3)	Measured Aerosol Conc, C (mg/m^3)	$\frac{C}{C_o}$	$\frac{U}{U'_o}$
96	0.8	850	850	1.0	8.5	11.5	1.35	-
97	0.8	850	850	1.0	8.5	7.6	0.89	-
98	0.8	850	850	1.0	8.5	9.0	1.06	-
99	0.8	850	850	1.0	8.5	9.0	1.06	-
100	0.6	654	654	1.0	9.5	9.0	0.95	-
101	0.6	654	654	1.0	9.5	10.0	1.05	-
102	0.6	654	654	1.0	9.5	8.5	0.89	-
103	0.6	654	654	1.0	9.5	9.3	0.98	-
104	0.6	654	654	1.0	9.5	9.6	1.01	-
105	0.6	654	654	1.0	9.5	11.0	1.16	-
106	0.6	654	654	1.0	9.5	10.5	1.11	-
107	0.6	654	654	1.0	9.5	9.2	0.97	-
108	0.6	654	654	1.0	9.5	10.3	1.08	-
109	0.6	654	654	1.0	9.5	9.3	0.98	-
110	0.6	654	654	1.0	9.5	8.6	0.91	-
111	0.6	654	654	1.0	9.5	8.9	0.94	-
112	0.6	654	654	1.0	9.5	8.8	0.93	-

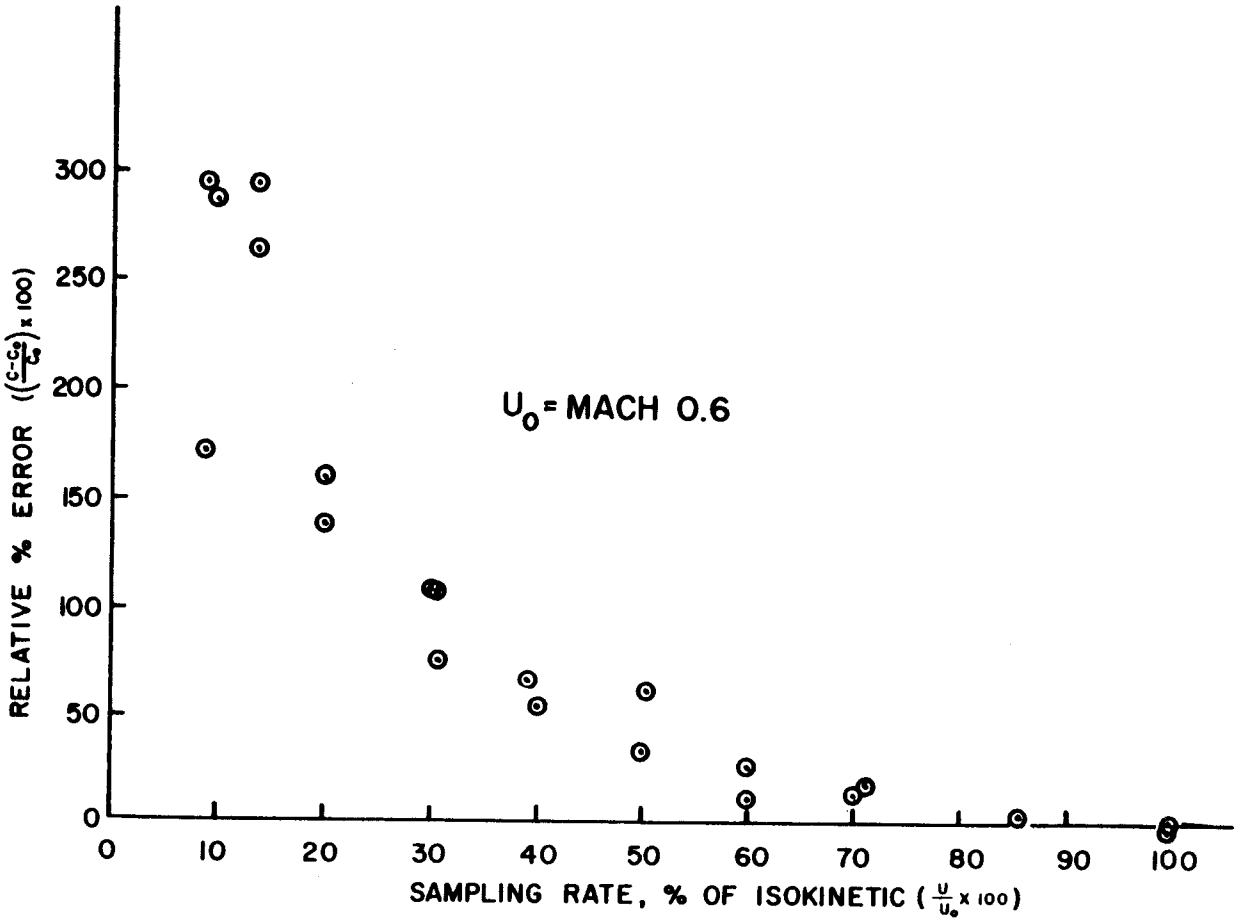

Figure J-1. Anisokinetic sampling errors, U_O = Mach 0.6.

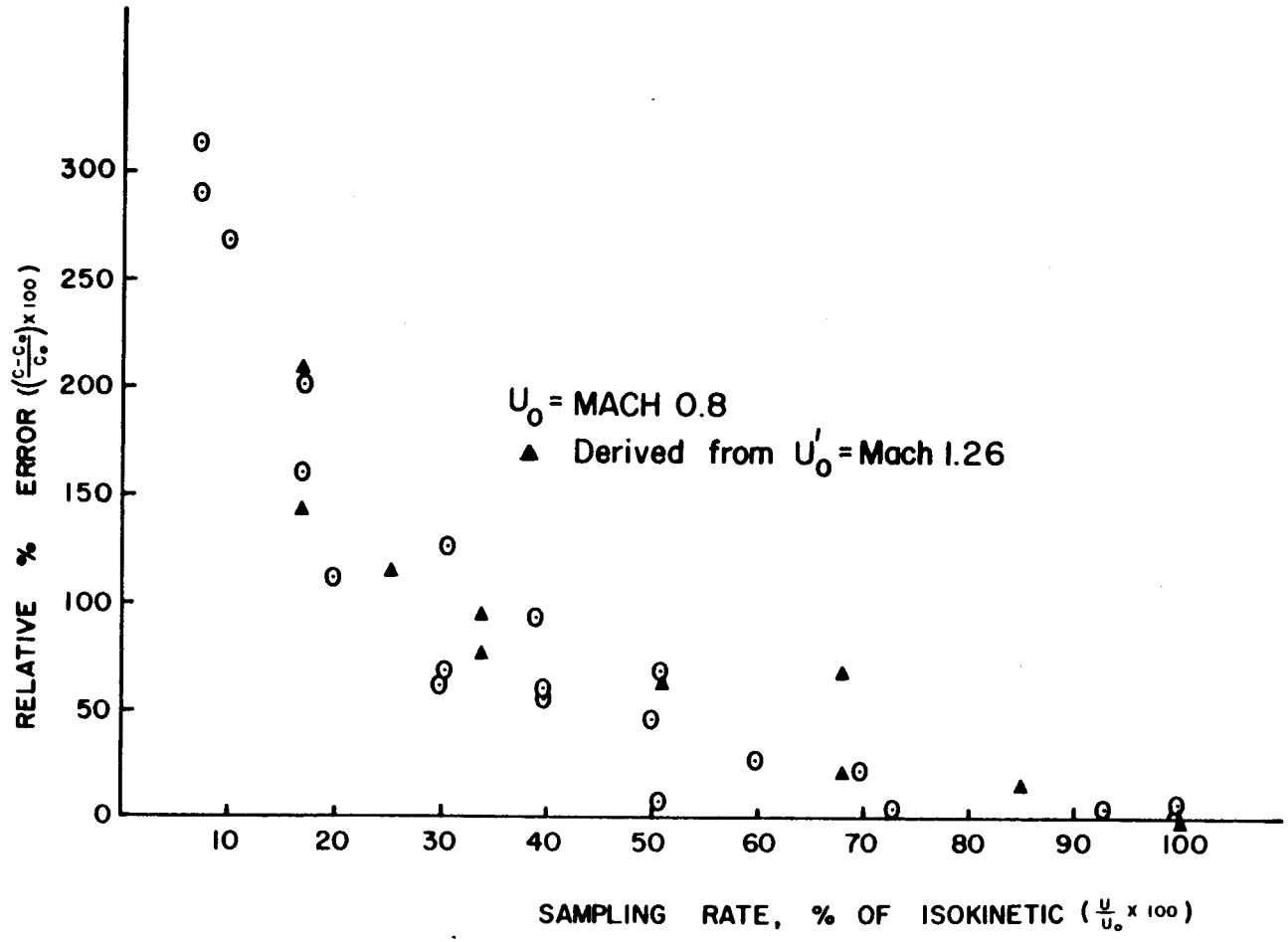

Figure J-2. Anisokinetic sampling errors, U_o = Mach 0.8.

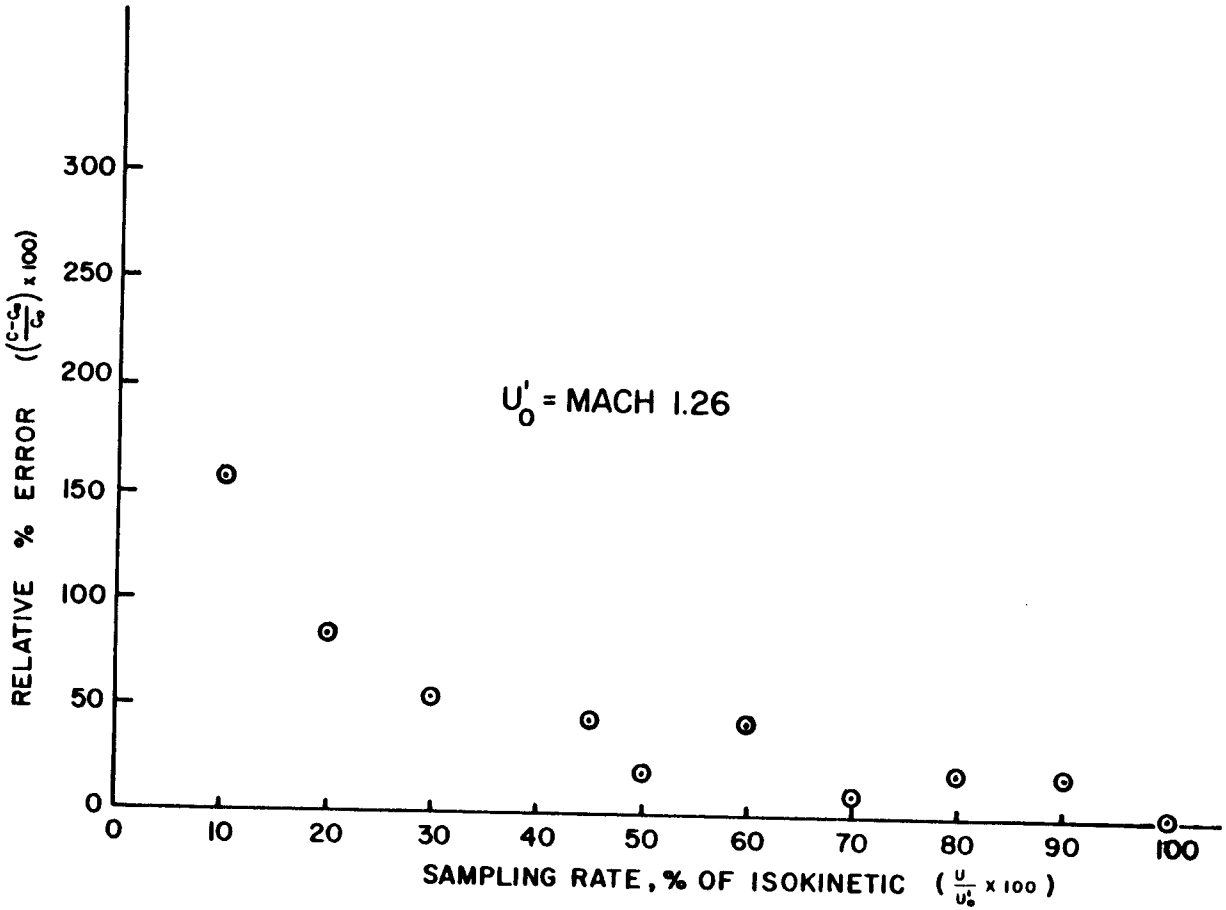

Figure J-3. Anisokinetic sampling errors, U'_O = Mach 1.26.

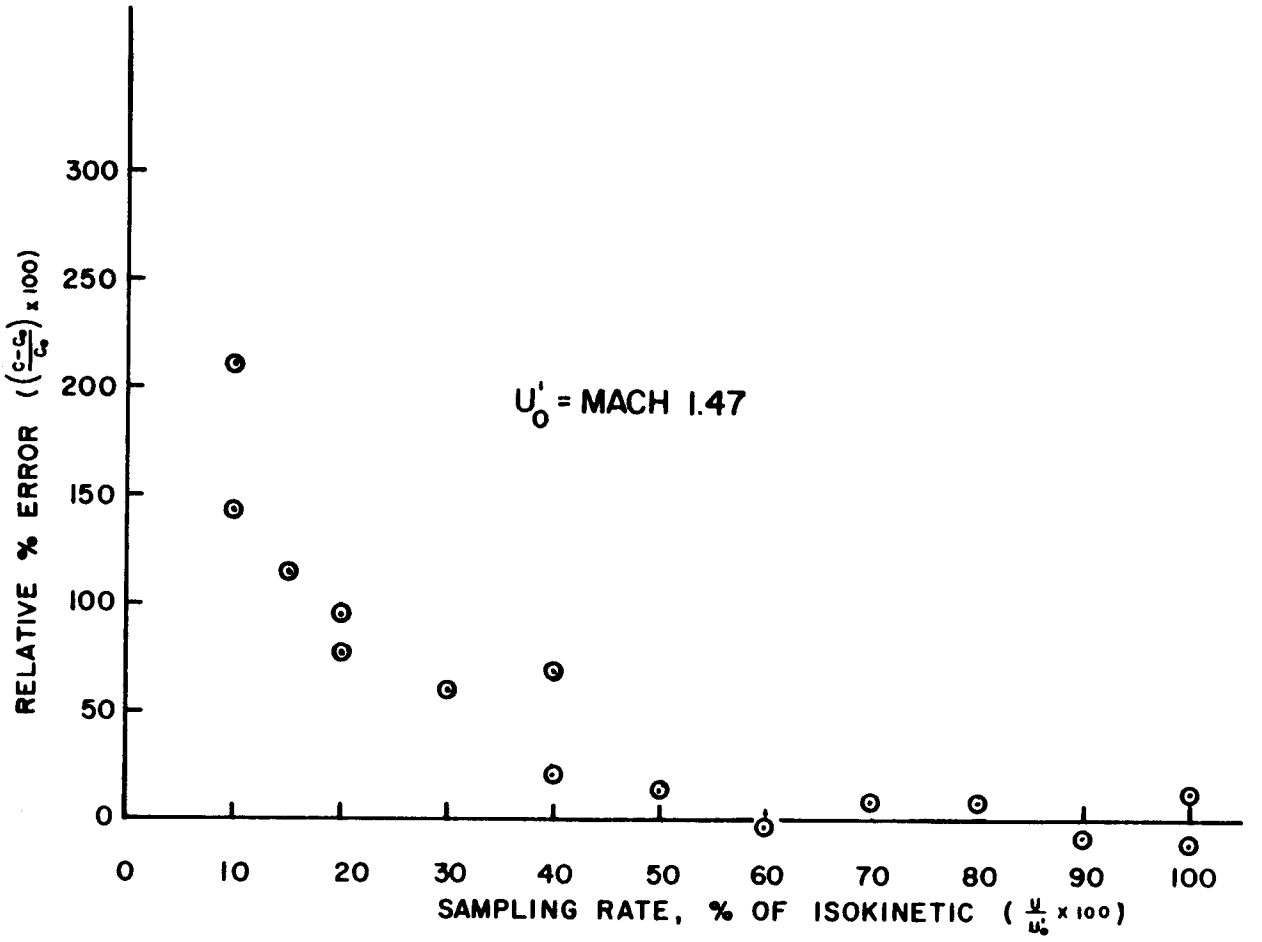

Figure J-4. Anisokinetic sampling errors, U'_O = Mach 1.47.

APPENDIX K

COMPARISON OF ANISOKINETIC RESULTS WITH RESULTS OF OTHER AUTHORS

Since the anisokinetic results of other authors are related to particle Stokes number, K, where

$$K = \frac{\rho_p \, d_p^2 \, U_o \, C_s}{18 \, \mu_g \, D_p} \qquad \text{(K-1)}$$

and,

ρ_p = particle density
d_p = particle diameter
U_o = free stream velocity
C_s = Cunningham correction factor
μ_g = gas viscosity
D_p = bore of sampling probe

K was calculated for the experimental conditions.

First, the Cunningham correction is given by (71):

$$C_s = 1 + \frac{\lambda^*}{R_p}\left[1.26 + 0.4 \exp\left(\frac{-1.1 \, R_p}{\lambda^*}\right)\right] \qquad \text{(K-2)}$$

where,

λ^* = mean free path of air molecules
= 0.65×10^{-5}cm at 20c at 1 atm
R_p = radius of particle = 0.4μm

and,

$$C_s = 1 + \frac{0.0065\times10^{-5}\text{m}}{0.4\times10^{-6}\text{m}}\left[1.26 + 0.4 \exp\left(\frac{-1.1\times0.4\times10^{-6}\text{m}}{0.0065\times10^{-5}\text{m}}\right)\right]$$

$C_s = 1.2$

Then, calculate Stokes number given that:

ρ_p = 58 Lbs/ft^3 (specification for Emersol 153 stearic acid)

d_p = 0.8 μm = 0.0262 x 10^{-4} ft

D_p = 0.177 in = 0.0148 ft

μ_g = 0.11 x 10^{-4} lb/ft-sec at 0C

U_o = 653.6 ft/sec (M_e = 0.6)

U_o = 850 ft/sec (M_e = 0.8)

For M_e = 0.6, K is:

$$K = \frac{58 \frac{\text{Lbs}}{\text{ft}^3} \times (2.62 \times 10^{-6} \text{ ft})^2 \times 653.6 \text{ ft/sec} \times 1.2}{18 \times 0.11 \times 10^{-4} \frac{\text{Lb}}{\text{sec} \times \text{ft}} \times 0.0148 \text{ ft}}$$

K = 0.10

For M_e = 0.8,

K = 0.14

Thus, the Stokes number range for experimental data is 0.10 - 0.14. For the supersonic cases the Stokes number calculation is based on U_o equal to the subsonic Mach number down stream of the normal shock in front of the probe which for M_e = 1.47 is M_2 = 0.81 and for M_e = 1.26, M_2 = 0.71. Thus, the Stokes number range of 0.10 - 0.14 includes all data. For this reason, the comparison of the experimental data with results for other authors was based on an average Stokes number of 0.12.

The present experimental anisokinetic data was correlated with the equation:

$$\frac{C}{C_o} = 0.69 + 0.31\ (U_o/U) \qquad \text{(K-3)}$$

Voloshchuck and Levin (21) gave a theoretical approximation:

$$\frac{C}{C_o} = 1 + \left(\frac{U_o}{U} - 1\right) \beta(K) \qquad \text{(K-4)}$$

Davies, as reported by Belyaev and Levin (23), suggested,

$$\beta(K) = 1 - [1/(1 + 4K)] \qquad \text{(K-5)}$$

or for K = 0.12,

$$\beta(K) = 0.32$$

and equation K-4 becomes:

$$\frac{C}{C_o} = 0.68 + 0.32\ \frac{U_o}{U} \qquad \text{(K-6)}$$

Belyaev and Levin (23) approximated their results with,

$$\beta(K)\ 1- [1/(1+BK)] \qquad \text{(K-7)}$$

where,

$$B = 2 + 0.62\ (U/U_o) \qquad \text{(K-8)}$$

Equation K-4 becomes:

$$\frac{C}{C_o} = 1 + \left[\frac{U_o}{U} - 1\right] \left[1 - \left(1/\left(1 + \left(2 + 0.62\ \frac{U}{U_o}\right)\right) K\right)\right] \qquad \text{(K-9)}$$

Zenker (22) found that,

$$\frac{C}{C_o} = N + \frac{U_o}{U}(1-N) \qquad \text{(K-10)}$$

N = dimensionless coefficient depending only on the Stokes number

Equating equation K-10 and K-4 and solving for ß(K) we have:

$$\frac{C}{C_o} = N + \frac{U_o}{U}(1-N) = 1 + \left(\frac{U_o}{U} - 1\right) ß(K) \qquad \text{(K-11)}$$

or,

$$ß(K) = \frac{N + \frac{U_o}{U}(1-N) - 1}{\frac{U_o}{U} - 1} \qquad \text{(K-12)}$$

$$ß(K) = \frac{N + \frac{U_o}{U} - N\frac{U_o}{U} - 1}{\frac{U_o}{U} - 1} \qquad \text{(K-13)}$$

$$ß(K) = \frac{N\left(1 - \frac{U_o}{U}\right) + \frac{U_o}{U} - 1}{\frac{U_o}{U} - 1} \qquad \text{(K-14)}$$

$$\beta(K) = \frac{-N\left(\frac{U_o}{U}-1\right) + \left(\frac{U_o}{U}-1\right)}{\frac{U_o}{U} - 1} \qquad \text{(K-15)}$$

$$\beta(K) = (1 - N) \qquad \text{(K-16)}$$

According to Zenker (22) for K = 0.12,

$$N = 0.71 \text{ and } \beta(K) = 0.29$$

and equation K-4 becomes:

$$\frac{C}{C_o} = 1 + \left(\frac{U_o}{U} - 1\right) 0.29 \qquad \text{(K-17)}$$

$$\frac{C}{C_o} = 0.71 + 0.29 \left(\frac{U_o}{U}\right) \qquad \text{(K-18)}$$

Badzioch (26) proposed that:

$$\frac{C}{C_o} = \eta \left(\frac{U_o}{U}\right) + (1 - \eta) \qquad \text{(K-19)}$$

where η is defined as an "inertial parameter".

Based on experimental data, Badzioch (26) gives values of η for various sampling probe diameters as a

function of the "range" of a particle, $\lambda = \frac{vU}{g}$ (cm).

where,

v = free falling velocity of a particle by Stokes law

$$v = \frac{[(\rho_p - \rho)\, d^2\, g] \times C}{18\, \mu g} \qquad \text{(K-20)}$$

For U_o = Mach 0.8 = 850 $\frac{ft}{sec}$:

$$\lambda = \frac{58\ \frac{Lb}{ft^3} \times (2.62 \times 10^{-6}\ ft)^2\ g \times 1.2}{18 \times 0.11 \times 10^{-4}\ \frac{Lb}{sec \times ft} \times g}$$

$$\lambda = 0.064 \text{ cm}$$

and from Badzioch (26),

$$\eta \approx 0.07$$

and equation K-19 becomes;

$$\frac{C}{C_o} = 0.07 \left(\frac{U_o}{U}\right) + 0.93 \qquad \text{(K-21)}$$

Watson's (27) analysis gave:

$$\frac{C}{C_o} = \frac{U_o}{U}\left[1 + f(K)\left[\left(\frac{U}{U_o}\right)^{1/2} - 1\right]\right]^2 \qquad \text{(K-22)}$$

where f(K) is an unknown function of the Stokes number, K.

Watson determined f(K) experimentally; for K = 0.12,

$$f(K) = 0.9$$

and equation K-22 becomes;

$$\frac{C}{C_o} = \frac{Uo}{U}\left[1 + 0.9\left(\left(\frac{U}{U_o}\right)^{1/2} - 1\right)\right]^2 \qquad \text{(K-23)}$$

Forney and McGregor (28) theoretically determined that the reduced probe efficiency, E_p, for a thin-walled cylindrical probe used in a supersonic stream is correlated with a a single universal curve and a function of $\Psi^{\frac{1}{2}}_f$ where:

$$\Psi_f = \text{inertial parameter} = K_1\ C_s\ \Phi_r\ \Phi_s \qquad \text{(K-24)}$$

and,

K_1 = Stokes number upstream of probe bow shock

$$K_1 = \frac{\rho_p\ d_p^2\ U_o'}{18\ \mu_1\ R} \qquad \text{(K-25)}$$

R = probe radius

C_s = Cunningham slip correction factor

Φ_r = non-Stokesian correction factor

$$\Phi_r = \frac{18}{Re_{p_2}}\left[Re_{p_2}^{1/3} - 2.52\ \tan^{-1}\left(\frac{Re_{p_2}^{1/3}}{2.52}\right)\right] \qquad \text{(K-26)}$$

where,

Re_{p_2} = particle Reynolds number

$$Re_{p_2} = Re_{p_1}\ \frac{(\rho 2)}{\rho 1} \qquad \text{(K-27)}$$

and,

$$Re_{p_1} = \frac{\rho_1\ U_o'\ d_p}{\mu_1} \qquad \text{(K-28)}$$

subscripts: 1 = stagnation conditions upstream of shock

2 = stagnation conditions downstream of shock

and

Φ_s = ratio of probe radius-to-shock detachment distance or R/δ

where,

$$\frac{\delta}{R} = \left(\frac{\delta}{R}\right)_{f=o} \cos\left(\frac{f_p \Pi}{2}\right) \qquad 0 \leq f_p \leq 1 \qquad \text{(K-29)}$$

and,

$$\frac{\delta}{R}_{f_p=0} = \frac{1.78}{M_e} \left[1 - 0.46\ (M_e-2) + 0.32\ (M_e-2)^2\right] \qquad \text{(K-30)}$$

The probe collection efficiency, E, is related to E_p by,

$$E_p = (E-f_p)/(1-f_p)$$

or

$$E = E_p\ (1-f_p) + f_p \qquad \text{(K-31)}$$

where,

f_p = probe mass fraction ingested

In terms of this work;

$$f_p = \frac{U}{U_o} \text{ and } E = \frac{C_o}{C} \qquad \text{(K-32)}$$

Table K-1 gives the appropriate terms calculated for $M_e = 1.26$ and $M_e = 1.47$.

Table K-1. Terms needed to calculate the inertial parameter, Ψ_f.

Term	$M_e = 1.26$	$M_e = 1.47$	Equation
$(\delta/R)_{fp=0}$	2.14	1.61	K-29
K_1	0.39	0.47	K-25
Re_{p_1}	33.2	43.7	K-28
Re_{p_2}	48	79	K-27
Φ_r	0.45	0.38	K-26
C_s	1.2	1.2	K-2
$(\delta)_{f=0}$	5.4 mm	4.1 mm	K-30

For $M_e = 1.26$,

$$K \times C_s \times \Phi_r = (0.39)\ (1.2)\ (0.45) = 0.21$$

For $M_e = 1.47$,

$$K \times C_s \times \Phi_r = (0.47)\ (1.2)\ (0.38) = 0.21$$

Table K-2 gives calculated values of ψ_f and corresponding values of E_p obtained from Figure 2. E, calculated from equation K-31 and C/C_o are also given.

Table K-2. Inertial parameter and probe collection efficiency for various probe injestion rates.

Probe Ingestion Rate (f)	Φ_s	Inertial Parameter Ψ_f	$(\Psi_f)^{\frac{1}{2}}$	Reduced Collection Efficiency E_p	Collection Efficiency E	$\frac{C}{C_o}$
0.1	0.47	0.099	0.31	0.15	0.24	4.25
0.2	0.49	0.10	0.32	0.17	0.34	2.98
0.3	0.53	0.11	0.33	0.18	0.43	2.35
0.4	0.58	0.12	0.35	0.20	0.52	1.92
0.5	0.66	0.14	0.37	0.22	0.61	1.64
0.6	0.79	0.17	0.41	0.24	0.70	1.44
0.7	1.04	0.22	0.47	0.37	0.81	1.23
0.8	1.51	0.32	0.57	0.49	0.90	1.11
0.9	2.93	0.62	0.79	0.76	0.98	1.02

The relationship between the probe ingestion rate and shock detachment distance, δ, given by equation K-29 is the result of a theoretical development by Forney et al (72) for $M_e = 2$. Table K-3 compares predicted values of δ from equations K-29 and K-30 with values measured directly from shadowgraphs of probe number 4 submerged in supersonic flow (Figure 14).

Table K-3. Measured shock detachment distance compared with predicted values.

Nozzle Exit Mach No. (M_e)	$\frac{U}{U_o}$	Shock Detachment Distance, δ (mm)	
		Measured	Predicted
1.26	0	4.4	5.4
1.47	0	3.1	4.1
1.26	0.7	2.4	2.4
0.47	0.9	1.3	0.7

Table K-4 compares the predicted values of C/C_o for values of U/U_o from 0.1 to 1.0 using the correlation equations developed by the various authors mentioned above. Table 5 compares the experimental conditions used by these authors in developing their predictive equations for anisokinetic sampling errors.

Table K-4. Comparison of anisokinetic sampling results of various authors.

U/U_o	C/C_o (eq K-3) (Martone)	C/C_o (eq K-6) (Davies)	C/C_o (eq K-9) (Belyaev-Levin)	C/C_o (eq K-18) (Zenker)	C/C_o (eq K-21) (Badzioch)	C/C_o (eq K-23) (Watson)	C/C_o (eq K-31) (Forney)
0.1	3.79	3.88	2.78	3.61	1.63	1.47	4.25
0.2	2.24	2.28	1.81	2.16	1.28	1.26	2.98
0.3	1.72	1.75	1.48	1.68	1.16	1.17	2.35
0.4	1.47	1.48	1.32	1.44	1.11	1.12	1.92
0.5	1.31	1.32	1.22	1.29	1.07	1.08	1.64
0.6	1.21	1.21	1.15	1.19	1.05	1.07	1.44
0.7	1.13	1.14	1.10	1.12	1.03	1.04	1.23
0.8	1.08	1.08	1.06	1.07	1.02	1.02	1.11
0.9	1.03	1.04	1.03	1.03	1.01	1.01	1.02
1.0	1.00	1.00	1.00	1.00	1.00	1.00	1.00

APPENDIX L

SUBISOKINETIC SAMPLING ERRORS FOR AIRCRAFT TURBINE ENGINE SMOKE PROBES

The Environmental Protection Agency (EPA) has promulgated emission standards and measurement procedures for smoke produced by aircraft turbine engines (1). Smoke, by EPA definition, is particulate matter in engine exhaust that obscures transmission of light. The EPA test methods are largely adoptations of the Aerospace Recommended Practice, ARP 1179, developed by the Society of Automotive Engineers (SAE) Committee on Aircraft Exhaust Emissions Measurement (E-31) (2). The procedure involves passing a known mass of engine exhaust gas through a filter and measuring the optical reflectivity of the collected particles. Dividing this result by the clean filter reflectance yields a dimensionless term used for quantifying aircraft engine smoke emissions called smoke number (SN) according to the following equation:

$$SN = 100\ [1 - (R_S/R_W)] \qquad \text{(L-1)}$$

R_S = sample reflectance

R_W = clean filter reflectance

ARP 1179 specifies a sample flow rate of 286 cm^3/sec using a single element sampling probe with an inlet diameter (D_p) of 2.0 mm. This means that a typical smoke probe located at the exit nozzle of an aircraft engine operates at about 20 to 33 percent of the isokinetic sampling velocity (73). Using this information and the

findings of this study, it is possible to estimate subisokinetic sampling errors associated with smoke probe operation. It should be noted that the EPA procedure (1) permits multipoint manifolded sampling probes with no specification for their physical dimensions, thus the entrance velocity at each orifice could be appreciably different from the velocity at the inlet of a single element smoke probe.

For Stokes numbers between 0.06 and 14 and values of U/U_o bewtween 0.4 and 2.5, Zenker (22) provides the following relationship:

$$C/C_o = N + (U_o/U)\ (1-N) \qquad \text{(L-2)}$$

where:

N = dimensionless coefficient depending only on the Stokes number

For Stokes numbers less than 0.5, a least squares fit (N vs $K^{1/2}$) to Zenker's (22) smoothed data gives:

$$N = 1.02 - 0.85\ (K)^{1/2} \qquad \text{(L-3)}$$

Since Equation L-2 was experimentally verified over a wider range of Stokes numbers than Equation 8, it was used in the following calculations to estimate subisokinetic errors associated with gas turbine engine smoke probe operation.

To apply Equation L-2, the first step is to

calculate appropriate particle-nozzle Stokes numbers. This requires a knowledge of engine exhaust temperature and velocity as well as information about the exit plane particle size distribution. For illustrative purposes, consider the JT9D turbofan engine which powers the Boeing 747 aircraft. According to the LAAPCD (11), at the take-off setting the JT9D has an exhaust temperature of approximately 480C and an exhaust velocity (U_o) near 400 m/sec (Mach 0.74). Although the size distribution of particles in a gas turbine engine exhaust is not known with much certainty, the result of the often cited work of Stockham and Betz (8) is used. Stockham and Betz (8) found particles at the exhaust plane of a J57 engine operating at 76% normal power to have a number median diameter (M_g) of 0.053 μm and a geometric standard deviation (σ_g) of 1.63. The number median diameter (M_g) can be converted to the mass median diameter (M_g') using (70):

$$\ln M_g' = \ln M_g + 3 (\ln \sigma_g)^2 \qquad \text{(L-4)}$$

For this example, M_g' equals 0.108

If the particle mass distribution is divided into size intervals which represent 10% of the particle mass, one can calculate Stokes numbers and use Equation L-3 to determine N values for the mid-point particle diameter in

each interval; Table L-1 summarizes this procedure. In the particle-nozzle Stokes number calculation a gas viscosity (μ_g) of 358.3 μ poise, a probe inlet diameter (D_p) of 2.0 mm, and a particle density of (ρ_g) of 1.0 gm/cm^3 were used.

With the computed N values (Table L-1), Equation L-2 can be used to estimate average relative percent sampling errors $[((C/C_o)/C_o) \times 100]$ for subisokinetic operation ($U/U_o<1$) of an ARP 1179 smoke probe. Table L-2 lists the computed values of C/C_o for the mid-point particle diameter of each 10% mass interval. In addition, Table L-2 contains arithmetic average values of C/C_o for selected sampling velocity ratios (U/U_o) ranging from 0.1 to 0.7. When U/U_o is greater than 0.7 the sampling error is negligible. Figure L-1 shows averaged C/C_o and selected U/U_o values plotted as relative % error versus the % of the isokinetic condition. As shown in Figure L-1, operation of an ARP 1179 smoke probe would produce an estimated 15-30% subisokinetic error at the assumed exhaust conditions.

Under aircraft turbine engine smoke testing procedures as specified in SAE ARP 1179 (2), the predicted subisokinetic sampling errors are not serious, since it has been shown by Champagne (3) that smoke filters which differ in collected particle mass by 50% can yield the same SAE smoke number. Thus, a smoke

Table L-1. Stokes numbers (K) and N values for a typical gas turbine engine exhaust particle size distribution.

Particle Diameter (μm)	Wt% Less than Stated Diameter	Mid-Point diameter, d_p (μm)	Stokes Number K	N (Eq. L-3)
0.023	0.1	0.040	0.0031	0.973
0.057	10	0.064	0.0052	0.959
0.070	20	0.077	0.0066	0.951
0.083	30	0.089	0.0078	0.945
0.095	40	0.102	0.0096	0.937
0.108	50	0.115	0.010	0.935
0.121	60	0.131	0.013	0.923
0.140	70	0.152	0.017	0.909
0.163	80	0.183	0.021	0.897
0.202	90	0.351	0.060	0.812
0.500	99.9			

Table L-2. Predicted aerosol concentration ratios (C/C_o) for selected sampling velocity ratios (U/U_o).

Particle Diameter, d_p (μm)	Aerosol Concentration Ratio, C/C_o				
	$U/U_o = 0.7$	$U/U_o = 0.5$	$U/U_o = 0.3$	$U/U_o = 0.2$	$U/U_o = 0.1$
0.040	1.01	1.03	1.06	1.11	1.24
0.064	1.02	1.04	1.10	1.16	1.37
0.077	1.02	1.05	1.11	1.20	1.44
0.089	1.02	1.06	1.13	1.22	1.50
0.102	1.03	1.06	1.15	1.25	1.57
0.115	1.03	1.07	1.15	1.26	1.59
0.131	1.03	1.07	1.18	1.31	1.69
0.152	1.04	1.09	1.21	1.36	1.82
0.183	1.04	1.10	1.24	1.41	1.93
0.351	1.08	1.19	1.44	1.75	2.69
Ave. C/C_o	1.03	1.08	1.17	1.30	1.68

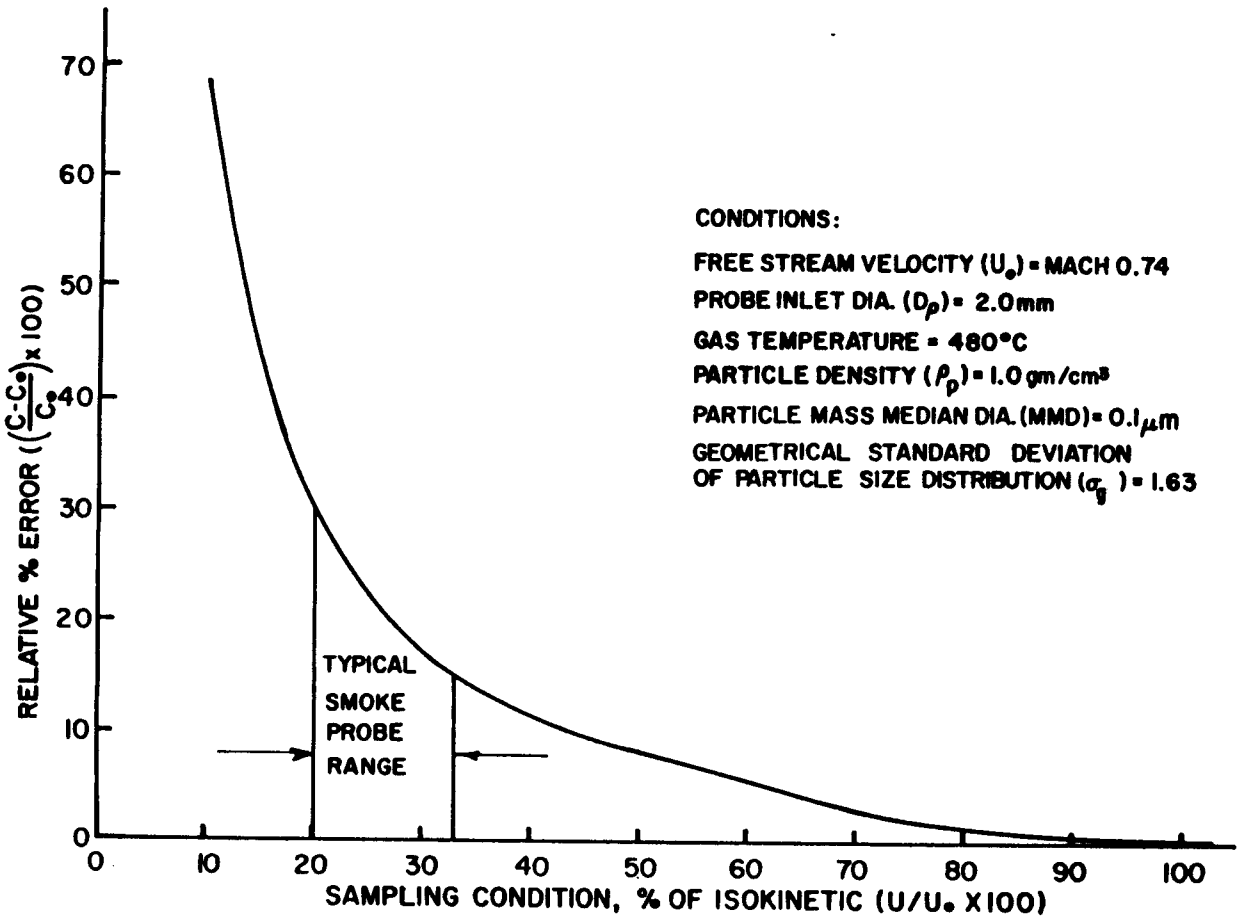

Figure L-1. Predicted subisokinetic sampling errors for a standard ARP 1179 smoke probe.

sample obtained isokinetically and a smoke sample obtained with U/U_o as low as 0.13 could produce identical smoke numbers. This can occur because smoke number is primarily influenced by the reflectivity of smaller particles on the filter paper. Larger particles will have little effect on the reading obtained, irrespective of their mass quantity. It must also be remembered that the error calculation was performed for a take-off engine power setting and therefore, must be considered a worst case analysis for a non-afterburning aircraft gas turbine engine.

The results are of special interest to those concerned with measuring the true smoke density (mass of particles/volume) of gas turbine engine exhausts. For this determination, especially at the take-off engine power setting, it is evident that subisokinetic sampling errors need to be considered. To insure representativeness, samplers should operate isokinetically or have a selection of sampling rates to maintain a sufficient U/U_o for all engine power settings.